



HAL
open science

Digital and multiplex detection of microRNAs for molecular diagnostics

Thomas Jet

► **To cite this version:**

Thomas Jet. Digital and multiplex detection of microRNAs for molecular diagnostics. Molecular biology. Université Paris Cité, 2021. English. NNT : 2021UNIP5004 . tel-03881412

HAL Id: tel-03881412

<https://theses.hal.science/tel-03881412>

Submitted on 1 Dec 2022

HAL is a multi-disciplinary open access archive for the deposit and dissemination of scientific research documents, whether they are published or not. The documents may come from teaching and research institutions in France or abroad, or from public or private research centers.

L'archive ouverte pluridisciplinaire **HAL**, est destinée au dépôt et à la diffusion de documents scientifiques de niveau recherche, publiés ou non, émanant des établissements d'enseignement et de recherche français ou étrangers, des laboratoires publics ou privés.

Université de Paris

Ecole Doctorale 563 Médicament, Toxicologie,
Chimie, Imagerie

Centre de Recherche des Cordeliers

Détection digitale et multiplexe de microARN pour le diagnostic moléculaire

Par Thomas Jet

Thèse de doctorat de Biologie moléculaire

Dirigée par Valérie Taly

Présentée et soutenue publiquement le 09/02/2021

Devant le jury composé de :

Niko Hildebrandt

Professeur, Université de Rouen Normandie

Claire Smadja

Professeur, Université Paris Saclay

Anne-Marie Gué

Directrice de Recherche, LAAS-CNRS

Florent Malloggi

Chargé de Recherche, CEA

Amel Bendali

Directrice générale, Inorevia

Valérie Taly

Directrice de Recherche, Université de Paris

Yannick Rondelez

Directeur de Recherche, ESPCI Paris

Rapporteur

Rapporteuse

Examinatrice

Examineur

Examinatrice

Directrice de thèse

Invité



Except where otherwise noted, this work is licensed under
<https://creativecommons.org/licenses/by-nd/3.0/fr/>

Université de Paris

Ecole Doctorale 563 Médicament, Toxicologie,
Chimie, Imagerie

Centre de Recherche des Cordeliers

Détection digitale et multiplexe de microARN pour le diagnostic moléculaire

Par Thomas Jet

Thèse de doctorat de Biologie moléculaire

Dirigée par Valérie Taly

Présentée et soutenue publiquement le 09/02/2021

Devant le jury composé de :

Niko Hildebrandt

Professeur, Université de Rouen Normandie

Claire Smadja

Professeur, Université Paris Saclay

Anne-Marie Gué

Directrice de Recherche, LAAS-CNRS

Florent Malloggi

Chargé de Recherche, CEA

Amel Bendali

Directrice générale, Inorevia

Valérie Taly

Directrice de Recherche, Université de Paris

Yannick Rondelez

Directeur de Recherche, ESPCI Paris

Rapporteur

Rapporteuse

Examinatrice

Examineur

Examinatrice

Directrice de thèse

Invité



Except where otherwise noted, this work is licensed under
<https://creativecommons.org/licenses/by-nd/3.0/fr/>

Contents

1	Introduction: Multiplex microRNA detection methods	1
1.1	Interest and challenges of miRNA detection	1
1.1.1	Challenges for miRNA detection.	4
1.1.2	Importance of multiplexed detection.	4
1.2	Amplification techniques applied to miRNA detection	6
1.2.1	RT-qPCR	6
1.2.2	Rolling Circle Amplification	8
1.2.3	Exponential Amplification Reaction	9
1.2.4	Duplex-specific Nuclease Signal Amplification	9
1.2.5	Enzyme-free amplification techniques	10
1.3	Multiplexed miRNA detection	12
1.3.1	Separation techniques	12
1.3.1.1	Northern Blot and size-separation gel-based techniques	12
1.3.1.2	Capillary electrophoresis	14
1.3.2	Homogeneous multiplex detection	14
1.3.2.1	Multiplex RT-qPCR	14
1.3.2.2	Isothermal multiplex homogeneous assays	15
1.3.2.3	Fluorescence-based digital methods	16
1.3.2.4	Next Generation Sequencing	17
1.3.3	Heterogeneous multiplex detection	18
1.3.3.1	On-sensor methods	18
1.3.3.2	Nanostring	19
1.3.3.3	Microarrays	21
1.3.3.4	Suspension arrays	23
1.3.4	Multiplex microRNA detection from live cells	29
1.4	Conclusions and perspectives	30
1.5	Objectives of the PhD project	36

2	Proof of Concept: Multiplex detection of synthetic DNAs	39
2.1	Introduction: Molecular programming for isothermal digital miRNA detection	39
2.1.1	Design of the molecular network	40
2.1.2	Isothermal detection of miRNA	45
2.1.3	Digital detection of miRNA	46
2.2	Design of multiplexed method	50
2.2.1	Multiplexing strategy	50
2.2.2	Particles selection	53
2.2.2.1	Droplets and particle size	53
2.2.2.2	Coating	53
2.2.3	Particle barcoding	57
2.3	On-particle detection of DNA analogs of miRNAs	60
2.3.1	On-bead converter template	60
2.3.2	Capture time optimization	63
2.3.3	On-bead reporting	64
2.3.4	Multiplex detection of DNA versions of miRNAs	67
2.4	Chapter summary	69
3	Particle enzyme scavenging	71
3.1	Discovery of the effect	71
3.1.1	Addition of a washing step	72
3.1.2	Effect of particles dilution	74
3.2	Effect characterization: Enzyme depletion experiments	77
3.3	Proposed solutions	80
3.3.1	Addition of "neutral" particles	80
3.3.2	Modification of the encapsulation microfluidic device	82
3.4	Chapter summary	87
4	From DNA to miRNA detection	89
4.1	Introduction: Inaccurate quantification of RNA	89
4.2	Trigger production rate	93
4.3	Proposed solutions	95
4.3.1	Addition of Klenow polymerase	95
4.3.2	1 dNTP capture step	98
4.3.3	Post-capture particle washing	102
4.4	Dynamic range of the method	103
4.5	Specificity of the method	105

4.6	Multiplex detection of synthetic miRNAs	108
4.7	Conclusion	111
5	Conclusion	113
6	Materials and methods	117
6.1	General material and methods	117
6.2	Buffers	120
6.2.1	miR Buffer	120
6.2.2	Binding and washing buffer	120
6.2.3	Particles storage buffer	120
6.3	Particles functionalization	121
6.4	MultimiR reaction mixture	121
6.5	Capture step	121
6.6	Post-capture particles washing	122
6.6.1	”Soft” washing procedure	122
6.6.2	”Hard” washing procedure	123
6.7	Microfluidics	123
6.7.1	Microfluidics material	123
6.7.2	Microfluidic devices preparation	124
6.7.2.1	Soft lithography	124
6.7.2.2	PDMS chip preparation	124
6.7.2.3	Plasma cleaning	124
6.7.2.4	Hydrophobic treatment	124
6.7.3	Single water inlet microfluidics	124
6.7.4	2-water inlet microfluidics	125
6.8	Amplification step	125
6.9	Flow cytometry analysis	126
6.10	ID3miR	127
6.11	Production rate experiments	127
6.12	Enzyme depletion experiments	128

List of Figures

1.1	Main miRNA-induced pathways for post-transcriptional regulation	2
1.2	Simplified miRNA biogenesis pathway	3
1.3	Principle of RT-qPCR	7
1.4	Principle of RCA	8
1.5	Principle of EXPAR	10
1.6	Principle of DSNSA	11
1.7	Principle of HCR	12
1.8	Schematic representation of the approaches to multiplex miRNA detection .	13
1.9	Multiplex miRNA detection strategies based on separation techniques	14
1.10	Principle of the Nanostring nCounter system	20
1.11	Principle of planar microarrays	22
1.12	Example of fluorescent particle barcoding	24
1.13	Principle of the SIMOA detection system	26
1.14	Examples of graphical particle barcoding	27
1.15	Photonic crystal particles	28
1.16	Examples of common approaches for miRNA detection from live cells	30
2.1	Principle of the bistable switch	41
2.2	Trigger amplification by the autocatalytic template	42
2.3	Trigger inactivation by the pseudo template	43
2.4	Conversion of the miRNA into a trigger molecule	44
2.5	Fluorescent reporting of amplification	45
2.6	qPCR-inspired miRNA quantification using molecular programming	47
2.7	Principle of the ID3miR method	48
2.8	On/off-bead repartition of the molecular program	50
2.9	Multiplexing strategy	51
2.10	Summarized workflow	52
2.11	Generation of false positive particles by coencapsulation	54

2.12	Evaluation of the exchange of oligonucleotides by Dynabeads at 30°C	55
2.13	Measurement of the oligonucleotide binding capacity of the two types of 1 μm streptavidin-coated particles	56
2.14	Distribution of particle fluorescence before and after encapsulation	57
2.15	Absorption and emission spectra of the used fluorophores	58
2.16	Flow cytometry Cy5 vs Cy3.5 fluorescence diagram of a mix containing 20 subpopulations of barcoded particles	59
2.17	Comparison of the on-bead cT designs	61
2.18	Optimisation of the biotin T7 cT concentration	62
2.19	Singleplex digital detection of 1 pM Let7a using on-bead biotin T7 cTs	63
2.20	Capture step kinetics	64
2.21	Generic scheme of a biotinylated rT	64
2.22	Comparaison of the reaction-inhibiting effects of rT designs	66
2.23	Simultaneous detection of 3 DNA analogs of miRNAs	68
3.1	Updated workflow with a post-capture washing step	73
3.2	Updated summarized workflow	74
3.3	Wash/no wash false positive rate comparison	74
3.4	Wash/no wash amplification kinetics	75
3.5	Theoretical distribution of enzymes in droplets	77
3.6	Schematic representation of the enzyme scavenging effect	78
3.7	Enzyme depletion experiment	79
3.8	Identification of the oligonucleotides responsible for the scavenging of enzymes	80
3.9	Working principle of neutral beads	81
3.10	Representation of a neutral particle	82
3.11	Results of the neutral particle range	83
3.12	Single water inlet microfluidic device	84
3.13	Co-flow microfluidic device	85
3.14	Fluorescence microscopy image of the nozzle of the co-flow microfluidic device	85
3.15	Implementation of 2-water inlet microfluidics for miRNA detection	86
4.1	Results of the 5-plex assay on RNA versions of miRNAs	90
4.2	Digital detection of Let7a in its DNA and RNA versions	91
4.3	Results of the addition of RNase inhibitors during capture	92
4.4	Comparison of on/off-bead trigger production rates of cTs when converting DNA or RNA targets	93

4.5	Comparison of the trigger production rates from RNA and DNA with or without Klenow polymerase	96
4.6	Range of Klenow polymerase in bulk detection reactions	97
4.7	Effect of Klenow polymerase during the amplification step	98
4.8	Evaluation of the trigger production rate by poly(T) spacers cTs	100
4.9	Evaluation of poly(T) cTs for the singleplex detection of Let7a (RNA version)	101
4.10	Evaluation of poly(T) cTs for the singleplex detection of miR 21 (RNA version)	101
4.11	Theoretical curves of the percentage of positive particles depending on the concentration of particles and miRNA	104
4.12	Comparison of the measured percentages of positive particles with the theoretical result at 2 different concentrations of particles	105
4.13	Specificity experiments	107
4.14	6-plex detection of miRNAs in their RNA version	110
6.1	Single water inlet microfluidic chip	125
6.2	Double water inlet microfluidic chip	126

List of Tables

1.1	Summary of the characteristics of the discussed multiplex miRNA detection methods	33
2.1	Summary of beads characteristics	57
2.2	Sequences of the potential on-bead converters	60
2.3	Comparison of the on-bead cTs	61
2.4	rT designs sequences	65
2.5	ON/OFF fluorescent signal ratios of on-particle rT designs	65
3.1	Composition of the particles mentioned in fig 3.8	79
4.1	Comparison of the false positive rates measured for the 2 proposed washing procedures	102
4.2	Summary of the effect of the tested optimization procedures	103
4.3	Sequences of the members of the Let7 family	105
4.4	Composition of the 2 miRNA mixes	108
6.1	Sequences of the oligonucleotides used in this study	118
6.2	Sequences of the oligonucleotides used in this study	119
6.3	Composition of the 1X miRNA detection buffer	120
6.4	Composition of the binding and washing buffer	120
6.5	Composition of the storage buffer	120
6.6	Typical enzymes concentrations for miRNA detection	121
6.7	Configuration of the detectors of the used flow cytometer	126
6.8	Reaction mixture for production rate experiments	127

List of abbreviations

AGO	argonaut protein
aT	autocatalytic template
cDNA	complementary DNA
CHA	catalyzed hairpin assembly
Cq	cycle of quantification
cT	converter template
ctDNA	circulating tumoral DNA
DNA	deoxyribonucleic acid
dPCR	digital PCR
ddPCR	droplet digital PCR
DSN	duplex-specific nuclease
DSNSA	DSN signal amplification
EXPAR	exponential amplification reaction
FC	flow cytometry
FFF	field-flow fractionation
FRET	Förster resonance energy transfer
FSC	forward scattering
HCR	hybridization chain reaction
HDL	high-density lipoprotein
HPLC	high-performance liquid chromatography
ID3miR	isothermal droplet digital detection of miRNA
miRISC	miRNA-induced silencing complex
miRNA	microRNA
MP	micro-particle
mRNA	messenger RNA
NASBA	nucleic acid sequence-based amplification
NB	northern blot
NGS	next generation sequencing
NP	nano-particle
LAMP	loop-mediated isothermal amplification
LNA	locked nucleic acid
LOB	limit of blank
LOD	limit of detection
PAP	poly(A) polymerase

PCR	polymerase chain reaction
PEN DNA	polymerase exonuclease nickase dynamic network assembly
PhC	photonic crystal
pre-miRNA	precursor miRNA
pri-miRNA	primary miRNA
pT	pseudo template
PTO	phosphorothioate
QD	quantum dot
qPCR	quantitative PCR
RNA	ribonucleic acid
RNAi	RNA interference
RCA	rolling circle amplification
RPA	recombinase polymerase amplification
rT	reporter template
RT	reverse transcription
RT-qPCR	reverse transcriptase quantitative PCR
SERS	surface-enhanced Raman scattering
SIMOA	single molecule assay
SPR	surface plasmon resonance
SSCP	single-strand conformation polymorphism
T _m	melting temperature
UTR	untranslated region

Chapter 1

Introduction: Multiplex microRNA detection methods

1.1 Interest and challenges of miRNA detection

MicroRNAs (miRNAs) are a class of short non-coding RNAs of about 19 to 25 nucleotides. They were first discovered in 1993 in *Caenorhabditis elegans*[1] and are said to be responsible for the post-transcriptional gene expression regulation of more than 60% of human protein-coding genes[2]. This regulatory process, called RNA interference (RNAi), was first described in 1998 by Andrew Fire and Craig Mello[3], who were awarded the 2006 Nobel Prize in Medicine and Physiology.

In order to regulate gene expression, miRNAs form complexes with protein GW182 and one of the proteins of the Argonaute (AGO) family[4, 5]. This complex is known as the miRNA-Induced Silencing Complex (miRISC). In this complex, the miRNA is used for target recognition through base pairing, whereas proteins actively induce repression[6]. Two main mechanisms of the miRISC complex are proposed (Fig. 1.1): in most cases, the miRNA binds the 3' untranslated region (UTR) thanks to a region known as the miRNA "seed", located between the second and the seventh nucleotides. The RISC proteins then recruit factors inhibiting mRNA translation and promoting mRNA deadenylation[4]. Another mechanism of action of miRISC involves the complete binding of the miRNA inside the coding region of the gene, which leads to mRNA cleavage by the AGO protein[7]. The shortness of the miRNA-recognition site on the 3' UTR of the mRNAs explains how only a few thousands miRNAs can regulate the expression of more than half of human genes.

The biogenesis of miRNAs is initiated in the nucleus, as miRNA genes are transcribed by RNA polymerase II into a primary miRNA (pri-miRNA) (Fig. 1.2). The pri-miRNA is generally over 1 kb long and partially hairpin-shaped, with single-stranded 3' and 5' ends.

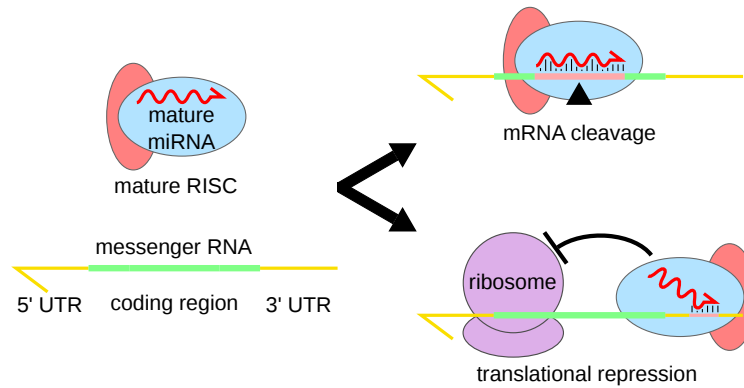


Figure 1.1: The two main miRNA-induced pathways for post-transcriptional regulation. Complete binding of the miRNA to the coding region of the mRNA leads to the cleavage of the mRNA by the proteins of the RISC complex. Alternatively, the "seed" region of the miRNA, typically located between the second and seventh nucleotide hybridizes to one of the untranslated regions (most commonly 3' UTR). This partial binding triggers the recruitment of translation-inhibiting factors and/or destabilizes the mRNA by promoting its deadenylation.

The mature miRNA sequence is part of the stem. Still inside the nucleus, this pri-miRNA undergoes maturation by the Microprocessor complex composed of nuclear RNase III Drosha and cofactor DGCR8[6]. Drosha cleaves the pri-miRNA and releases a 65 bases long hairpin-shaped RNA called precursor-miRNA (pre-miRNA). The pre-miRNA is exported in the cytoplasm, where it undergoes a second maturation step by Dicer endonuclease. Dicer cleaves pre-miRNA near both ends of the loop, releasing a duplex of small RNAs. This duplex is loaded onto an AGO protein to form a pre-RISC. The duplex is then unwinded by a helicase and only one of the RNAs remains in the complex, forming a mature RNA-induced silencing complex. For a more complete overview of miRNA biogenesis and physiological role, we refer the reader to dedicated reviews[6, 8, 9].

The role of miRNAs in cancer was first evidenced by Croce's group in 2002 when they discovered that a genomic region on which were located two miRNA genes was commonly deleted in chronic lymphocytic leukemia[10]. Since then, a plethora of disease-related miRNA dysregulations have been reported, not only in cancer [11], but also for Parkinson's disease[12], diabetes[13] and cardiovascular diseases[14], among others. The causes of these dysregulations are for example gene deletions[10, 15] or amplifications[16, 17] and defects in miRNA transcriptional control[18, 19, 20] or biogenesis machinery[21, 22]. In cancer, due to their gene expression-regulating role, the miRNA dysregulations could contribute to most of the cancer hallmarks. Among countless examples, miR92a's upregulation has been described as promoting cell proliferation[23], miR21 was found upregulated in lung cancer and inducing

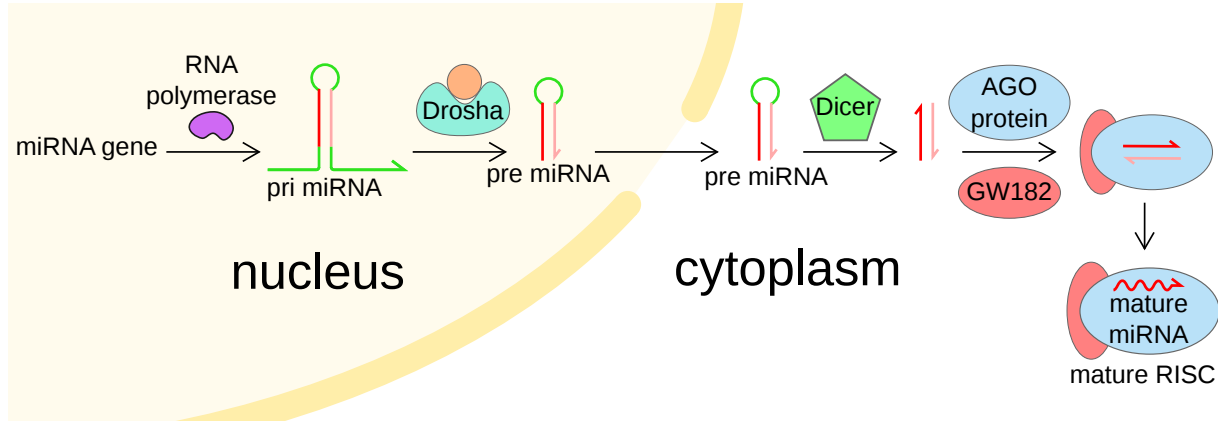


Figure 1.2: Simplified miRNA biogenesis pathway. The miRNA gene is transcribed into a 1kb-long primary miRNA (pri-miRNA). The pri-miRNA then undergoes two successive maturations, first forming an hairpin-shaped precursor miRNA (pre-miRNA) and then an RNA duplex composed of the miRNA and its complementary sequence. The complex binds a protein of the Argonaute (AGO) family and is unwinded by an helicase, releasing the complementary strand. The mature miRNA remains bound to the complex composed of AGO and other proteins, such as GW182, called the miRNA-induced silencing complex (miRISC).

apoptosis resistance[24], whereas miR203 downregulation was observed in metastatic breast cancer cells[11].

Tumor tissue biopsy is currently the main biomarker analysis method for cancer diagnostics. This procedure however presents serious drawbacks, such as limited capacities to recapitulate tumor heterogeneity, high cost and invasiveness. Moreover it is also not appropriate for tumor real time characterization which could be of great interest for patient follow up and treatment management. To circumvent these limitations, liquid biopsies are being developed. Liquid biopsy relies on the analysis of circulating biomarkers (including circulating tumoral DNA, circulating tumoral cells, proteins and miRNAs) in bodily fluids, such as blood or urine. MiRNAs have been shown to be released by healthy and tumor cells in the bloodstream and other biofluids[25]. These circulating miRNAs are thought to be not only passively released by apoptotic or necrotic cells, as it has mainly been described for ctDNA, but also actively secreted by living cells in extracellular vesicles. Studies suggest that secreted miRNAs could be addressed and delivered to specific cells. Once inside target cells, recovered miRNAs would modify the gene expression pattern, thus playing a long distance cell-to-cell signaling role[26]. Moreover, released miRNAs are protected, by conjugation to RNA-binding proteins such as AGO2 or high-density lipoprotein (HDL)[5], and are thus very stable even under harsh conditions[27]. These characteristics make miRNAs very promising biomarkers for liquid biopsy strategies.

1.1.1 Challenges for miRNA detection.

In spite of their attractiveness as biomarkers, several challenges need to be addressed in order to apply miRNA detection to cancer diagnosis. First, miRNAs are very short sequences, displaying a high level of homology, especially if they belong to the same family: The Let-7 miRNA family, involved in numerous pathologies including cancers, is comprised of 10 miRNAs sharing the same seed and most other nucleotides[28]. Let-7a and Let-7e, for example, are perfectly identical with the exception of their 9th nucleotide. Hence, a very high level of specificity is required to selectively quantify each miRNA.

MiRNAs only represent 0.01% of total RNA mass[29], and additionally need to be detected from highly complex media. In blood plasma, the concentrations of miRNAs are in the sub-picomolar (pM) range[27, 30]. In addition to sufficient sensitivity, miRNA detection methods need to display a dynamic range spanning at least four orders of magnitude.

The aim of a miRNA-based liquid biopsy is to detect miRNA concentrations changes, as both healthy and tumor cells release miRNAs, but in different relative quantities. Since these dysregulations may be subtle, the accuracy and precision of the assay is thus of utmost importance.

1.1.2 Importance of multiplexed detection.

The study of the dysregulation of single miRNAs is, in most cases, insufficient for a reliable diagnosis. Some members of the Let-7 family, which work as inhibitors of cell growth, are down-regulated in different cancers, such as lung, breast and cervical cancers[31]. Similarly, miR-21, an apoptosis inhibitor, is found upregulated in glioblastoma, B-cell lymphoma and ovarian cancer, among others[32]. Consequently, the diagnostic, predictive and prognostic potential of miRNAs is most likely the determination of miRNA-signatures associated to a disease with which a patient miRNA profile can be compared[33]. A plethora of such signatures were described for both diagnostic[34, 35, 36] and prognostic applications[37, 38, 39]. The determination of disease signatures opens the way for diagnosis, which requires the quantification of multiple miRNAs in order to establish the miRNA profile of the patient. Such profiles can be determined either by running multiple single-plex detection reactions or a single multiplex reaction. In the case of parallel single-plex reactions, the sample is splitted in aliquots, one for each miRNA target. The required amount of sample thus increases proportionally to the number of miRNA targets, which is not the case of multiplexed detection methods. Alternatively, the sample can be diluted. Both of these strategies come at the cost of lowered sensitivity. Additionally, performing multiple single-plex assays in parallel significantly increases the workload, the cost and error risks. For all these reasons, the

Chapter 1. Introduction: Multiplex microRNA detection methods

development of multiplex techniques has drawn considerable research efforts.

1.2 Amplification techniques applied to miRNA detection

The detection of miRNA targets, present in concentrations within the 1-100 femtomolars (fM) range, requires a high sensitivity and accuracy. The amplification of the target sequence or of an intermediate molecule is in most cases mandatory to detect such diluted targets by conventional readout strategies, such as fluorescence. While the pool of DNA amplification chemistries comprises a plethora of techniques, most of them are not fitted for the amplification of short RNA sequences such as miRNAs.

Here we briefly describe conventional amplification methods and the developments that were made in an attempt to adapt these methods to the amplification of miRNAs and to increase the accuracy and the specificity of the quantification. For a more detailed overview of nucleic acids amplification techniques applied to miRNA detection, we refer the readers to a dedicated review from our group[40].

1.2.1 RT-qPCR

Of all miRNA detection techniques herein presented, RT-qPCR is undoubtedly considered as the gold-standard method. It allows for the detection of miRNA targets down to the attomolar (aM) range[41, 42] and displays single-nucleotide specificity[43] while being relatively low-cost. RT-qPCR also features a wide dynamic range, spanning up to 8 orders of magnitude.

Quantification of RNA molecules by RT-qPCR, in general, comprises two steps: (i) Reverse Transcriptase (RT) is first used to synthesize the complementary DNA (cDNA) of the RNA target. (ii) this cDNA is then amplified by PCR thanks to a thermostable DNA polymerase and a pair of primers. The amplification is monitored in real-time by fluorescence, using either a double-stranded DNA specific dye (e.g. SYBR Green I) or specific fluorescence probes (e.g. hydrolysis or molecular beacon probes) labeled with orthogonal dyes in the case of multiplex RT-qPCR (cf. 3.2.1)(Fig. 1.3b). The target is quantified by measuring the number of temperature cycles necessary to cross a fluorescence threshold (C_q) and comparing it to a standard range of samples of known concentrations.

Adapting qPCR to miRNA quantification requires some ingenuity. Indeed, RT-qPCR was initially developed to quantify long RNA sequences: typical PCR primers are approximately 20 bases long, which is the size of a full miRNA. This problem was solved by designing stem-loop[41] or linear[44] RT primers partially complementary to the miRNA (Fig. 1.3a, left) or by using the poly(A) polymerase (PAP)[42] (Fig. 1.3a, right). Although convenient,

this method may reduce the specificity and sensitivity of the assay[40]. This observation is however contradicted by a study by Mestdagh *et al.*[45], where the authors systematically analysed seven RT-qPCR kits. They show that minimal cross-reactivity is obtained using the polyA strategy, in combination with LNA-modified universal RT primer. Another limitation of miRNA RT-qPCR is that the interval of melting temperatures (T_m) of the miRNA-specific primer/miRNA duplex is rather large due to the heterogeneous GC content of miRNAs. According to Benes *et al.*, the sensitivity is reduced if the T_m is below 55°C, which can be the case for GC-poor miRNA sequences[46]. Moreover, the RT step efficiency can also depend on the miRNA sequence or structure, which has been shown to introduce biases in the transcribed cDNA library[47, 48].

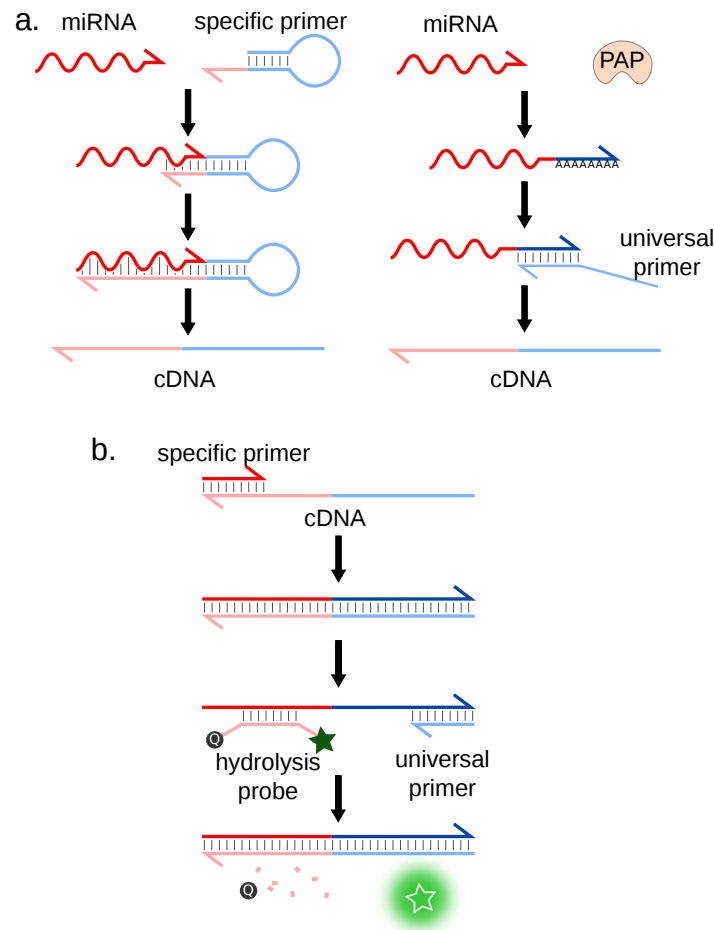


Figure 1.3: Principle of RT-qPCR. (a) Reverse-transcription strategies. Left: The miRNA is reverse-transcribed using a miRNA-specific hairpin-shaped primer that partially hybridizes to the miRNA 3' end. Right: The 3' ends of all miRNAs are extended using the poly(A) polymerase (PAP). This allows the reverse transcription of all miRNAs using a universal primer. (b) The produced complementary DNA (cDNA) strands are quantified by qPCR, using a miRNA-specific and an universal primer.

RT-related biases can be reduced by using two-tailed primers[49], or by replacing the RT by a miRNA-induced ligation step[50, 51]. The ligated oligonucleotide is the cDNA strand that will be then quantified by qPCR. This ligation step is however also most likely prone to sequence-specific biases, as shown in the context of library preparation for small RNA sequencing[52]. Two-tailed primers and ligation-mediated qPCR also increase the specificity of the detection[49, 53]. In the case of ligation-mediated qPCR, the choice of the ligase is especially important to specificity. Jin and coworkers demonstrated a detection of several members of the let-7 family with excellent specificity by using the SplintR ligase instead of the commonly used T4 ligase[53]. This strategy has also been adapted to recombinase polymerase amplification (RPA)[54].

As it was already mentioned, qPCR-based measurement only provides a relative quantification of the sample with respect to a calibration curve established from standard samples, which may introduce quantification biases (e.g. due to the presence of PCR inhibitors in the sample).

1.2.2 Rolling Circle Amplification

Rolling circle amplification (RCA) was originally designed by Kool’s group as a method for the linear amplification of single-stranded RNA[55] or DNA[56]. The amplification uses circular single-stranded DNA as a template. Once a forward primer (P1, the miRNA in this case) hybridizes to the circular template, it is elongated by a DNA polymerase. The polymerase progresses around the circular template multiple times, producing a long concatemer composed of numerous copies of the sequence complementary to the template (Fig. 1.4).

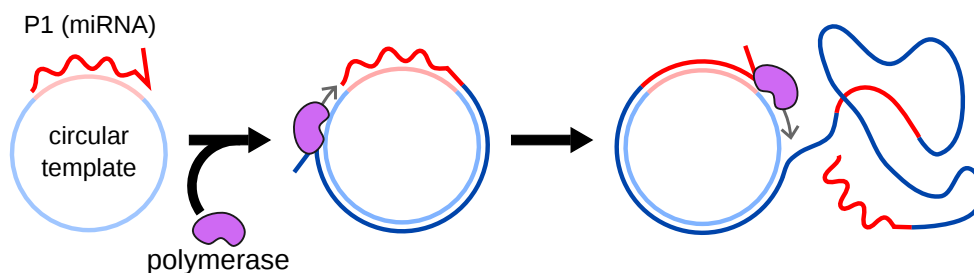


Figure 1.4: Principle of RCA. The miRNA hybridizes to a circular DNA template, and acts as a primer for elongation by a DNA polymerase. The polymerase keeps progressing around the circular template, producing a long DNA strand composed of repeats of the same sequence. Amplification is reported by the hybridization of fluorescent probes complementary to the repeat sequence.

RCA was first applied to miRNA detection by Jonstrup *et al.*[57]. The sensitivity of the method was low, due to its northern blot readout. Interestingly, the assay relied on linear

detection probes that were circularized by ligation upon miRNA hybridization, therefore increasing specificity. The use of SplintR ligase[58, 59], dumbbell probes[60] or graphene-oxide nanosheets[61] further improved detection specificity. The sensitivity of RCA-based detection can be enhanced by adding additional primers, turning the concatemer into a template for further amplification[62]. RCA can also be modified to be an exponential amplification method by integrating nicking enzyme recognition sites to the template sequence, as demonstrated for miRNA detection by Liu *et al.*[63].

1.2.3 Exponential Amplification Reaction

Exponential amplification reaction (EXPAR) was designed by Galas and coworkers as an alternative to PCR[64, 65]. EXPAR allows the amplification of a nucleic acid sequence using a DNA template, a DNA polymerase and a nicking enzyme[66] (Fig. 1.5). The DNA template is composed of two miRNA-complementary sequences separated by a nicking enzyme recognition site. Upon hybridization, the miRNA is used as a primer for elongation. The nicking enzyme then recognizes its specific site, and cleaves only the miRNA-containing strand, releasing a DNA analog of the miRNA. This DNA strand can in turn hybridize to a probe and generate more miRNA analogs. The miRNA sequence is therefore exponentially amplified.

While being an efficient signal-amplification method (10^6 to 10^9 -fold amplification)[67], EXPAR is however prone to unspecific amplification, which limits its sensitivity[68, 69]. This problem has been solved by Montagne and coworkers by introducing an additional template (referred as pseudotemplate) that drives the deactivation of unspecifically produced triggers[70], allowing accurate miRNA quantification using a digital readout (see section 3.2.3)[71]. Additionally, the specificity of the assay by Jia's group within the Let7 family was rather low: The chemical network designed for Let7-a detection was triggered almost simultaneously by Let7-a and Let7-e. Several groups adapted the original EXPAR design in order to improve the specificity, such as using dumbbell or hairpin-shaped probes[72, 73].

1.2.4 Duplex-specific Nuclease Signal Amplification

Duplex-Specific Nuclease Signal Amplification (DSNSA) is commonly used for multiplex miRNA detection. Originally isolated from the Kamchatka crab[74], the duplex-specific nuclease (DSN) was first characterized as an exonuclease that specifically degrades double-stranded DNA. Anisimova *et al.* later demonstrated that in the presence of DNA:RNA duplexes, DSN specifically degrades the DNA strand, leaving the RNA strand untouched[75]. Based on this property, Yin *et al.* first applied DSN for the simultaneous detection of 3

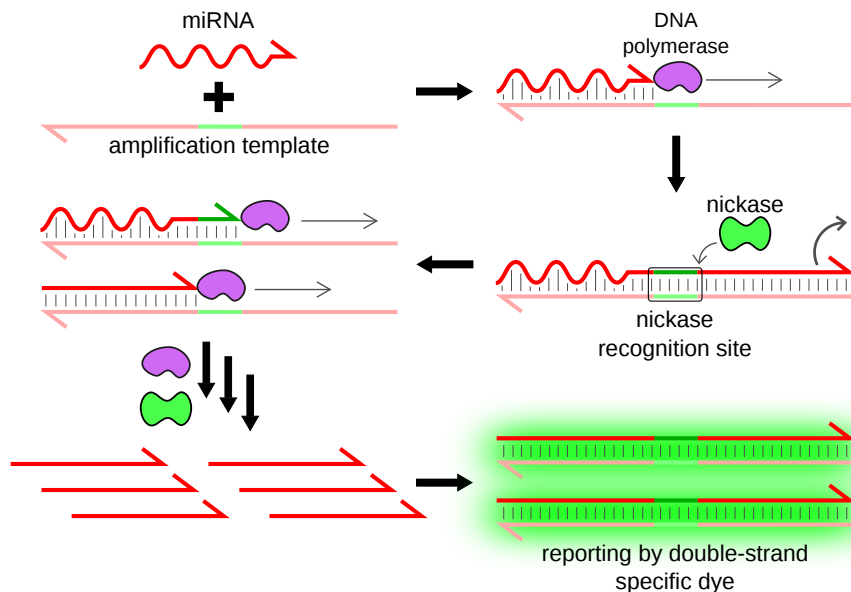


Figure 1.5: Principle of EXPAR. The miRNA is captured by a DNA template composed of two miRNA-complementary sequences separated by a nicking enzyme recognition site. Binding of the miRNA initiates the production of multiple DNA analogs of the miRNA following polymerization/nicking cycles. The produced miRNA analogs are released in the solution and can in turn initiate the production of more analogs, resulting in exponential amplification.

miRNAs with sub-pM sensitivity[76]. The assay was based on the hybridization of hydrolysis DNA probes on the miRNA, thus forming a DNA:RNA duplex. The hydrolysis probe was preferentially degraded by DSN, and the unaffected miRNA was free to hybridize to another probe, resulting in linear signal amplification (Fig. 1.6). The sensitivity of the assay was improved using different reporter probes, such as molecular beacons[77] or G-quadruplex specific probes[78]. Alternatively to DSN, CRISPR-associated nucleases (Cas)[79] or T7 exonuclease[80] were successfully applied to similar methods for miRNA detection.

1.2.5 Enzyme-free amplification techniques

Contrary to most other amplification methods presented herein, hybridization chain reaction (HCR) and catalyzed hairpin amplification (CHA) are enzyme-free amplification techniques. First described by Dirks and Pierce[81, 82], HCR only uses two short DNA hairpins (H1 and H2) and a single-stranded initiator hairpin (Fig. 1.7). The loop region of the initiator hybridizes to the target. The 5' and 3' ends of the initiator become available and hybridize to H1, opening it in the process. The part of H1 that remains single-stranded is complementary to H2, which in turn opens and binds H1, resulting in the sequential concatemerization of

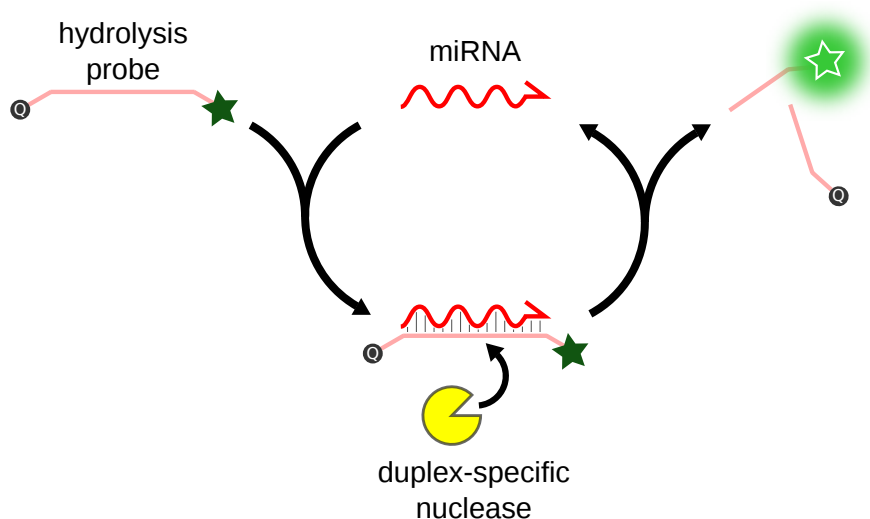


Figure 1.6: Principle of DSN. Hybridization of the miRNA to a complementary DNA hydrolysis probe forms a RNA/DNA duplex. The duplex-specific nuclease recognizes the duplex and selectively degrades the probe, producing fluorescence. The miRNA remains untouched and is free to bind to another hydrolysis probe, triggering its degradation.

H1 and H2. The amplification can be monitored by fluorescence using molecular beacons as H1 and H2[83] or thanks to an intercalating dye[84]. This technique was applied by Pierce's team for the detection of mRNAs[83, 85] and miRNAs[86], with a limit of detection (LOD) of 25 attomoles (amol).

Developed by the same team, CHA also relies on toehold-mediated strand displacement[87]. The nucleic acid target triggers the opening of a first hairpin by hybridizing in the stem region. The target is then displaced by the binding of a second hairpin, and is thus recycled in the process. CHA can be coupled to various readout strategies, and provides an amplification ratio of around 100-fold[87, 88, 89, 90].

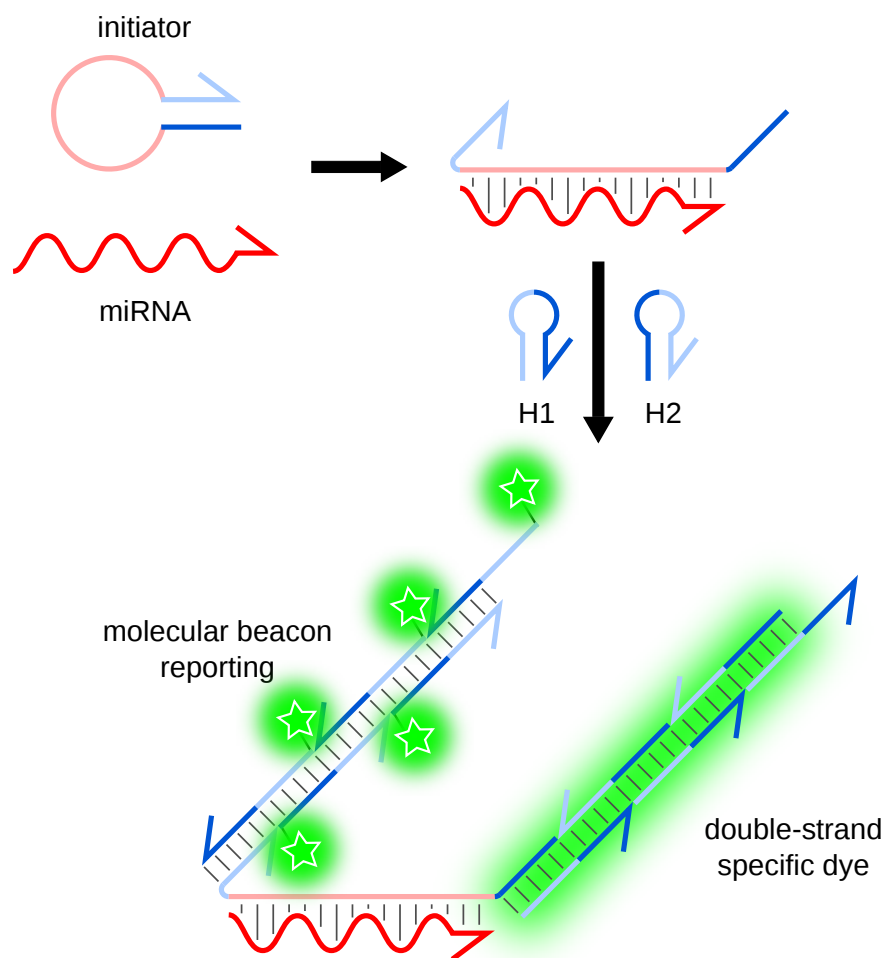


Figure 1.7: Principle of HCR. The hybridization of the miRNA to the initiator strand triggers sequential concatenation of hairpins H1 and H2, forming long regions of double-stranded DNA. The amplification can be reported by a double-strand specific dye or by using molecular beacons as H1 and H2.

1.3 Multiplexed miRNA detection

1.3.1 Separation techniques

1.3.1.1 Northern Blot and size-separation gel-based techniques

Northern blotting (NB) is a well-established miRNA detection method, for example involved in the first identification of a miRNA[1]. In this method, cells RNA extracts first undergo a size-separation step on a denaturing polyacrylamide gel (Fig. 1.9). Separated RNAs are then fixed on a membrane, on which sequences of interest are labeled by hybridization of complementary DNA probes. Historically radiolabeled with ^{32}P , these probes are now more commonly labeled using fluorescent or chemiluminescent dyes.

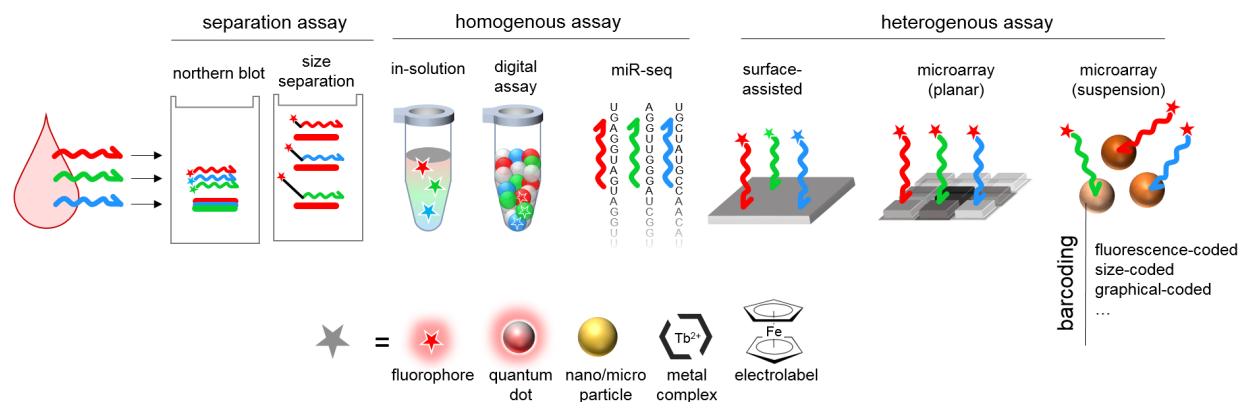


Figure 1.8: Schematic representation of the approaches to multiplex miRNA detection presented in this chapter.

Although it has been described as robust and reliable, NB is a cumbersome and time-consuming technique. Since gel electrophoresis cannot distinguish different sequences of the same molecular weight, as is the case for miRNAs, specificity relies only on probe hybridization, resulting in rather poor specificity and sensitivity. Both sensitivity and specificity can be improved by using Locked Nucleic Acid (LNA)-modified probes[91]. Additionally, target quantitation is only relative and lacks accuracy[92].

NB can be implemented into a multiplex miRNA detection method using color-coded detection probes, as was demonstrated by Schwarzkopf *et al.*[86]. Interestingly, NB was in this work coupled to HCR amplification in order to improve sensitivity (100 amol). This multiplexing strategy is however limited by the availability of spectrally-resolved fluorescent probes.

In spite of the narrow size distribution of miRNAs, size-separation can be useful for multiplex miRNA detection by using the miRNAs to generate size-coded molecules. For example, Arefian *et al.* used miRNAs as a scaffold for the ligation of 2 miRNA-specific DNA sequences, one of which is of different length depending on the target miRNA[93]. The method allowed the simultaneous detection of 9 miRNAs of the Let-7 family, also showing great specificity, but rather low sensitivity (1 pM). Chandrasekaran and coworkers proposed another method, based on agarose gel separation[94]. This assay allows miRNA detection using only a double-stranded DNA probe with two miRNA-specific overhangs. The presence of the miRNA brings the 2 overhangs together, forcing the double-stranded DNA probe to form a loop. In this method, the barcoding strategy is only based on the distance between the two overhangs, which defines the size of the loop once the miRNA is captured and allows electrophoresis separation. The authors demonstrated multiplexing for up to five targets as well as single-nucleotide specificity, with a LOD around 100 fM.

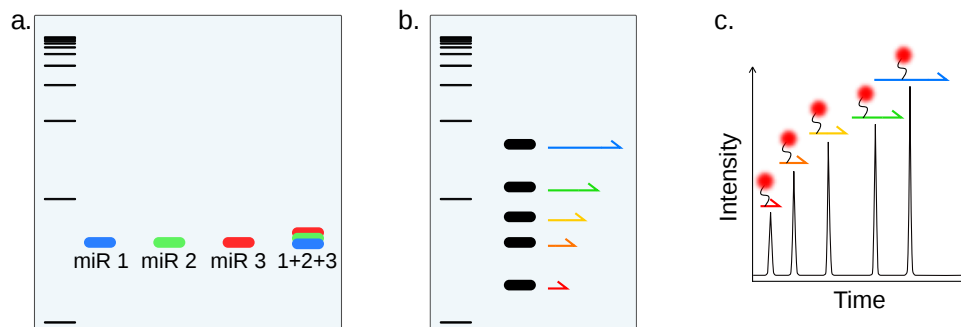


Figure 1.9: Multiplex miRNA detection strategies based on separation techniques. Since the size distribution of miRNAs is very narrow, miRNAs can not be directly separated based on size. Multiplex detection is however possible by using miRNA-specific detection probes (a), or by using the miRNA to generate size-coded DNA molecules that can be separated on slab gels (b) or by capillary electrophoresis (c).

1.3.1.2 Capillary electrophoresis

Also a size-based separation technique, capillary gel electrophoresis monitors the time needed for a molecule migrating in a gel-filled capillary to reach a detector (Fig. 1.9c). As for aforementioned slab gel techniques, multiple miRNAs can be indirectly detected by generating miRNA-specific size coded molecules. Jiang *et al.* demonstrated an amplification-free method based on the hybridization of target miRNAs to a capture probes presenting a poly(A) tail of different lengths, allowing separation based on the molecular weight of the duplex[95]. An amplification step, such as PCR[96], DSNSA[97] or EXPAR[98] can be added prior to separation to improve sensitivity. In terms of multiplexing, Na *et al.* managed to detect up to 8 miRNAs simultaneously using conformation-sensitive separation (single strand conformation polymorphism, CE-SSCP)[98], demonstrating the multiplexing potential of these methods. High-performance liquid chromatography (HPLC) was also used in a similar assay coupled to DSNSA, displaying sub-fM sensitivity[99].

1.3.2 Homogeneous multiplex detection

Most conventional miRNA detection methods are fully realized in solution, such as RT-qPCR, EXPAR or RCA. Such techniques are therefore named homogeneous methods.

1.3.2.1 Multiplex RT-qPCR

One of the biggest RT-qPCR limitations lies in its multiplexing ability. The reverse transcription step can be performed simultaneously for all target miRNAs by using any of the RT strategies presented in section 2.1, but the qPCR, however, can only be performed on

a few miRNAs simultaneously. This is due to fluorescence emission spectra overlap that limits the number of fluorescence colors simultaneously distinguishable. In the best cases, multiplex qPCR is limited to six colors. Noteworthy, a 15-plex qPCR detection of 16S RNAs was performed by using different combinations of two spectrally distinct fluorophores out of six to identify bacterial species[100]. This strategy is not adapted however to the profiling of multiple RNA species present in the same sample, as multiple combinations of targets would generate the same signal, leading to a degeneracy issue. This problem can be solved mathematically by adjusting the probes concentrations so that the output signal corresponds only to one possible input combination[101]. To our knowledge, this strategy has not been implemented to increase the multiplexing capabilities of RT-qPCR in miRNA quantification. In addition, multiplying the number of primers increases the risk of primer dimer reaction and thus, requires careful design and tuning of the experimental conditions to guarantee specific amplification of all targets.

To circumvent this specificity issue, qPCR mix is typically diluted after one-pot reverse transcription, and distributed in 96- or 384-well plates, each well containing different miRNA-specific primers as well as universal primers and fluorescent probes[102].

1.3.2.2 Isothermal multiplex homogeneous assays

Fluorescence is the most common readout for in-solution detection assays, but spectral overlap therefore limits their multiplexing capabilities.

Hildebrandt's group developed several amplification-free multiplex detection methods in solution, using either fluorescent dyes[103] or quantum dots (QD)[104, 105]. These methods use the miRNA to bring FRET donor and acceptor within close proximity either by ligation or base stacking. Interestingly, they reported the simultaneous detection of two miRNAs using a single FRET pair (terbium complex / QD), whose photoluminescence is tuned by the distance between the donor and the acceptor, reaching sub-nanomolar sensitivity. By coupling this temporal multiplexing with enzyme-free amplification, the same team reported a gain in sensitivity of three orders of magnitude[106, 107]. More recently, they combined spectral and temporal multiplexing to detect four DNA analogues of miRNAs with RCA[108]. Quantum dots were also used by Ye *et al.* in a 4-plex microfluidics-based assay[109]. RCA was also used by Wang *et al.* in a 3-plex assay displaying a LOD of 90 fM[110].

Interestingly, the chromogenic cationic polymer poly[(9,9-bis(60-N,N,N-trimethylammonium)-hexyl)-fluorenylene phenylene dibromide] (PFP) has been used as a universal FRET donor, allowing the detection of three miRNAs, combined with orthogonal fluorescent probes and DNase-based amplification[111].

Color-coded fluorescent reporters were also widely applied to amplified homogeneous de-

tection methods, such as the first DSN SA miRNA multiplex detection by Yin and coworkers[76]. The LOD of the method (100 fM) was indeed improved compared to amplification-free techniques. Other DSN-based fluorescent methods were since then reported, most notably Xiao’s 3-plex assay, using fluorescent probes embedded in MoS₂ nanosheets to improve specificity[112, 80, 113].

1.3.2.3 Fluorescence-based digital methods

Fluorescence intensity level encoding is a possible way to perform multiplex detection past the “one target per color” barrier. In previously described fluorescence-based methods, however, signal intensity (referring either to an amplification time or a luminescent intensity) was used to compute the miRNA concentration. Additionally, these methods only provide relative quantification of their target requiring assay calibration with standard samples. Digital readout refers to methods where the absolute target concentration is directly computed from a ratio of positive (target-containing) and negative (empty) partitions, following the poissonian distribution of target molecules throughout these partitions. Digital PCR (dPCR) is undoubtedly the most widespread method for digital nucleic acid quantification. This method relies on the partitioning of the sample into microchambers[114] or microdroplets[115] (the latter referred as droplet digital PCR, ddPCR) thanks to microfluidics, in such a way that every partition contains either zero, one or a few cDNA or RNA molecules, according to the Poisson distribution. The RT step can either be performed before or after sample partitioning. Following thermocycling, the partitions are analyzed by imaging or in-line fluorescence readout. Absolute quantification of the cDNAs is achieved by counting the fluorescence-emitting (i.e. cDNA-containing) partitions and assuming the cDNA repartition followed a Poisson distribution. This quantification mode does not rely on fluorescence intensity, which is thus available for multiplexing. Introducing different probe concentrations, several groups managed to break the one target per color barrier for the detection of DNA molecules[116].

Our group recently reported a multiplex isothermal amplification method using orthogonal EXPAR-like designs[117]. By solving the problem of cross-reactivity often observed in one-pot multiplex reactions, they demonstrated a 3-plex assay using a droplet digital readout.

Smith *et al.* recently reported an ingenious use of RCA for single-molecule miRNA detection[118]. Following one-pot multiplex RCA, RCA products are labelled with probes tagged with different fluorophores, which allows miRNA indexation. They achieved as a proof of concept a duplex miRNA detection with sub-pM sensitivity. The analysis was performed by single-molecule flow cytometry, as DNA molecules produced by RCA were large enough (48 kb) to be detected using conventional instruments. Although the authors only demonstrated a duplex detection as their proof of concept, it is clear that the barcoding capacity can reach

hundreds or even thousands of combinations. The sensitivity of the assay, however, still needs to be improved to match the requirements of miRNA profiling in biological samples. This may be caused by non-specific initiation of RCA, which could be reduced by using padlock probes[119]. Hu and coworkers however reported a similar method using padlock probes displaying similar sensitivity (1 pM)[120]. One can note the development of a similar strategy applied to multiplex nucleic acid detection, combined with a microfluidic-driven enrichment step to improve the sensitivity[121].

1.3.2.4 Next Generation Sequencing

Next Generation Sequencing (NGS) is an emerging technology for miRNA profiling. In order to perform RNA sequencing (RNA seq), the RNAs of the sample first need to be extracted and purified. After purification, universal adapters are ligated, typically to the 5' and 3' ends of each RNA strand (alternatively, a single adapter can be ligated to the 3' end followed by circularization of the product[122]). A reverse-transcription step is then performed, followed by a PCR amplification and finally, sequencing.

NGS historically allowed the discovery of a plethora of miRNAs[123], as NGS instruments are able to read millions to billions of sequences in a few days. This very high throughput is one of the advantages of NGS, and is extremely important for miRNA profiling. NGS is indeed the miRNA detection method that displays the highest multiplexing ability, since all RNAs in the sample can theoretically be detected, thanks to the use of universal RT and PCR primers[124]. RNA seq thus requires no prior information or specified target sequence. This ability makes RNA seq unique among miRNA detection methods, because most other techniques require the design of specific primers and/or probes for each targeted miRNA, which reduces the spectrum of the analysis. The specificity of NGS miRNA detection depends on the error rate of the sequencing platforms, which is typically around 1-10 errors for 1,000 bases called[125]. Since miRNAs are around 20 bases long, NGS is very accurate for the differentiation of miRNAs, even highly homologous sequences.

While it displays undeniable advantages, NGS still suffers from several flaws. Owing to its lack of sensitivity, sequencing analysis always requires a pre-amplification step traditionally achieved by RT-qPCR (which also converts the RNA sequence into DNA material readable by DNA sequencing). The reverse-transcription and PCR steps can generate sequence-dependent biases[126, 127], making this technique poorly quantitative. Additionally, rare sequences are often dropped out because of abundant RNAs drawing most of the reads, thus reducing the sensitivity. NGS equipments are still very expensive, which makes, so far, routine diagnosis impossible. Each analysis provides a great amount of useful information, the extraction of which requires time and skilled bioinformaticians.

In spite of its drawbacks, comprehensive miRNA analysis by NGS is progressively becoming a benchmark to identified disease-linked miRNA signatures[128, 129]. Coenen-Stass *et al.*, for example, reported a dysregulated miRNA profile for the diagnosis of Duchenne muscular dystrophy using NGS[130].

1.3.3 Heterogeneous multiplex detection

1.3.3.1 On-sensor methods

Several readout strategies require a surface to be performed, forbidding their use in fully in-solution - homogeneous - format. On-sensors methods refer to the use of a surface for performing the readout, coupled to orthogonal signals for multiplexing (as opposed to microarrays that use universal reporting for all targets, combined with spatial indexation, see section 3.3.3.1). That is the case for electrochemical readout, since electrodes are needed to measure the intensity in the solution.

This method has been applied to multiplex miRNA detection in a planar format by Yuan's group. The team first coupled electrochemical readout to DSNSA, achieving detection limits of a few fM[131]. The sensitivity was further improved to reach a LOD around 50 aM by designing a DNA bot triggering the degradation of electrochemical labels upon miRNA capture[132]. The group so far demonstrated the simultaneous detection of two targets using methylene blue and ferrocene as electrochemical labels. Xu and coworkers reported a LOD of 20 aM for a similar assay relying on a DNA framework changing conformation upon miRNA capture[133].

Similar designs were developed in suspension, using the target miRNA to modify the distance between a magnetic microparticle and a miRNA-specific electrochemical label[134, 135, 136]. To our knowledge, all of the so far reported electrochemical on-particle methods demonstrated a duplex miRNA detection. The most sensitive of those methods reported a limit of detection around 1 fM[135].

In all aforementioned electrochemical assays, each target is quantified using a different electrochemical label. As for fluorescence-based homogeneous assays, the multiplex ability of this method is limited by the number of electrochemical dyes simultaneously distinguishable by square wave voltammetry. Alternatively, mass spectrometry has demonstrated a high multiplexing potential using dozens of orthogonal metal isotopes[137]. Such readout was for example combined with lanthanide-tagged recognition probes and DSNSA in a triplex assay[138].

Surface-enhanced Raman scattering (SERS) is a powerful technique allowing the enhancement of Raman light scattering signals by up to 11 orders of magnitude[139]. The method

requires the interaction of two surfaces brought within close proximity to amplify the signal, and is therefore a heterogeneous-only detection method. SERS can for example be applied to sandwich assays using Raman-barcoded particles[140, 141]. Su *et al.* designed SERS "nano-mushrooms"[140], composed of a gold core linked to a silver cap by DNA spacers. The gap between the gold and silver surfaces forms a signal-enhancing "hotspot", in which Raman labels are inserted. The gold core of the mushroom is coupled to DNA probes specific to one miRNA target, and are accordingly barcoded by inserting different Raman dyes in the hotspot. In this assay, the miRNA forms a bridge between a magnetic microparticle and its specific SERS nano-mushroom. After hybridization, the microparticles are recovered and each target is quantified by measuring the intensity of the corresponding Raman signals. The authors demonstrated a 3-plex assay with a 1 pM detection limit. Zhou and coworkers increased the sensitivity by a 100-fold by using gold-Raman Nanobridge Nanogap Probes (Au-RNNP)[141]. Instead of a sandwich detection, Wang *et al.* designed the "Inverse Molecular Sentinel" (IMS) assay[142]. They used gold particles specifically engineered for signal enhancement, called Nanostars. Raman-labeled hairpins were immobilized on the particles. In the absence of the miRNA, the hairpins are opened and partially hybridized to the miRNA capture probe. The miRNA is perfectly complementary to its capture probe and can hybridize to it, strand-displacing the hairpin in the process. The hairpin then closes, bringing the Raman dye close to the SERS-inducing tips of the Nanostar particle, which amplifies the Raman signal of the dye. This technique enabled the duplex detection of miRNAs from total RNA cell extracts.

While most of the herein presented SERS-based assays rely on the use of Raman dyes, Sim's group developed a label-free miRNA detection method, able to recognize the Raman signature of the miRNA directly[143]. Although the label-free approach reduced the sensitivity (5 fM) compared to other assays from the same group (section 3.3.3, planar microarrays), the multiplexing potential of the method appears promising.

1.3.3.2 Nanostring

The NanoString nCounter system is an emerging technology for multiplexed miRNA detection. It was originally developed for gene expression monitoring by quantifying messenger RNAs[144, 145, 146] and adapted for miRNA detection[147, 148]. This system allows single-molecule detection using a microarray-inspired principle. As for a classical microarray, the miRNA hybridizes to a capture probe and a detection probe (Fig. 1.10). The capture probe, 35 to 50 base-long and coupled to biotin on its 3' end, binds the 5' half of the miRNA. The detection probe is composed of a 3' end complementary to the miRNA and a chain of fluorescently labeled RNA sequences, forming a fluorescent barcode associated with the target

Digital and multiplex miRNA detection for molecular diagnostics

miRNA. After hybridization of both probes, the complex is immobilized on a surface thanks to the biotin tag on the capture probe, and fluorescence imaging is performed. Analysis consists simply in counting fluorescent barcodes, each of them indicating the capture of one miRNA molecule.

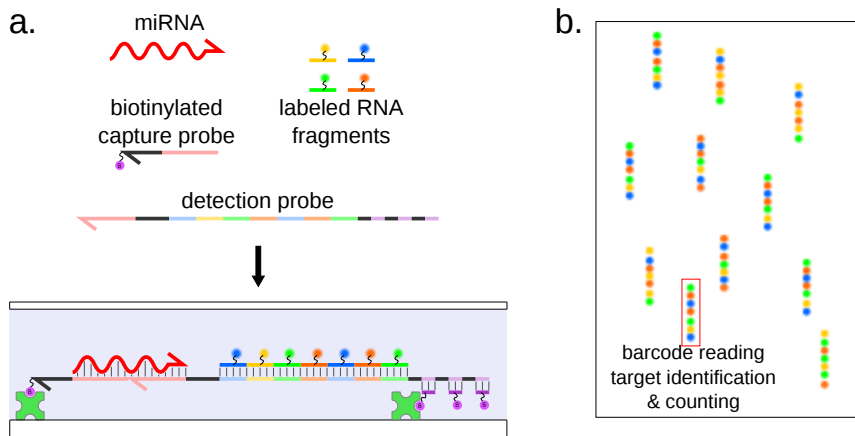


Figure 1.10: Principle of the Nanostring nCounter system. (a) The miRNA bridges between biotinylated capture probe, allowing immobilization on a glass slide, and a detection probe carrying a combination of fluorescent labels allowing identification of the target miRNA. (b) The immobilized sets of labels are counted, each one of them reporting the capture of a single miRNA molecule.

This single-molecule approach grants the nCounter system with great sensitivity, in the sub-fM range[144], without requiring any amplification. This technology still displays some limitations in terms of specificity and assay duration[148, 45].

The multiplexing ability of the nCounter system lies in the fluorescently barcoded RNA fragments on the reporter probe. They are prepared separately by incorporating amino-allyl-modified UTPs during transcription of the fragments and coupling the modified uracil residues to four different dyes[144]. The reporter probe is then assembled from a template by ligating seven fluorescent RNA fragments and the miRNA-specific 5' end together. This strategy of seven fluorescent RNAs, with four possible colors for each of them, allows more than 15,000 possible combinations. Taking into account that two consecutive fragments must be of different colors, the number of combinations is still 2916, while only 2654 miRNA sequences are referenced for *Homo Sapiens* in miRbase[149]. In practice, Nanostring proposes detection panels of up to 800 human miRNAs. This effective barcoding strategy places this technology among the highest multiplexing methods, in the same range as density-based microarrays, while supposedly outperforming them in terms of sensitivity and sample requirement thanks to single-molecule counting[144]. This observation is however contradicted by a study by Mestdagh *et al.*[45], where the authors benchmarked 3 microarray platforms

(including Agilent, Affimetric and Nanostring) and concluded that the nCounter system did not display higher sensitivity and was even poorly performing with low-input amount of RNA. The nCounter system was recently used to screen for possible cancer miRNA signatures, for example in breast[150] and ovarian[151] cancers.

1.3.3.3 Microarrays

Microarrays are detection methods enabling multiplexing by spatially separating the specific receptors of each target. These methods can be divided into two main categories: Planar arrays and suspension (i.e. on-particle) arrays. In suspension arrays, each particle is coupled to capture probes for a single analyte and is given a corresponding “barcode”, indicating what is the target of the particle. Given the diversity of available particles, various barcoding strategies were implemented, such as size, graphical and most commonly fluorescence encoding. Planar arrays, or flat-arrays, use spatial separation as a multiplexing strategy: Specific capture probes are spotted on a flat surface, each spot targeting a different analyte. Both approaches display interesting characteristics, especially in terms of multiplexing.

Planar microarrays Planar arrays are composed of high-density spots of DNA probes immobilized on a flat glass or polymer support[152] (Fig. 1.11). These probes can capture one specific target by Watson-Crick base-pairing. Each spot comprises only one kind of DNA capture probes, and can therefore in theory only capture one kind of target. The sample is flown on the support, and every target sequence is captured on its specific probe spot. Multiple targets can thus be simultaneously quantified by measuring the signal on each spot. The spatial target separation allows microarrays to detect up to hundreds to thousands of nucleic acid sequences simultaneously [Yin, 2008]. Thanks to this excellent multiplexing ability, microarrays are often used for miRNA screening assays, leading for example to the identification of disease miRNA signatures[153, 154].

Most conventional microarrays require the enrichment and labelling of potential targets prior to hybridization. In the case of miRNAs, the enrichment step consists in the separation of short RNAs (usually under 200 nt) from total RNA. All short RNAs are then labelled, typically using radioactive or fluorescent labels[155]. The labelling can be performed either directly on the RNA strands, by ligating a fluorescent dye[156, 157] or a biotin residue[158] to one of the miRNA ends, or indirectly following a reverse-transcription step[159] and possibly a PCR amplification[160, 161].

Despite being high-throughput and highly multiplexed, classic miRNAs microarrays display a relatively low sensitivity, with detection limits within the nanomolar range. Moreover, since the yield of labelling, enrichment and/or amplification steps often varies depending

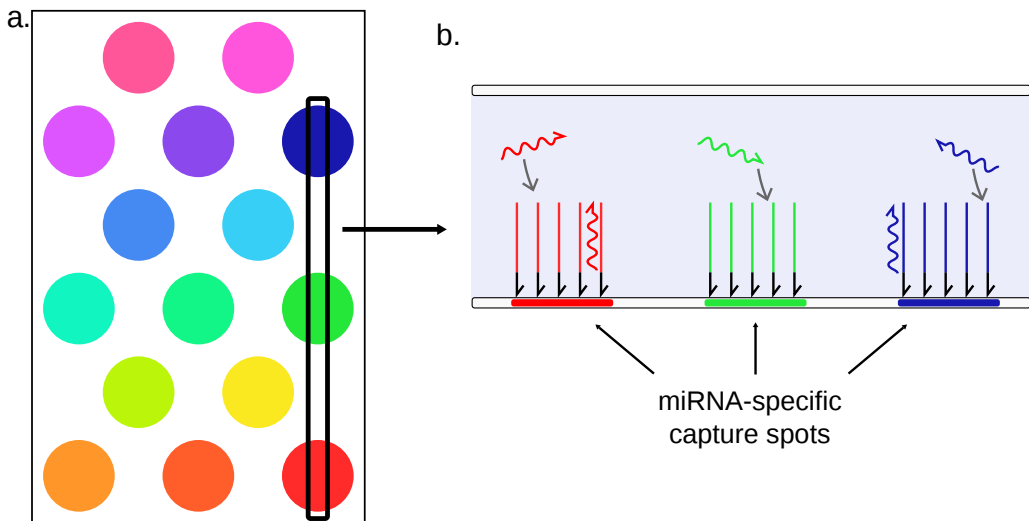


Figure 1.11: Principle of planar microarrays. (a) Capture probes are immobilized on a surface, forming separated spots. (b) Each spot is exclusively composed of capture probes for the same miRNA. Multiple readout strategies can be employed to quantify the miRNAs.

on the sequence, these steps can introduce quantification biases. The hybridization step is also prone to biases due to the variable miRNA hybridization thermodynamics[162]. The specificity of conventional microarrays is also relatively low towards highly homologous miRNAs, which requires long hybridization steps (up to several days). The implementation of LNA-modified[163] or stem-loop capture probes[164] is reported to improve the specificity.

The relatively low sensitivity of conventional microarrays is a critical issue for the detection of low-abundant miRNAs in real samples. In order to detect lower concentrations, two main options are available: Improving the sensitivity of the detector, or increasing the target concentration. In this section, we will focus on new detectors and readout strategies applied to the detection of miRNAs.

As was already presented, SERS is a very powerful surface-based signal amplification technique. Sim's group for example reported significant advances for SERS-based multiplex miRNA detection[165, 143]. The group designed a sensor composed of gold nanopillars, the tips of which are coupled to miRNA-specific DNA capture probes. The sensor allowed the sensitive detection of 3 miRNAs simultaneously, either by amplifying the Raman signal of the miRNA itself[143] or in a labeled sandwich assay format[165]. The assays are indeed more sensitive than conventional microarrays: The LOD of the direct detection method is a few fM, and the sandwich assay can even detect concentrations in the attomolar range, with a 9 orders of magnitude dynamic range. Liu *et al.* also designed a SERS-based microarray[166]. The method uses Raman-labeled nanoparticles that compete with miRNA to bind miRNA-specific capture probes coupled to the sensor. The concentration of target miRNA for each

spot is thus inversely related to the intensity of the Raman signal. Interestingly, the proof of concept assay was an 8-plex detection of the members of the Let7 family, showing the excellent specificity of the method. The LOD was around 100 fM, not as good as previously reported nanopillar-based methods.

Other reporting strategies for amplification-free miRNA sensing were developed, such as surface-plasmon resonance[167, 168], microring resonators[169], electrochemistry[170, 171] or gold nanoparticles aggregation[172]. None of these technologies have however surpassed SERS in terms of sensitivity.

The high multiplexing ability of microarrays can also be used to enhance the potential of conventional techniques, such as RT-qPCR[173, 174] or LAMP[175]. Choi *et al.* for example proposed an on-support version of RT-qPCR[173]. In this method, following the RT step, the cDNA mix is introduced in a microfluidic channel. Hydrogel microposts were formed in the middle of the microchannel. The microposts are photochemically coupled to miRNA-specific PCR primers, allowing each post to capture its specific cDNAs. Quantitative PCR is performed using a universal reverse primer in solution, and amplification is reported by SYBR Green I fluorescence. Although less sensitive than in-solution RT-qPCR, this assay displays increased multiplex potential, because the independent PCR amplifications are spatially separated, mitigating cross-reactivity issues. A similar assay using LAMP amplification coupled to an electrochemical readout was developed by Hashimoto and coworkers[175]. A 5-plex detection with a LOD in the 100 aM range was demonstrated. Alternatively, Ishihara *et al.* used a dendritic amplification step by flowing fluorescent streptavidin and biotinylated anti-streptavidin antibodies[176]. Instead of capturing the target and then amplifying the signal, the other approach is to perform an amplification in solution prior to capturing and labeling the amplified target. Mader *et al.* performed a 14-plex detection based on nucleic acids sequence-based amplification (NASBA) using this approach[177].

1.3.3.4 Suspension arrays

The fundamental difference between planar and suspension microarrays is the mobility of detection particles. Instead of being tethered on a surface, analyte receptors are therefore spread throughout the entire volume[178]. As both targets and capture probes diffuse in the sample, the analyte-receptor encounter probability is increased, resulting in faster capture kinetics. This feature is of crucial importance given the duration of hybridization protocols for planar microarrays (up to several days).

One of the main challenges for multiplexed detection is that several output signals not only need to be measured, but also attributed to the corresponding target. For homogeneous methods, target identification is mostly based on two strategies: The use of different fluo-

rescent reporters or the coupling to separative techniques. In the case of planar arrays, the indexation is encoded in spatially distinct spots. Barcoding designates the various indexation methods for suspension microarrays. Thanks to the diversity and versatility of particles and functionalization techniques, the field of suspension arrays offers a greater variety of barcoding strategies and shows excellent multiplexing potential.

Fluorescence As for homogeneous assays, fluorescence is the most common barcoding strategy for particle-based methods. In this case, it is however possible to surpass the typical limitation of six colors by encoding the particles with different intensities for a single fluorescent channel.

Fluorescently barcoded particles can be prepared using various techniques. The easiest of them is the functionalization of the surface of the particle with fluorescent oligonucleotides, either using affinity or covalent coupling[179]. Alternatively, dyes can be integrated to the core of the particle, in the form of dyes[180] or Quantum Dots (QD)[181, 182].

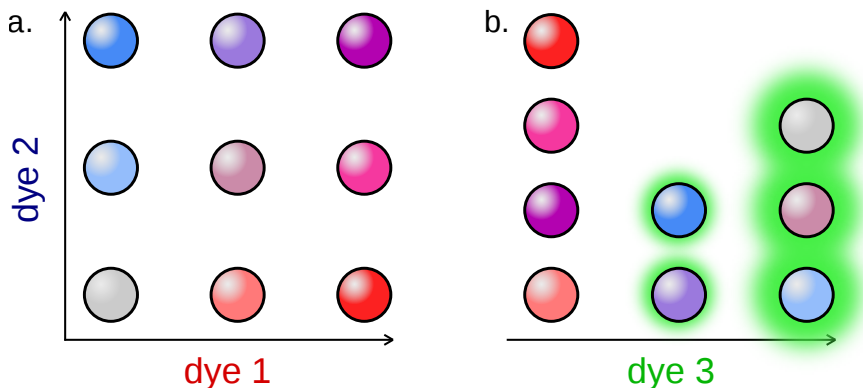


Figure 1.12: Example of fluorescent particle barcoding. (a) Fluorescent particle barcoding allows to overcome the "one color per target" barrier by combining intensity levels of fluorophores. In this example, using 2 dyes, each of which can be introduced in 3 distinct intensity levels, allows the barcoding of up to $3^2=9$ subpopulations. (b) Reporting is performed using an independent fluorescence channel, the intensity of which can be used to compute the miRNA concentration.

The Luminex xMAP system is a commercial set of more than 100 fluorescent microparticles subpopulations, widely used for multiplex detection assays. Li *et al.* applied this system for the amplification-free detection of 4 miRNAs in a single assay[183]. The technique displayed a relatively high detection limit (500 fM). Causa and coworkers notably reported another amplification-free 3-plex method using fluorescent hydrogel particles, displaying remarkable sensitivity for such assays, in the fM range[180]. A similar limit of detection was achieved by Tao's group[184]. Additionally, the authors managed to break the "one tar-

get per color” barrier by relying on particle colocalization for reporting: 6 miRNAs were simultaneously detected using only 4 fluorescent particles populations.

Fluorescent particles are also compatible with amplification techniques, such as DSNSA[182], strand-displacement amplification[105] or SIMOA detection. The single molecule array (SIMOA) is a suspension array designed by Quanterix corporation. This system allows the detection of analytes down to the single-molecule level thanks to microfluidics[185, 186]. Originally developed for the detection of proteins[185, 187, 188], the assay was later adapted to digital nucleic acid detection[189]. In this technology, microparticles are functionalized with miRNA-specific capture probes. The target miRNA is used to bridge the capture probe and a reporter oligonucleotide tagged with a beta-galactosidase. The particles are then isolated in individual wells carved on a microfluidic chip. The hydrolysis of a fluorogenic substrate by the beta-galactosidase reports the capture of the target in each well. Fluorescent imaging of the microfluidic chamber, followed by poissonian analysis allows the absolute quantification of the target. Cohen *et al.* reported a 3-plex digital detection of miRNAs using the SIMOA system[179]. The assay showed good sensitivity, as the limit of detection was approximately 10 fM. In order to improve the specificity of the multiplex detection, LNA capture probes were designed, which prevented any cross-reactivity between the three targets. The method was further validated by a comparison with gold-standard RT-qPCR, showing convincing results even from total RNA cell extracts.

Graphical barcoding Graphical barcoding consists in shaping or engraving visual patterns in order to differentiate beads subpopulations. This strategy allows for highly multiplexed assays, as the pool of potential symbols or patterns that can be encoded in the particles is only limited by patterning resolution[190]. Doyle’s group extensively used such encoded particles for multiplexed miRNA detection[191, 192, 193]. Their hydrogel particles are bar-coded by a set of five length-coded stripes, using stop-flow lithography. As there are three possible lengths for each stripe, there are $3^5=243$ possible combinations. The authors demonstrated the potential of these particles for miRNA detection in real samples, such as formalin-fixed paraffin-embedded tissue[192] or raw cell lysates[193]. The introduction of a RCA amplification step increased the sensitivity of the assay by a 100-fold[191]. The same group also designed polygon-shaped, easily recognizable particles for mobile phone readout[194]. Doyle’s group also designed digital patterns, with a set of 8 spots, each of them being in a 0 (No engraving) or 1 (Engraved) state, for a similar capacity (256 combinations)[195]. As a proof of concept, the authors demonstrated a multiplex assay where barcoded hydrogel particles targeting 3 different miRNAs are individually trapped in a microfluidic chamber prior to an enzymatic (β -galactosidase) signal amplification, achieving a 10 fM limit of de-

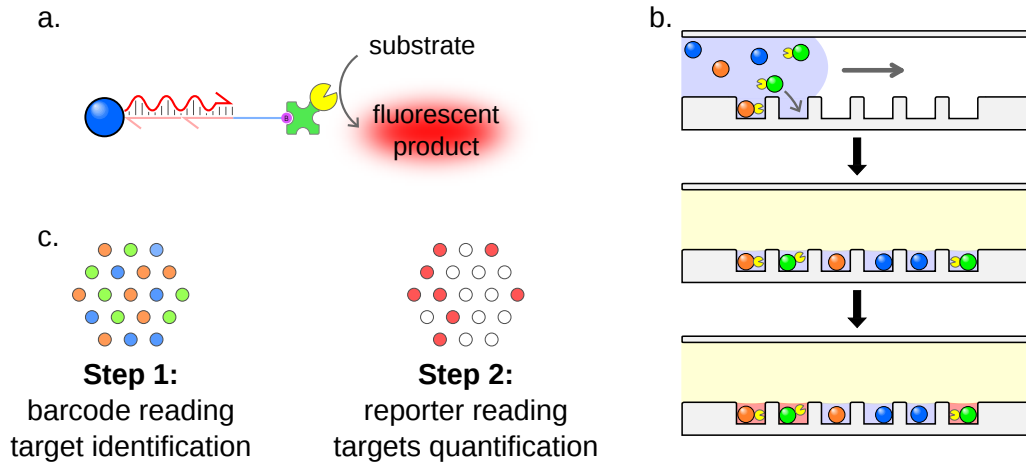


Figure 1.13: Principle of the SIMOA detection system. (a) The hybridization of the miRNA to its specific capture probes allows the capture of β -galactosidase on a barcoded microparticle. (b) Simplified workflow. After enzyme capture, particles are trapped in individual microwells and incubated. (c) Readout is performed in two steps. First, particle barcodes are read, enabling target identification. Then, reporter fluorescence is measured, indicating whether the targeted miRNA was captured or not. Since the capture of miRNAs by particles follows a Poisson distribution, absolute quantification of the target can be achieved by simply counting "ON" and "OFF" wells for each miRNA.

tection. A similar digital encoding was used by Liu on silica particles, reaching 128 possible sub-populations and demonstrating a duplex assay[196]. The experimental design included a RCA step to improve sensitivity, reaching 1 fM. Jung and co-workers reached an exceptional 3^{12} combinations with radially-encoded polyethylene glycol half-spheres, which they used in combination with qPCR-based detection method[190]. MiRNA specific primers are chemically grafted in the gel matrix, and the particles are graphically encoded by lithography. Following a common RT step, cDNAs are specifically captured by the immobilized primers, inside the pores of the corresponding particle. RT-qPCR is then performed using universal reverse primers in solution. After each cycle, the fluorescence of each particle is measured by microscopy. The method allowed to perform a 10-plex detection from purified extracellular vesicles. The sensitivity of the assay was significantly reduced (1 pM) compared to conventional RT-qPCR. The authors report that the specificity of this supported qPCR is superior to that of solution qPCR. In spite of this exceptional multiplexing ability, such techniques are neither as easy, nor as commonly used as fluorescence barcoding strategies, possibly because of the need for special equipment and expertise for generating the particles.

Photonic crystals A photonic band-gap crystal, or photonic crystal (PhC), is a spatially periodic structure composed of materials having different dielectric constants[197]. In such

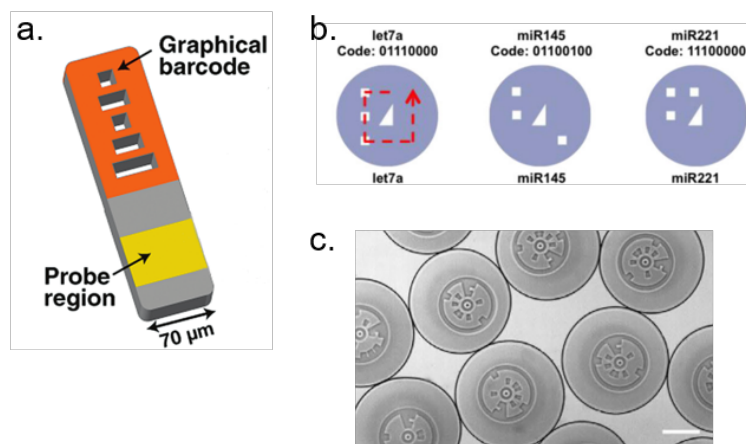


Figure 1.14: Examples of graphical particle barcoding. (a) Hydrogel particle encoded by 5 stripes of various lengths. Picture extracted from Chapin and Doyle[191]. (b) Example of digital encryption: Each particle presents 8 spots that can be engraved (1 state) or not (0 state). The central triangle is used for orientation. Picture from Kim *et al.*[195]. (c) Each particle carries a circular barcode divided in 16 angular sectors. Picture from Jung *et al.*[190].

structures, photons of a chosen wavelength can not propagate and are therefore reflected, whereas all other wavelengths are transmitted. The excluded wavelength, or bandgap, depends on dielectric constants of the materials and on the characteristics of the periodic lattice itself. The reflected wavelength range is thus highly tunable. The advantages of using photonic crystals as particle barcodes are numerous: PhCs are highly stable and are not affected by photobleaching. Being a fluorescence-free strategy, photonic crystal particles do not interfere with fluorescent reporting[198, 199, 200]. Contrary to fluorescence barcoding, photonic crystal particles can not be intensity-encoded. Moreover, the reflection spectra of PhCs are gaussian peaks with a typical half-height width of 25nm[199], which limits the number of simultaneously distinguishable populations, just like overlapping emission spectra do for fluorescence barcoding. The preparation of such particles is also a limitation, as it is very expertise-demanding. These drawbacks may explain why, in spite of their attractive qualities, PhC particles are still an uncommon barcoding strategy.

The use of PhC particles for multiplexed miRNA detection was demonstrated by Zhao's group, either coupled to RCA[199] or HCR[198, 200]. The highest sensitivity was obtained using a RCA step, with a LOD of 20 fM. All designs allowed the detection of up to 3 miRNAs simultaneously. Due to overlapping reflection spectra, the maximum multiplicity of PhCs appears to be 5 subpopulations.

Size encoding Particle size encoding is an easy way for subpopulations barcoding. Size-coded particles can simply be differentiated by microscopy, or flow cytometry by measuring

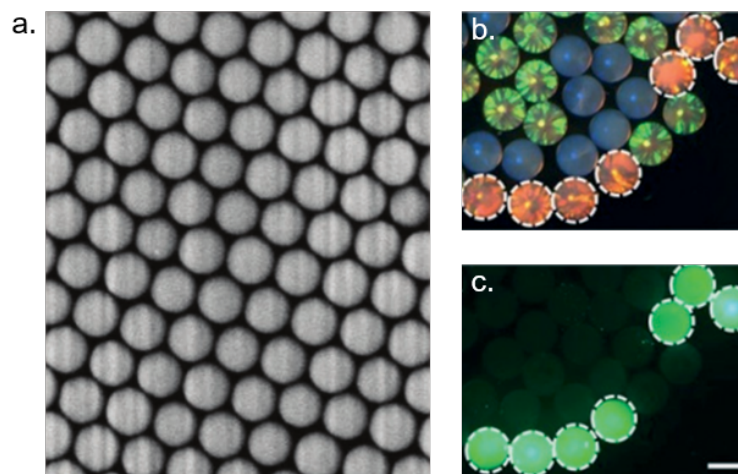


Figure 1.15: Photonic crystal particles. (a) Electron microscopy image of the surface of a photonic crystal particle. (b) Reflection images of photonic particles with blue, green and red structural colors. (c) Fluorescence image of the particles shown on (b). Green fluorescence intensity allows quantification of the corresponding target. White light reflection by the photonic crystal and fluorescence emission are completely independent. Pictures from Bian *et al.*[198].

particles forward light scattering (FSC)[201, 202]. Particles of different sizes but similar densities can also be distinguished based on their mass, using separative techniques such as field-flow fractionation (FFF)[203] or acoustic levitation[204]. Size-based barcoding is however a relatively uncommon strategy, mostly because of its low multiplexing potential, as none of the aforementioned techniques can detect subtle size variations. To our knowledge, the highest demonstrated multiplex miRNA detection using size-coded particles was a 4-plex assay by Wang *et al.*[202].

Although size coding may not be easily scalable, the main quality of this method is its compatibility with other barcoding strategies. The combination of fluorescent barcoding with an additional size-based encryption level appears as particularly promising: Both approaches can easily be combined, as affinity tag-coated particles of various sizes are widely available. Moreover, both particle size and fluorescence can be measured simultaneously by flow cytometry, which makes this multimodal strategy particularly convenient.

Other barcoding strategies Among the numerous suspension-based methods for multiplexed miRNA detection, Kim and coworkers proposed a unique barcoding strategy[205]. Their approach is based on three encryption levels: First, they used plasmonic nanoparticles as detection particles. The three different kinds of particles (gold-silver nanorods, gold nanospheres and silver nanospheres) had different light-scattering signatures (red, green and blue, respectively). The second unique feature of this work is kinetic encoding: The particles

were also discriminated based on their mobility. For each kind of plasmonic particles, half was functionalized with lipids that could interact with an immobile 2D lipid bilayer, hindering the mobility of the particle. The other half was left free in solution, creating a new dimension of barcoding composed of two levels (mobile and immobile). The third encryption level was linked to the reporting, as target detection was signaled by the colocalization of an immobilized particle with a mobile one. This method allowed for the detection of 9 miRNA targets using only six particle subpopulations. The sensitivity was rather low, however, since the LOD is around 10 pM.

1.3.4 Multiplex microRNA detection from live cells

Although most of the miRNA detection methods presented in this chapter aim at quantifying miRNAs in cell extracts or bodily fluids, some multiplex methods were also developed to detect miRNAs in live cells. The detection of miRNAs from live cells presents different challenges than detection from biofluids: The quantification method needs to be particularly robust to resist to the complex environment of the cell, while being perfectly biocompatible to avoid damaging it. Most of the reported methods rely on color-coded fluorescent probes quenched by nanoparticles[206, 207] or nanosheets[208, 209, 210, 211]. Zhou et al designed an assembly of DNA strands forming a tetrahedron that changes its conformation to emit fluorescence upon miRNA hybridization[212]. Similar DNA framework was applied by several groups to multiplex miRNA detection thanks to the great versatility and biocompatibility of this approach[213, 214].

Signal amplification in live cells is particularly challenging, since it requires biocompatibility, which is not required for ex vivo detection. Lu et al managed to implement DSNSA in live cells[215], while Meng and coworkers combined strand-displacement and DNAzyme amplifications in order to increase the sensitivity of their assay[216]. Interestingly, Wang *et al.* took advantage of the cells expression machinery by introducing plasmids promoting the production of fluorescent proteins (e.g. GFP, mRFP) once the miRNA is captured[217]. All of the aforementioned techniques rely on fluorescence for detection, and are limited by the one-color-per-target barrier. Wang and coworkers implemented successive cycles composed of an HCR amplification step, fluorescence imaging followed by the degradation of HCR hairpins by DNase I to increase the multiplexing ability of their method to 12[218]. As an alternative to fluorescence, Zhou et al used SERS to detect 2 miRNAs simultaneously in live cells[219].

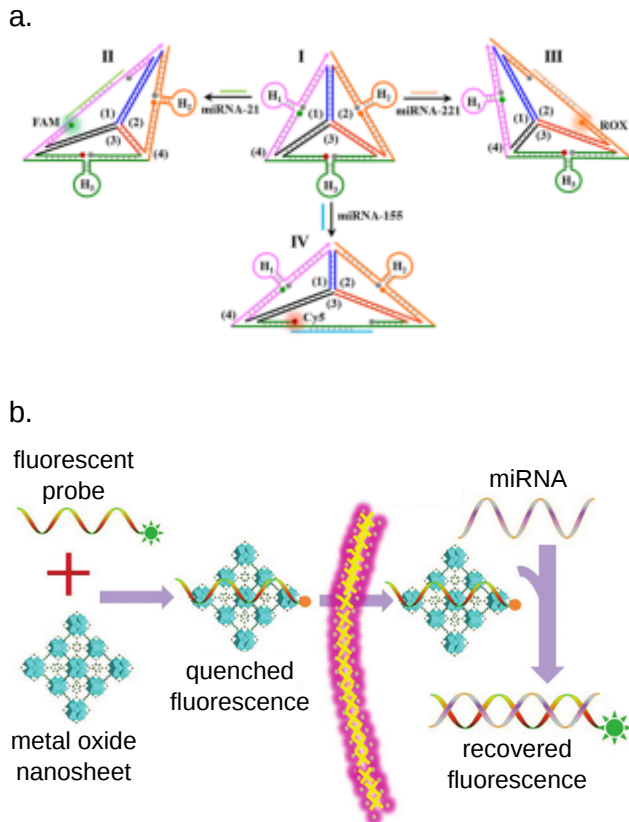


Figure 1.16: Examples of common approaches for miRNA detection from live cells. a. DNA framework allowing the simultaneous of 3 miRNAs simultaneously. All 3 fluorophores are initially quenched. The binding of a miRNA changes the conformation of the framework, taking the corresponding fluorophore and its quencher apart. Picture from Zhou *et al.*[213]. b. MiRNA detection based on metal oxide nanosheets. The fluorescent probes are initially embedded in the nanosheet, which quenches their fluorescence. Upon miRNA hybridization, the probe is freed from the nanosheet, and fluorescence is recovered. Picture from Wu *et al.*[209].

1.4 Conclusions and perspectives

Conventional miRNA detection methods suffer from symmetrical limitations: RT-qPCR is highly sensitive, but its multiplex capacity is limited by the lack of spectrally-resolved fluorescent probes, whereas planar microarrays can detect up to thousands of miRNAs simultaneously but display relatively low sensitivity. In this chapter, we reported innovative miRNA sensing methods aiming at detecting very low concentrations while being highly multiplexable. Signal overlap still limits the multiplex ability of methods using an independent reporter for each targeted miRNA. This is not only the case for fluorescence-based methods, but also applies to electrochemical or Raman-scattering readouts. Consequently, alternative target indexation methods were implemented to boost the multiplex capacity. Suspension arrays are

currently emerging as very promising detection methods. The wide diversity and versatility of functionalizable particles offers high multiplexing potential and compatibility with multiple readout strategies, while the suspension format allows higher sensitivity and throughput than planar microarrays. Although the low concentrations of miRNAs in bodily fluids are still challenging to reach for numerous methods, the field greatly benefited from the design of novel nucleic acid amplification techniques. The development of highly sensitive readout methods, such as SERS, SPR or electrochemical labels, has also been instrumental in the improvement of the sensitivity of assays.

Due to the high sequence homology encountered in the miRNA world, multiplex assays would also need to be highly specific. Different strategies have been explored to increase target specificity. These include the design of selective capture oligonucleotides that discriminate miRNAs taking into account the difference in free energy (using secondary-structured probes or chemical modifications such as LNA). Similarly, specific reporting probes (e.g. hydrolysis probes) may be used to discriminate the target sequence from nonspecific reactions. In enzyme-based systems, the choice of the enzyme(s) (polymerase, ligase, restriction enzyme, RNase or other nucleases) is crucial to maximise the assay selectivity with respect to homologous target sequences. Finally, support-assisted designs seem promising leads for improving specificity in multiplexed format[220, 174, 113]. We refer the readers to a recent review from Ouyang *et al.*, in which the specificity of microRNA is thoroughly discussed[92].

In all the above-mentioned multiplex methods, each miRNA target is individually quantified using independent bioreceptors and data analysis allows to reconstruct the sample profile. These techniques are ideally suited to accurately profile miRNAs and discover novel disease-related signatures. Complementary approaches are focusing on the *in vitro* integration of the data processing step. Conceptually, a DNA circuit is built to integrate the presence or absence of a set of miRNAs, transduce this information *in moleculo*, and report an output that depends on the programmable circuit's architecture. More than a decade ago, Seelig and coworkers conceived a 11-gate amplification-free DNA circuit that accept 6 miRNA sequences as input (let-7c AND miR-124a AND (miR-15a OR miR-10b) AND (miR-143 OR miR-122a)), resulting in the classification of the samples according to the presence or absence of DNA analogues of the target sequences[221]. Other groups have cascaded HCR and/or DNAzyme amplification to assemble boolean logic circuits, using fluorescence[222], colorimetric[223] or nanopore readout[224]. Although conceptually elegant, these demonstrations use hundreds of nanomolars to subnanomolar of discrete concentrations of miRNA input, making them unsuitable for clinical applications without substantial sensitivity improvement. Yet another path exploits DNA architectures that emulate neural networks to perform sample classification based on biomolecules concentrations[221, 222]. Coupled to

PCR and RCA amplification, such approach has recently proven capable of cancer diagnosis from plasma samples[225]: after training an *in silico* classifier from publicly-available miR-seq profile and identified a 4-miRNA signature of non-small cell lung cancer, Zhang *et al.* implemented a DNA classifier that computes the weighted sum of all 4 miRNA targets and return a yes/no diagnosis. To reach clinically relevant sensitivity, miRNA from plasma samples were first amplified by RT-PCR and converted to circular single-stranded DNA, subsequently used as input for the molecular computation. Yet to be confirmed, an advantage of these emerging concepts is that the complexity to measure independently miRNA markers is transferred from the technology (microarray, microfluidics, sequencing, etc.) to the molecular chemistry, opening the door to miRNA profiling kits for rapid testing, for example for routine screening of cancer diseases from minimally invasive, low-cost procedure, that would expand the arsenal of multiplexed microRNA detection technologies.

Table 1.1: Summary of the characteristics of the discussed multiplex miRNA detection methods. Asterisks indicate that the limit of detection was calculated by adding 3 standard deviations to the average blank. Non-asterisk references did not indicate how the LOD was calculated. Please note that the specificity criterium is not included in the table as it is often partially or not assessed in the listed references.

Type	Amplification	LOD	Readout	Target indexation	Highest multiplex	Ref.
Homogeneous	HCR	25 amol	NB	Fluorescent dye	3	[86]
Homogeneous	Ligation PCR	1 pM	PAGE	Size separation	9	[93]
Homogeneous	No	130 fM	Agarose gel	Conformation separation	5	[94]
Homogeneous	No	190 fM*	CE	Size separation	5	[95]
Homogeneous	Ligation PCR	200 aM	CE	Size separation	5	[96]
Homogeneous	EXPAR	2 fmol	CE	Conformation separation	8	[98]
Homogeneous	DSNSA	260 aM	HPLC	Size separation	3	[99]
Homogeneous	No	200 pM*	Fluorescence	Fluorescent dye	3	[103]
Homogeneous	No	40 pM*	Fluorescence	Fluorescent dye	3	[104]
Homogeneous	No	500 pM*	Fluorescence	FRET decay time	2	[105]
Homogeneous	No	40 pM	Fluorescence	Fluorescent dye	4	[109]
Homogeneous	RCA	90 fM*	Fluorescence	Fluorescent dye	3	[110]
Homogeneous	HCR	0.88 pM*	Fluorescence	FRET decay time	2	[106]
Homogeneous	CHA	1.8 pM*	Fluorescence	FRET decay time	2	[107]
Homogeneous	RCA	0.3 fM*	Fluorescence	FRET dye and decay time	4	[108]
Homogeneous	DNAzyme	15 fM	Fluorescence	Fluorescent dye	3	[111]
Homogeneous	DSNSA	100 fM*	Fluorescence	Fluorescent dye	3	[76]
Homogeneous	DSNSA	9 pM*	Fluorescence	Fluorescent dye	3	[112]
Homogeneous	DSNSA	0.8 pM*	Fluorescence	Fluorescent dye	2	[137]
Homogeneous	DSNSA	10 fM*	Fluorescence	Fluorescent dye	3	[113]
Homogeneous	EXPAR-like	10 fM	Fluorescence (digital)	Fluorescent dye	3	[117]

Continued on next page

Table 1.1 – Continued from previous page

Type	Amplification	LOD	Readout	Target indexation	Highest multiplex	Ref.
Homogeneous	RCA	47 fM*	Flow cytometry	Combination of dyes	2	[118]
Homogeneous	RCA	1 pM*	Flow cytometry	Combination of dyes	3	[120]
On-sensor	DSNSA*	3 fmol	Voltammetry	Electrolabels	2	[131]
On-sensor	DNAzyme	50 aM*	Voltammetry	Electrolabels	2	[132]
On-sensor	No	20 aM	Voltammetry	Electrolabels	2	[133]
On-sensor	No	50 fM*	Voltammetry	Electrolabels	2	[134]
On-sensor	No	0.2 fM	Voltammetry	Electrolabels	2	[135]
On-sensor	No	0.3 pM*	Voltammetry	Electrolabels	2	[136]
On-sensor	DSNSA	58 fmol*	MS	Lanthanide tags	3	[138]
On-sensor	No	1 pM	SERS	Raman labels	3	[140]
On-sensor	No	10 fM*	SERS	Raman labels	3	[141]
On-sensor	No	N/A	SERS	Raman labels	2	[142]
On-sensor	No	2 fM*	Raman spectrometry	miRNA Raman signature	3	[143]
Microarray (plan.)	No	1 aM	SERS	Spatial	3	[165]
Microarray (plan.)	No	200 fM*	SERS	Spatial	8	[166]
Microarray (plan.)	No	500* fM	SPR	Spatial	4	[167]
Microarray (plan.)	No	30 fM	SPR	Spatial	3	[168]
Microarray (plan.)	No	10 pM	Microring resonator	Spatial	4	[169]
Microarray (plan.)	No	1 pM	Electrochemical	Spatial	8	[170]
Microarray (plan.)	Trapped enzyme	1 aM*	Electrochemical	Spatial	3	[171]
Microarray (plan.)	No	260 fM*	Au NP aggregation	Spatial	3	[172]
Microarray (plan.)	RT-qPCR	10 pg/ μ L	Fluorescence	Spatial	5	[173]
Microarray (plan.)	RT-qPCR	2 amol	Fluorescence	Spatial	5	[174]
Microarray (plan.)	LAMP	20 copies/ μ L	Voltammetry	Spatial	5	[175]

Continued on next page

Table 1.1 – Continued from previous page

Type	Amplification	LOD	Readout	Target indexation	Highest multiplex	Ref.
Microarray (plan.)	Dendritic	50 fM	Fluorescence	Spatial	3	[226]
Microarray (plan.)	DSNSA	N/A	Fluorescence	Spatial	14	[177]
Microarray (susp.)	SIMOA	1 fM*	Fluorescence	Fluorescent barcodes	3	[179]
Microarray (susp.)	No	1 fM	Fluorescence	Fluorescent barcodes	3	[180]
Microarray (susp.)	Strand displacement	400 aM	Fluorescence	Fluorescent barcodes	3	[181]
Microarray (susp.)	No	500 fM	Fluorescent	Fluorescent barcodes	4	[183]
Microarray (susp.)	No	1 fM*	Particle colocalization	Fluorescent barcodes	6	[184]
Microarray (susp.)	DSNSA	0.5 pM	Fluorescence	Fluorescent barcodes	2	[227]
Microarray (susp.)	RT-qPCR	100 fM	Fluorescence	Graphical barcodes	5	[190]
Microarray (susp.)	RCA	300 aM*	Fluorescence	Graphical barcodes	3	[191]
Microarray (susp.)	Trapped enzyme	4 pM*	Colorimetry	Graphical barcodes	3	[194]
Microarray (susp.)	No	2 amol*	Fluorescence	Graphical barcodes	5	[192]
Microarray (susp.)	No	2 amol*	Fluorescence	Graphical barcodes	5	[193]
Microarray (susp.)	Trapped enzyme	60 zmol*	Fluorescence	Graphical barcodes	3	[195]
Microarray (susp.)	RCA	500 aM*	Fluorescence	Graphical barcodes	2	[196]
Microarray (susp.)	HCR	10 pM	Fluorescence	Photonic crystals	3	[198]
Microarray (susp.)	RCA	20 fM	Fluorescence	Photonic crystals	3	[200]
Microarray (susp.)	HCR	1 nM	Fluorescence	Photonic crystals	3	[199]
Microarray (susp.)	DNAzyme	30 pM*	Fluorescence	Particle size	4	[202]
Microarray (susp.)	No	10 fM	SERS	Particle size	3	[203]
Microarray (susp.)	No	2 pM*	Acoustic levitation	Particle size	2	[204]
Microarray (susp.)	No	3 pM	Particle colocalization	Optical + mobility	9	[205]

1.5 Objectives of the PhD project

A plethora of studies reported the role of miRNA dysregulations in cancers, and demonstrated their potential as diagnostic or prognostic biomarkers. They are released in a stable form in bodily fluids, which makes them attractive targets for the development of liquid biopsy technologies. Moreover, the clinical applications of miRNA quantification are not limited to diagnostics: miRNA detection from biofluids could also be a particularly useful tool for patient follow-up, for example in response to a treatment, given its non-invasive nature.

However, miRNAs are short sequences, presenting in some cases high levels of homology, and are only present in very low concentrations in highly complex media. Relevant miRNA detection methods therefore need to display high specificity and sensitivity while being quantitative and robust. Additionally, relevant clinical applications of miRNAs rather rely on panels of biomarkers than single ones. Such multiplex information can be obtained in two different ways, either by repeating a singleplex assay multiple times, which is costly in terms of time, consumables and sample requirement, or by designing a more complex assay simultaneously measuring multiple miRNA concentrations. The current gold-standard method for miRNA analysis, RT-qPCR, is mostly a singleplex or low-multiplex method, but possesses excellent sensitivity and robustness. On the other hand, microarrays and NGS-based technologies are highly multiplexable techniques but lack sensitivity. Moreover, well-established miRNA detection methods only provide a relative quantification and require prior calibration to be quantitative.

Considerable efforts were deployed in recent years to design innovative technologies or improve existing ones in order to overcome these issues. Heterogeneous assays, in particular, display enhanced multiplexing ability while being compatible with conventional amplification strategies or sensitive detectors, which allows the quantification of miRNAs at lower concentrations. Unfortunately, sensitivity is still an issue for many of these methods. Moreover, most of the reported approaches still rely on a calibration step to provide a quantitative information, which is a potential source of biases. Only a few multiplex methods claim to provide absolute quantification of miRNAs, namely the nCounter (Nanostring) and SIMOA (Quanterix) systems.

Our group previously developed a novel singleplex digital miRNA detection method, based on a noise-reducing molecular amplification network and droplet microfluidics. The aim of this PhD project was first to design a multiplex miRNA detection method based on this singleplex assay. This method is referred to as the MultimiR method. Simultaneously, we wished to obtain an excellent sensitivity, within the fM range, in order to be relevant for miRNA detection from biofluids.

Our first challenge was to achieve multiplexing. Our strategy relied on the immobilization of part of the chemical network on fluorescently barcoded particles. In addition to multiplexing, this supported approach enables digital and high-throughput readout by flow cytometry. DNA analogs of miRNA sequences were first used as target analytes for the early stages of development of the method. Once multiplex quantification of DNA targets was achieved, experimental conditions were further optimized for the detection of synthetic miRNAs. A limit of detection of about 1 fM was reached. A proof-of-concept 6-plex miRNA detection was performed.

Once validated on synthetic miRNAs, our second aim was to detect endogenous miRNAs from human biological samples. First, we intended to detect miRNAs from extracted total RNA from healthy and tumoral tissue. Our final aim was miRNA analysis from blood plasma, as it is a crucial step towards the development of liquid biopsy technologies. This work is still ongoing, but holds good potential.

Chapter 2

Proof of Concept: Multiplex detection of synthetic DNAs

2.1 Introduction: Molecular programming for isothermal digital miRNA detection

The aim of our approach is to simultaneously quantify multiple miRNAs from human biofluids. The first step to validate our detection method is to detect synthetic miRNA targets spiked in a buffer of controlled composition.

In this chapter, we first describe the low-background isothermal amplification molecular network we applied to miRNA detection. The network is based on the PEN DNA toolbox (Polymerase Exonuclease Nickase Dynamic Network Assembly) and is composed of four DNA templates, each of which fulfils a specific function: conversion, amplification, thresholding and reporting. This system enables miRNA detection either in tubes or in microdroplets. The droplet format allows absolute quantification of the miRNA target as well as enhanced sensitivity.

We then present how this singleplex method was modified to quantify multiple miRNAs simultaneously. Our approach is based on the use of functionalizable microparticles on which part of the detection machinery is immobilized.

The barcoding of the particles is key to the multiplexing ability of suspension arrays, as presented in chapter 1. We chose to use fluorescent oligonucleotides that can efficiently be coupled to the beads. We were able to create up to 20 subpopulations of microparticles thanks to this approach, which also allows high-throughput particle analysis by flow cytometry.

Finally, we present the preliminary results we obtained by progressively adapting our singleplex digital miRNA quantification method to a multiplex digital miRNA quantification.

Since DNA displays a higher stability than RNA, here we demonstrate a 6-plex detection of synthetic DNA versions of miRNAs.

2.1.1 Design of the molecular network

The isothermal amplification method we designed is based on the principle of exponential amplification reaction (EXPAR)[64]. As explained in chapter 1, EXPAR is an attractive isothermal amplification method. However, its main disadvantage is nonspecific amplification. In practice, negative controls tend to amplify shortly after target-containing samples. This problem makes the design of an EXPAR-based digital method especially challenging, because the short time gap separating positive samples from negative controls would certainly result in false positive signal, negatively affecting sensitivity.

To reduce background noise in EXPAR amplification, we used the polymerase exonuclease nickase dynamic network assembly (PEN-DNA) toolbox, a chemical programming system developed by our lab to design networks performing various functions, such as switches or oscillators. The toolbox is composed of three enzymes (polymerase, exonuclease and nicking enzyme) performing chemical reactions on tailored DNA oligonucleotides, called templates. Typically, an input strand binds the template, and undergoes polymerization/nicking cycles to generate output strands, the sequence of which is determined by that of the template. The exonuclease degrades all unprotected single strands, keeping the system out of equilibrium. Each template is a module of the chemical network, fulfilling a specific function. Combining different modules, our group designed networks displaying complex behaviours, such as oscillations[228, 229] or multistability[230].

Basic EXPAR uses an amplification template that, once activated by a trigger sequence, undergoes polymerization/nicking cycles to generate more trigger strands. The trigger production rate thus increases linearly with the concentration of trigger, until all amplification templates are hybridized to trigger strands. At this point, the production rate saturates. EXPAR amplification in the presence of a first order decay mechanism (such as an exonuclease) is modeled on Fig 2.1a. The system possesses one unstable state, before amplification, in total absence of trigger, and only one stable equilibrium state, after amplification, at high trigger concentration. In this configuration, the presence of the slightest amount of trigger inevitably leads to amplification, explaining the already discussed generation of background noise by EXPAR. Montagne *et al.* reported a bistable network by coupling the exonuclease degradation to a trigger-specific degradation pathway[70]. The exonuclease provides an unspecific and linear degradation, while a tailored DNA template, referred to as "pseudo-template", specifically disables triggers. Once the concentrations of all components were optimized, the system possesses two stable steady states: one in the absence of trigger, the

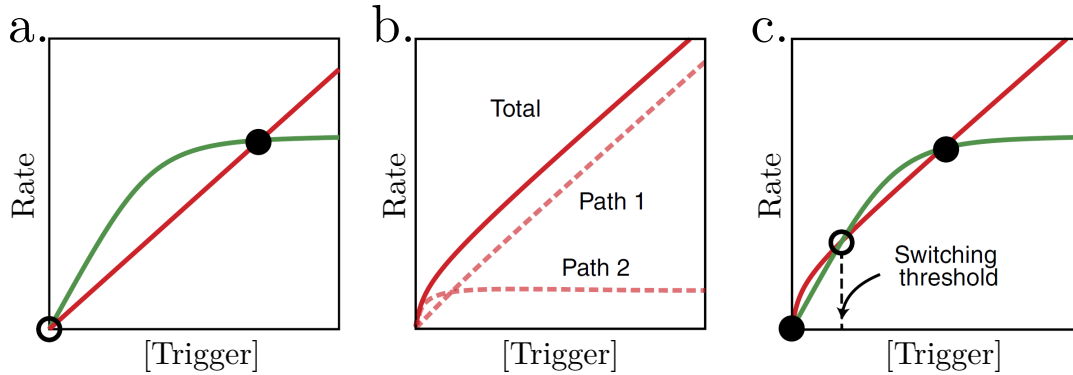


Figure 2.1: Trigger production (green curves) and degradation (red curves) rates depending on trigger concentration. a. No drain template. The system is initially at the unstable steady state at 0 trigger. If trigger is produced - specifically or not - production is faster than degradation and the amplification is triggered. b. The combination of the exonuclease (path 1) and drain template (path 2) degradation pathways increases the slope of the overall degradation rate at low trigger concentration only. c. The combination of both degradation pathways, when properly adjusted, generates a system presenting two stable steady states. Above the threshold trigger concentration, the amplification is triggered, while a trigger concentration below the threshold will not allow amplification. Figure extracted from Montagne *et al.*

other after amplification, at high trigger concentration (Fig 2.1c). Additionally, the saturation of the template-induced degradation pathway creates an unstable equilibrium state, defining a threshold concentration of trigger. Below this threshold concentration, degradation is faster than amplification, leading to stabilisation at the "no trigger" steady state. If trigger concentration surpasses the threshold, however, the amplification occurs. This bistable switch is the base module of our detection machinery.

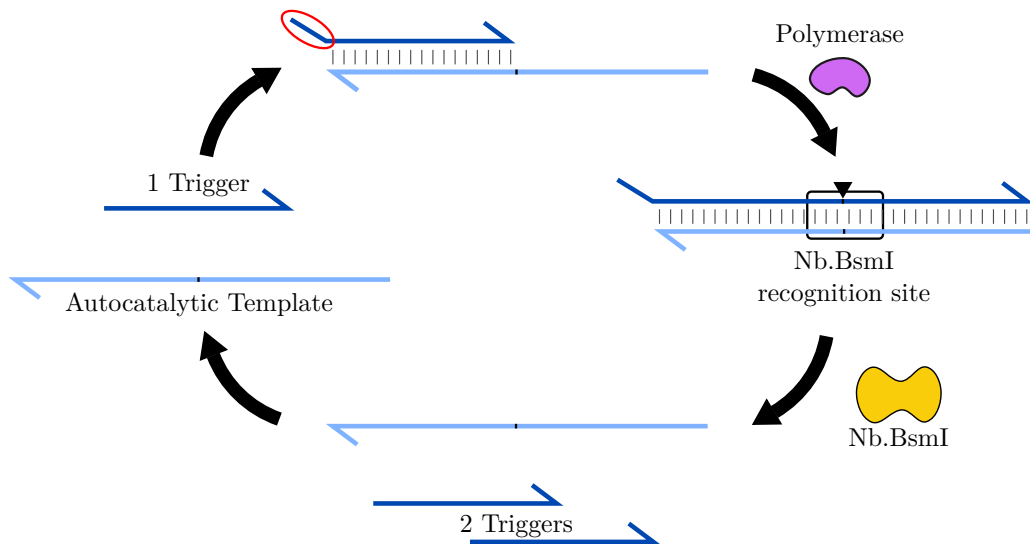


Figure 2.2: Trigger amplification by the autocatalytic template. One trigger molecule hybridizes to the 3' half of the aT. One can note that the two bases on the 5' end of the trigger sequence do not hybridize to the aT (red circle). This overhang is of prime importance to the prevention of non-specific amplification. The trigger molecule acts as a primer for polymerization. The trigger molecule is designed so that a repeat of this sequence presents a Nb.BsmI recognition site. Nicking by Nb.BsmI separates the elongated strand into two trigger sequences. The amount of trigger molecules is thus regularly doubled, resulting in exponential amplification.

Our miRNA detection network is composed of 4 DNA templates, each fulfilling a different function: amplification, thresholding, conversion and reporting. The autocatalytic template (aT) and pseudo-template (pT) were already mentioned as part of the bistable switch. The aT catalyses exponential amplification of a 12 bases DNA sequence, called trigger sequence. The 3' end of the aT is complementary to the trigger sequence. The captured trigger sequence acts as a primer for polymerase elongation. The 5' end of aT is also complementary to the trigger, the sequence of the elongated strand is thus two trigger sequences. The trigger is engineered in such way that the middle of this elongated strand forms a Nb.BsmI recognition site, leading to the nicking and release of two trigger sequences. The amount of trigger is therefore regularly doubled by polymerization/nicking cycles.

The pT also hybridizes to the trigger and extends it with a few bases (2-5 bases typically). This short polynucleotide tail prevents the modified trigger from being elongated along its cognate aT. Moreover, the produced strand can not be converted back to a functional trigger by nicking. Pseudo-templates is therefore a specific, fast but saturable trigger degradation pathway. The aim of the pT is to deactivate triggers produced by leaky reactions, while still allowing amplification if enough trigger is present. The concentration threshold required for

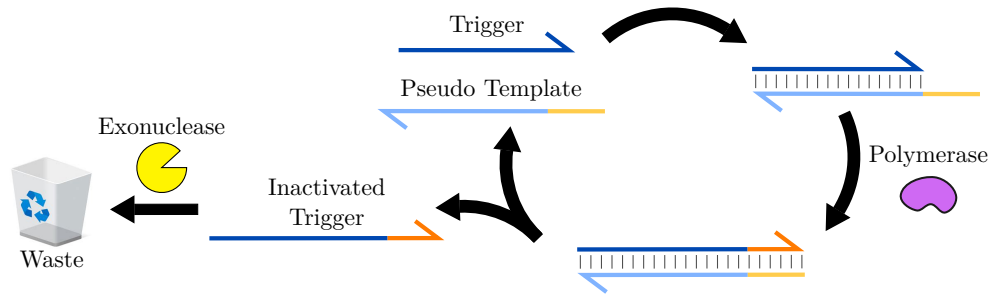


Figure 2.3: Trigger inactivation by the pseudo template. The pT hybridizes to the trigger molecule. A few bases (typically 5 bases) are added to the 3' end of the trigger, preventing its amplification by the aT. The inactivated trigger is unprotected and eventually degraded by the exonuclease. The inactivation is catalytic for the pT. Noteworthy, contrary to the aT, the trigger molecule completely hybridizes to the pT. The trigger therefore preferentially binds a pT rather than an aT, increasing the leak-absorbing effect of the pT.

the amplification to start can be tuned by modifying the pT concentration. Noteworthy, the pT is complementary to all 12 bases of the trigger sequence, whereas aT is only complementary to 10 bases, leaving a 2 bases overhang on the 5' end of the trigger. Consequently, a trigger sequence is more likely to bind a pT than an aT if one is available, making the pT pathway the preferential one at low concentrations of trigger.

The conversion template (cT) is the link between the target miRNA and the amplification/thresholding module. The cT specifically captures the target miRNA by hybridization, and uses it as a primer to produce multiple trigger strands via polymerisation/nicking cycles. The system is thus highly versatile, as only the cT needs to be changed to detect a different miRNA. The nicking enzyme used for the converters is Nt.BstNBI.

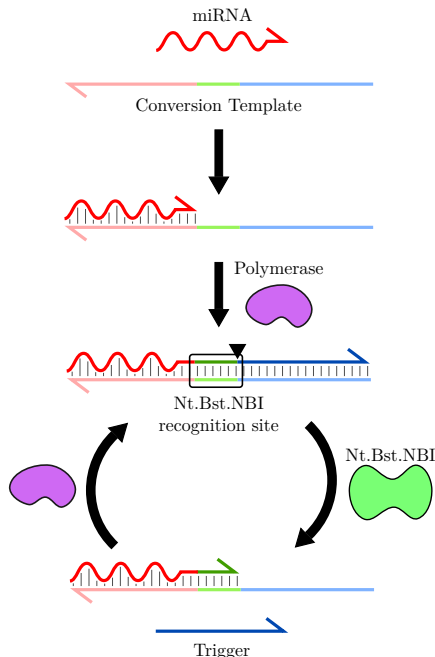


Figure 2.4: Conversion of the miRNA into a trigger molecule. The miRNA hybridizes to the 3'end of the cT and is elongated by the polymerase. The cT sequence is composed of 3 regions: The miRNA complementary sequence in 3', the trigger complementary sequence in 5' and a Nt.Bst.NBI restriction site in between. The elongated strand is therefore cleaved by Nt.Bst.NBI, freeing a trigger molecule. The miRNA does not melt away, and undergoes polymerization/nicking cycles, generating multiple trigger strands.

Finally, the reporting template (rT) produces a fluorescent signal in the presence of trigger sequence (fig 2.5a). The rT is a stem-loop oligonucleotide coupled to a fluorophore on one end and to a fluorescence quencher on the other end. In the absence of trigger sequence, the rT is in closed conformation and fluorescence is quenched. The hybridization and extension of a trigger strand opens the hairpin, releasing fluorescence. Cleavage by Nb.BsmI reverts probe opening. If the restriction enzyme BsmI is added to the reaction mix, the double-stranded rT can be cleaved, making fluorescent emission irreversible, and avoiding the consumption of a trigger strand.

This set of 4 DNA templates is referred to as the molecular program. Each template forms a node of the chemical network, and the trigger sequence links each node to the others. Noteworthy, DNA templates are protected against exonuclease degradation thanks to phosphorothioate (PTO) modifications. The organisation of the network is summed up on figure 2.5b. First, the converter template captures the target miRNA and uses it to generate trigger molecules. If the number of activated cTs is sufficient to increase the concentration of trigger above the threshold concentration of the bistable switch, the amplification is triggered. If the trigger production is too low to surpass the threshold concentration, the combination of

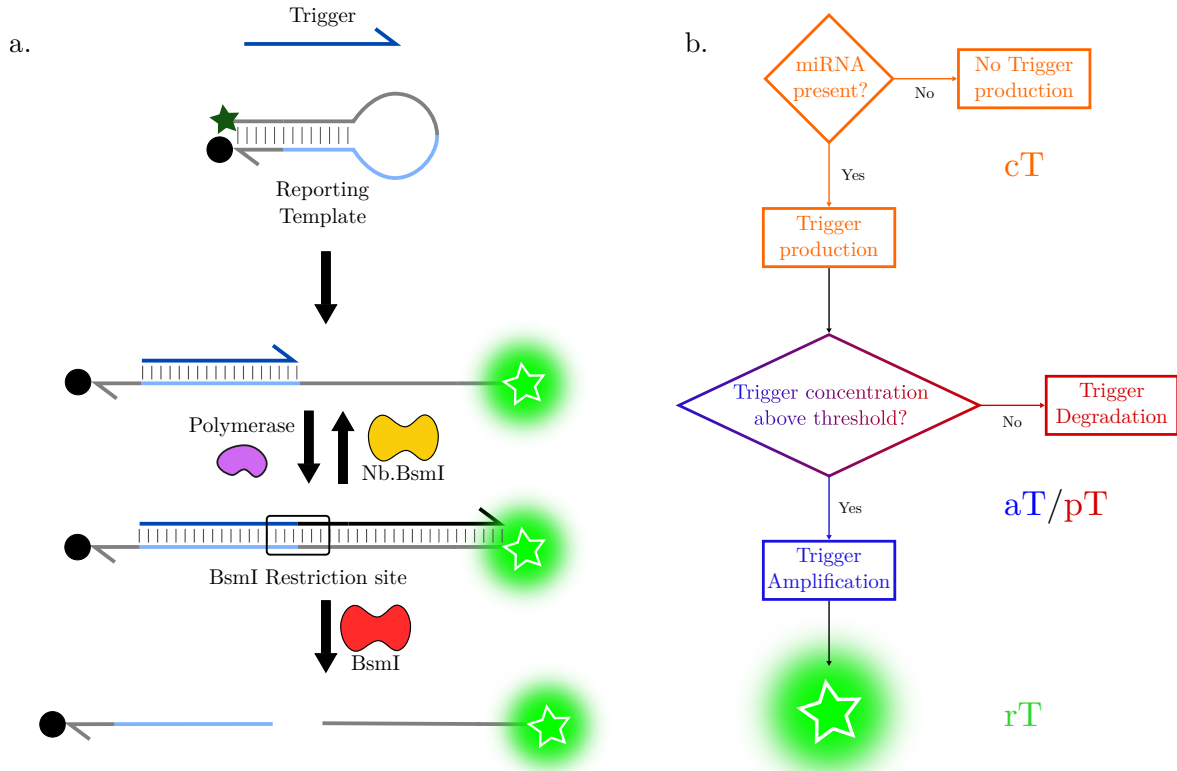


Figure 2.5: (a) Fluorescent reporting of amplification. The rT is originally hairpin-shaped, and coupled to a fluorophore on one of its ends and a fluorescence quencher on the other end. In the stem-loop conformation, the fluorophore and the quencher are close, and fluorescence is quenched. Upon hybridization of a trigger molecule, the hairpin opens, enabling fluorescence emission. The opening of the hairpin is reversible, as the trigger molecule can melt away, but extension by the polymerase stabilizes this conformation. Adding BsmI restriction enzyme to the reaction renders the opening irreversible by cleaving the rT. (b) Summary of the functions of each template of the molecular program.

the exonuclease and pT degradation pathways prevents the amplification from being initiated. Once the amplification takes place, the exponentially increasing amount of trigger allows the opening of the rTs and the emission of a fluorescent signal. Based on this molecular program, our group developed isothermal analogs of qPCR and ddPCR for miRNA detection [71].

Sections 2.1.2 and 2.1.3 present the singleplex quantification methods developed by Guillaume Gines and Roberta Menezes, upon which our multiplex detection method is based.

2.1.2 Isothermal detection of miRNA

The 4 DNA templates presented in the previous section were first applied to an isothermal qPCR-inspired miRNA detection method. In this real-time approach, the miRNA concentration is computed based on the time needed for the exponential amplification to be triggered.

As for RT-qPCR, the miRNA quantification is relative, and requires a calibration using standard samples of known miRNA concentration.

The molecular program of 4 DNA templates is mixed with the enzymes of the PEN DNA toolbox (Vent(exo-) DNA polymerase, exonuclease ttRecJ, nicking enzymes Nt.Bst.NBI and Nb.BsmI) and the miRNA-containing sample (Fig. 2.6). The reaction tube is incubated at 50°C and rT fluorescence is monitored in real-time. A high concentration of miRNA will allow the quick activation of numerous cTs, and therefore a quick initiation of the amplification. Reversely, a low amount of targets requires more time and activates less converters, which delays the amplification. Figure 2.6a shows the normalized fluorescence signals over time of a range of samples of known Let7a concentration. The amplification times indeed increase when the miRNA concentration decreases. For the 1 fM sample and the no target control (NC), the amplification does not take place. A calibration curve can be established by measuring the time needed to reach 20% of the maximum, as was done on figure 2.6b. We observe a range of concentration over which the amplification time varies proportionally to the logarithm of the concentration. The miRNA can be accurately quantified within a dynamic range going from 10-100 fM to 100 pM.

The pT improves the limit of detection compared to EXPAR, at the cost of longer incubation times. For most miRNAs, the LOD is 10 fM detected in real-time within 16 hours. As is the case for qPCR and EXPAR, this amplification method suffers from non-specific amplification, which limits the limit of detection around 10 fM for most miRNAs.

2.1.3 Digital detection of miRNA

To improve the sensitivity of our method, we decided to implement our chemical network in a digital detection design. The principle is close to that of droplet-based digital PCR. The reaction mixture is composed of the same components as the previous design. The mixture is then partitioned in millions of picoliter droplets. The distribution of miRNA copy numbers per droplet is poissonnian. In our method, the sample dilution is adjusted in such a way that most droplet contains either zero or one miRNA. In this droplet-based approach, the internal concentration can take only one out of two values (0 or 3 pM for a 0.5 pL droplet), and the amplification reaction takes place or not in each droplet independently of the others, depending on whether or not the droplet contains a miRNA. The droplets are incubated at 50°C. The reporter fluorescence is again monitored in real time during incubation. Contrary to a bulk detection, the amplification reaction takes place independantly in every droplet, resulting in a much slower fluorescence increase. Droplets incubation is stopped when the fluorescent signal reaches a plateau, meaning that the amplification was completed in all miRNA-containing droplets. The droplets are imaged by fluorescence microscopy. In miRNA-

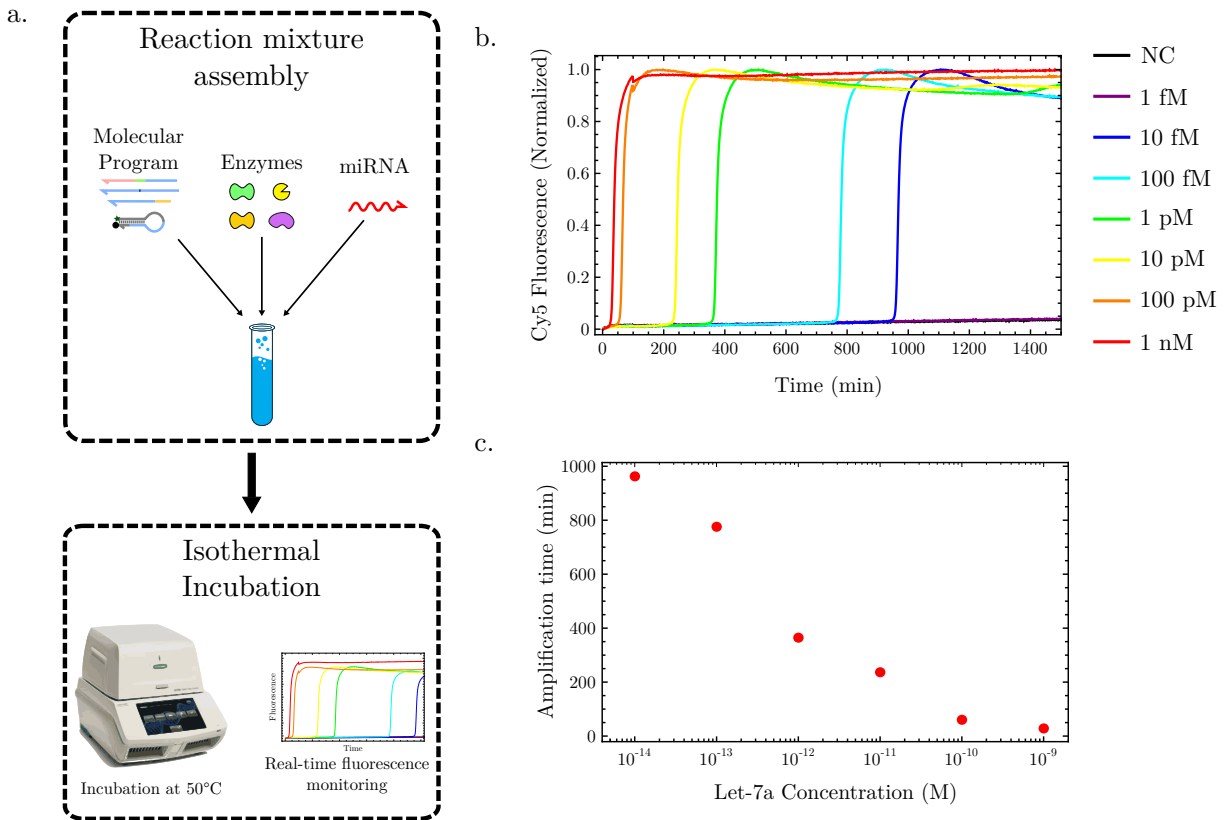


Figure 2.6: qPCR-inspired miRNA quantification using molecular programming. a. The reaction mixture, containing the 4 DNA templates, the enzymes and the miRNA-containing sample is assembled and incubated at 50°C. b. Fluorescence over time curves. The higher the miRNA concentration, the sooner the amplification is triggered. c. The amplification start times are measured to generate a calibration curve. In this experiment, the linear range spans from 100 pM to 10 fM.

containing droplets, the trigger molecule was amplified and rT fluorescence was activated, whereas droplets that do not contain any miRNA remain non-fluorescent. The readout is said digital, as the information carried by each droplet can only take two values. The miRNA concentration is computed from the percentage of fluorescent droplets by assuming the distribution of miRNAs in droplets was poissonian. This digital detection method is referred to as isothermal digital droplet detection of miRNAs (ID3miR)[71].

Digital and multiplex miRNA detection for molecular diagnostics

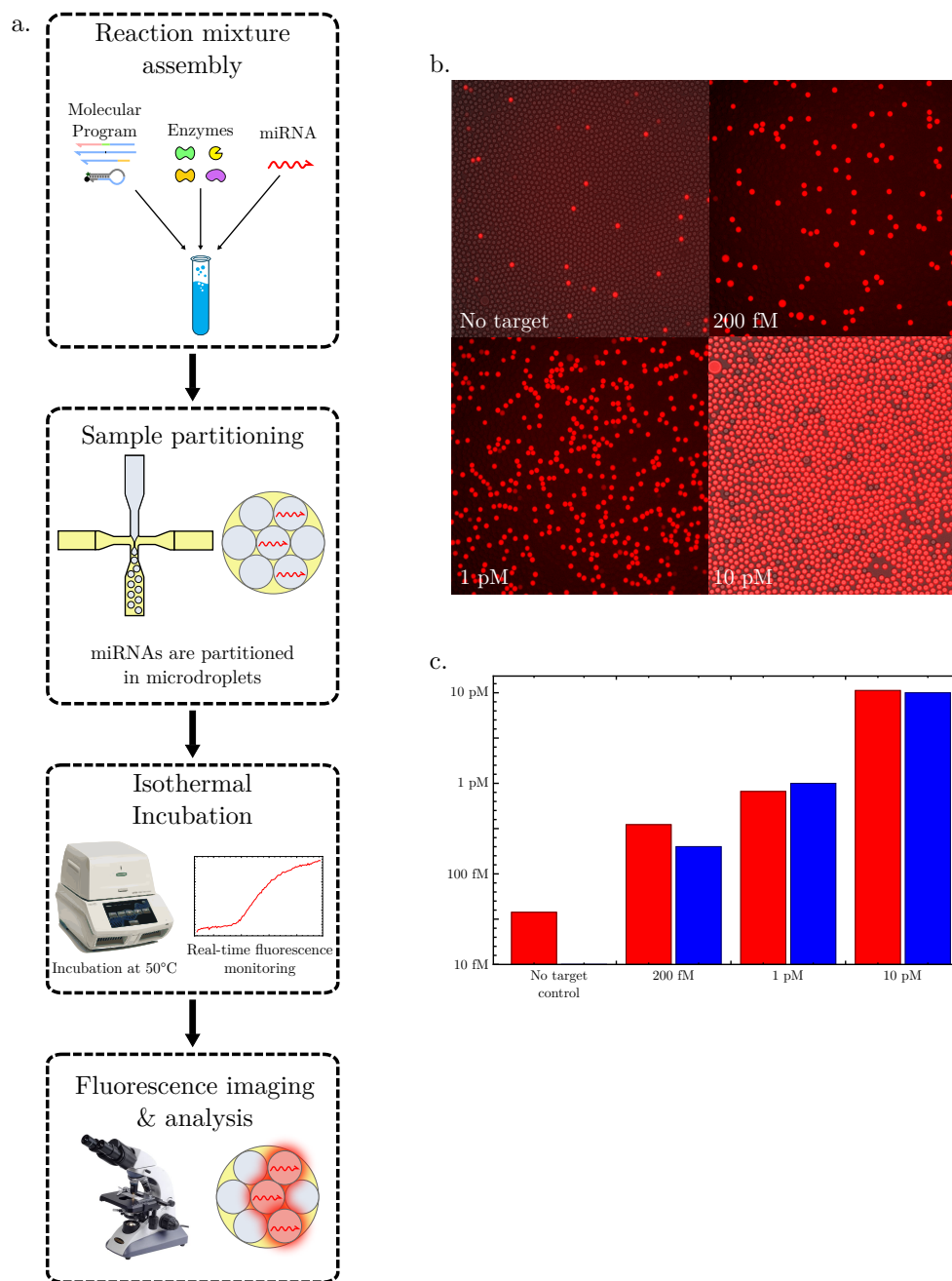


Figure 2.7: ID3miR method. a. Workflow of the method. The reaction mixture is composed of the 4 DNA templates of the molecular program, the PEN enzymes and the miRNA-containing sample. The sample is then partitioned in $10 \mu\text{m}$ droplets using a flow-focusing microfluidic device. The droplets are incubated at 50°C until fluorescence reaches a plateau, at which point incubation is stopped and droplets are imaged. b. Fluorescence microscopy images of a range of Let7a. c. Results of the Let7a range. The results are in good accordance with the expected concentration.

This method allows the detection of miRNA down to the single molecule level, and is

therefore more sensitive than its bulk counterpart. Additionally, this technique allows absolute target quantification.

2.2 Design of multiplexed method

The aim of the project is to implement this molecular programming approach into a multiplex miRNA detection method. Here, we present our strategy, based on functionalizable microparticles, to achieve this objective. We also discuss the selection of the particles we used for our multiplex technology. Finally, we report the formation of beads subpopulations by fluorescent barcoding.

2.2.1 Multiplexing strategy

The previously described singleplex method relies on fluorescence to report detection. As discussed in chapter 1, fluorescence-based homogeneous assays are limited in terms of multiplexing by the spectral overlap of fluorophores and chemical crosstalk [117]. To circumvent this limitation, we decided to design a suspension microarray based on the same chemical network by immobilizing part of the molecular program on particles. Each bead would be coupled to converter templates for a specific miRNA target and a corresponding fluorescent barcode. The reporter template, common to all targets, is also bound to the particles, allowing the high throughput analysis of barcodes and reporters simultaneously by flow cytometry. The bistable switch, composed of the autocatalytic template and pseudo-template is left in solution.

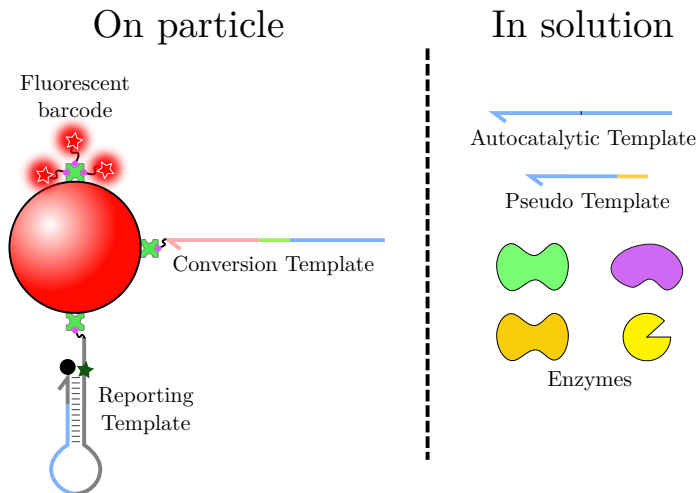


Figure 2.8: Repartition of the molecular program components. Converters and reporters are immobilized on fluorescent barcoded particles. The autocatalytic templates and pseudo templates remain free in solution, as well as the enzymes.

The detection process is similar to the one presented on figure 2.7. A capture step is however added at the beginning of the procedure (figure 2.9). During this step, the reaction

mixture is incubated at 40°C for 2 hours so that miRNAs can hybridize to their corresponding cTs. The capture of a miRNA by a particle is a random process and therefore follows the Poisson law. After capture, the mixture is partitioned in microdroplets and incubated at 50°C. When the fluorescence reaches a plateau, incubation is stopped and the emulsion is broken to allow flow cytometry analysis of the particles. For each particle, barcode and reporter signals are measured. The beads are first sorted based on their barcode, each subpopulation corresponding to a different target miRNA. Then, the reporter fluorescence is examined for each subpopulation separately. The reporter fluorescence histograms is typically composed of two peaks: One at low fluorescence intensity, indicating that the particle did not capture any miRNA, the other at high fluorescence, meaning that the particle captured at least one miRNA target.

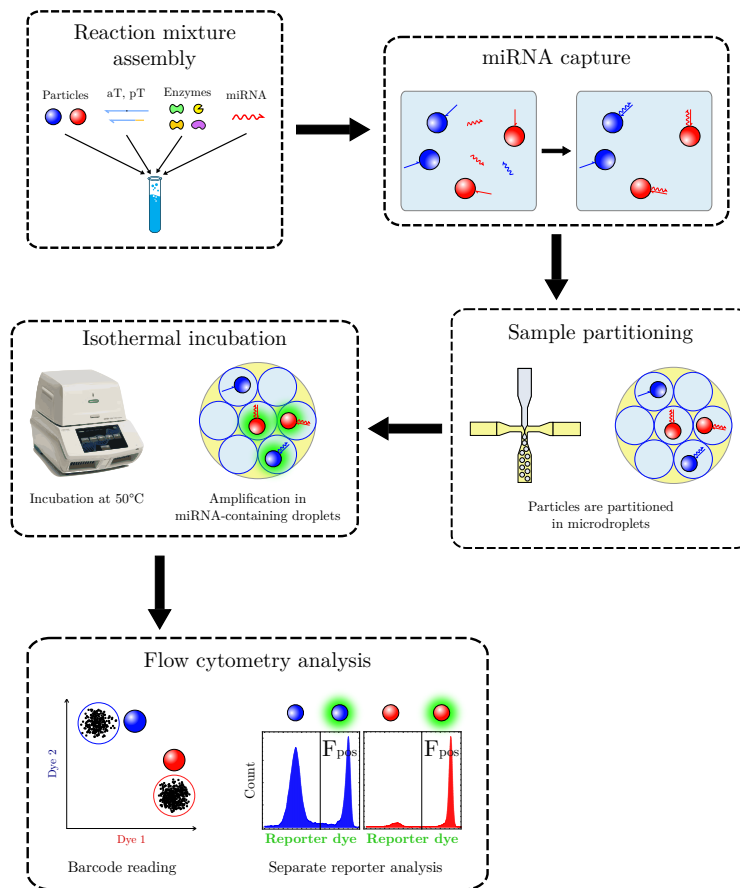


Figure 2.9: Multiplexing strategy. The reaction mixture contains the functionalized particles, aT and pT in solution, the PEN enzymes and the miRNA-containing sample. The mixture is incubated prior to partitioning to allow the capture of miRNAs on the immobilized cTs. Following encapsulation, droplets are incubated. Droplets are then broken in order to recover the beads for flow cytometry analysis. The barcode fluorescence is first measured, and then reporter fluorescence is analyzed for each subpopulation separately.

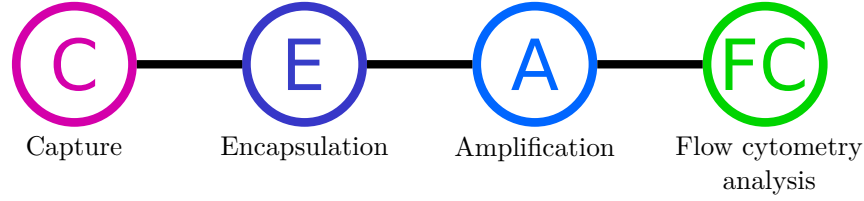


Figure 2.10: Summarized workflow. This summary will be used to indicate what step is being optimized in a section.

The concentration of each targeted miRNA in the original sample can be computed thanks to these fluorescence histograms. Since miRNA capture is a random process, the distribution of miRNAs on their specific particles follows a Poisson law. Hence, the probability $P(k)$ for a particle to capture k miRNA targets is given by equation 2.1:

$$P(k) = \frac{\lambda^k \cdot e^{-\lambda}}{k!} \quad (2.1)$$

where λ is the mathematical average number of miRNAs per specific particle:

$$\lambda = \frac{C_{\text{miRNA}}}{C_{\text{particles}}} \quad (2.2)$$

with C_{miRNA} the concentration of the miRNA and $C_{\text{particles}}$ the concentration of detection particles targeting the miRNA. Considering that the probability for a particle to be positive F_{pos} is equal to the probability of having captured one miRNA or more, we get equation 2.3.

$$F_{\text{pos}} = \sum_{k=1}^{\infty} P(k) = 1 - P(0) = 1 - e^{-\lambda} \quad (2.3)$$

Hence,

$$\lambda = -\ln(1 - F_{\text{pos}}) \quad (2.4)$$

The concentration of the miRNA in the original sample is thus given by equation 2.5:

$$C_{\text{miRNA}} = -\ln(1 - F_{\text{pos}}) \cdot C_{\text{particles}} \quad (2.5)$$

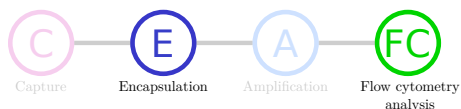
Since $C_{\text{particles}}$ is known, the concentration of the miRNA can be calculated directly from the reporter fluorescence histogram of the corresponding subpopulation by measuring the percentage of beads in the ON state.

This approach theoretically allows the absolute quantification of multiple miRNAs simultaneously based on our amplification chemical network.

2.2.2 Particles selection

A plethora of functionalizable microparticles are commercially available, presenting a wide variety of materials, sizes, affinity coatings, etc.

2.2.2.1 Droplets and particle size



The choice of a particle size is indirectly conditioned by particle coencapsulation. Figure 2.11 shows an example of two coencapsulated particles, only one of which has captured its target miRNA. During incubation, the miRNA-bound particle will induce amplification of the trigger sequence in the whole droplet, inevitably leading the opening of all rTs in the droplet. Both particles will therefore be counted as positive during flow cytometry analysis, whereas only one captured its target miRNA. Since the distribution of particles in droplets also follows a Poisson law of parameter Λ :

$$\Lambda = N_A \cdot C_{\text{particles}} \cdot V_{\text{droplet}} \quad (2.6)$$

with N_A the Avogadro constant, $C_{\text{particles}}$ the concentration of particles in the reaction mixture and V_{droplet} the volume of a droplet. Given equation 2.2, and in order to keep λ within a reasonable range (between 0.1 and 10), the typical $C_{\text{particles}}$ would be around 1 pM. The target Λ is 0.1, which limits the probability of coencapsulation to 1%. Equation 2.6 thus gives us an ideal droplet diameter of about 7 μm . In order to avoid any clogging and sedimentation inside the microfluidic chip, we chose a particle size of 1 μm .

2.2.2.2 Coating



We selected two sets of 1 μm particles to be further tested: Polystyrene particles from Bangs Laboratories and magnetic Dynabeads from Thermo Fisher Scientific. Both types of particles can be coated to allow the coupling of DNA oligonucleotides to their surface. Such coupling can either be covalent, relying on thiol/maleimide or amine/carboxylic acid reactions, or non-covalent, by using affinity coupling such as biotin/streptavidin. Covalent bonding provides a nearly irreversible coupling, which prevents any exchange of oligonucleotides between particles, whereas biotin/streptavidin coupling is reversible and promoted by heating but is

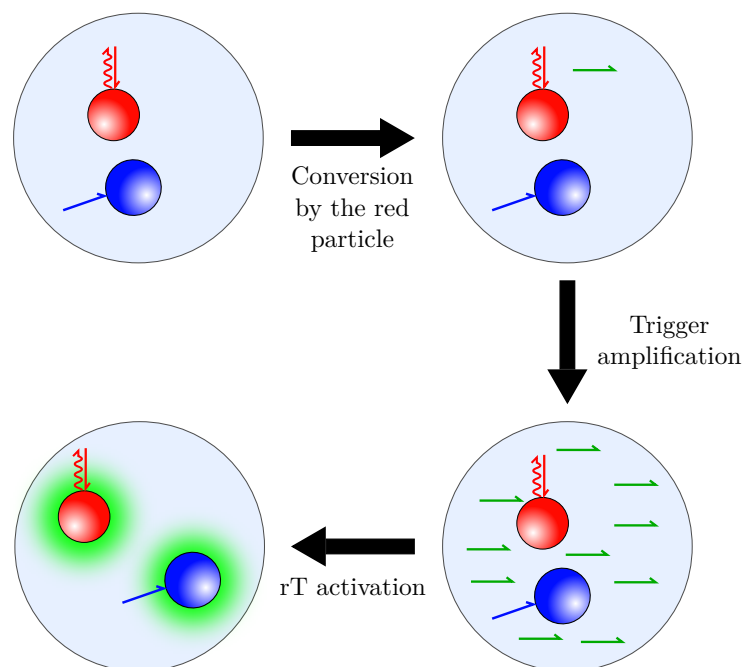


Figure 2.11: Generation of false positive particles by coencapsulation. In this example, a miRNA-carrying particle is encapsulated along with a particle that did not capture any miRNA target. During amplification at 50 °C, the loaded converter produces trigger molecules, which are then exponentially amplified by the machinery in solution. After amplification, the droplet contains numerous copies of the trigger sequence free in solution. Since the rTs carried by the particles are identical, the trigger strands open indiscriminately the rTs carried by both beads. During flow cytometry analysis, both particles are counted as positive, whereas only the red particle captured its target.

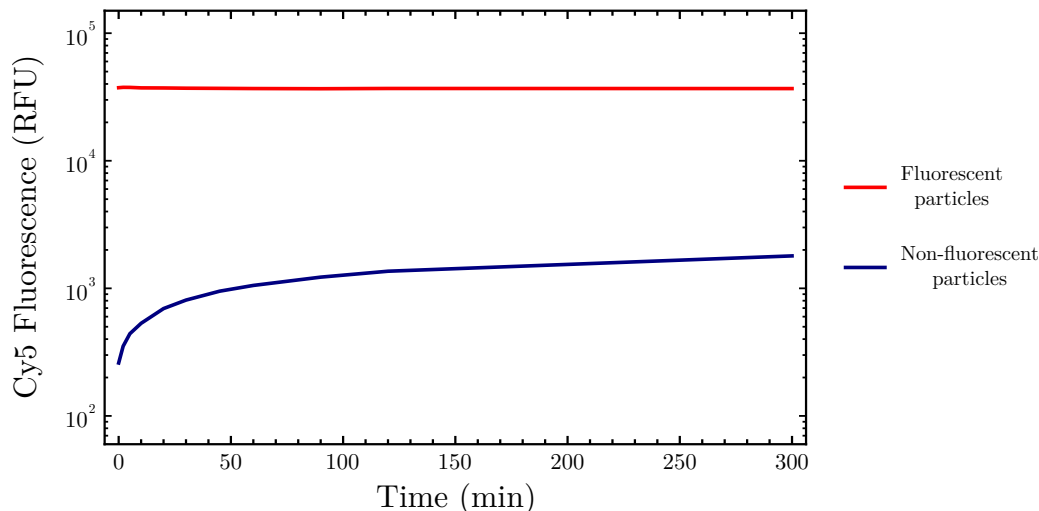


Figure 2.12: Evaluation of the exchange of oligonucleotides by Dynabeads at 30°C. At this temperature, it appears that particles can indeed exchange immobilized oligonucleotides. After 5 hours, 4% of the oligonucleotides were exchanged

far more convenient to perform, as the number of oligonucleotides displayed on the surface can be reproducibly controlled.

In order to determine the extent of interparticle oligonucleotide exchange, we incubated together streptavidin-coated magnetic particles, half of which were coupled to biotinylated fluorescent oligonucleotides (50% of saturation). The beads were incubated several hours at 30°C under strong stirring (2000rpm) in order to mimic the conditions during the capture step, which is most prone to interparticle exchange. A fraction of the particles are regularly collected and analyzed by flow cytometry to follow the exchange of the labeled oligonucleotides. Figure 2.12 shows the results of the experiment. The fluorescent signal emitted by the originally non-fluorescent beads quickly increases in the first minutes of the incubation. The exchange then slows down, but the fluorescent signals continues to steadily increase even after 5 hours of incubation. After 5 hours, we estimate that 4% of the fluorescent oligonucleotides were transferred.

As presented in section 1.2.1, detection particles carry 3 types of oligonucleotides: converters, reporters, and fluorescent barcodes. Reporter templates are the same for all particles, their exchange during capture is thus inconsequential. The exchange of a cT can trigger false positive signal, but only if the transferred cT was bound to a miRNA, which is a rare event, given that the cT/miRNA ratio is typically around 100. Moreover, converters only represent 0.1% of the oligonucleotides carried by the particles. We therefore considered cT exchange as negligible. The main consequence of oligonucleotides is its effect on bead barcoding, since fluorescent barcodes can occupy up to 85% of the streptavidin sites of the particles. Bar-

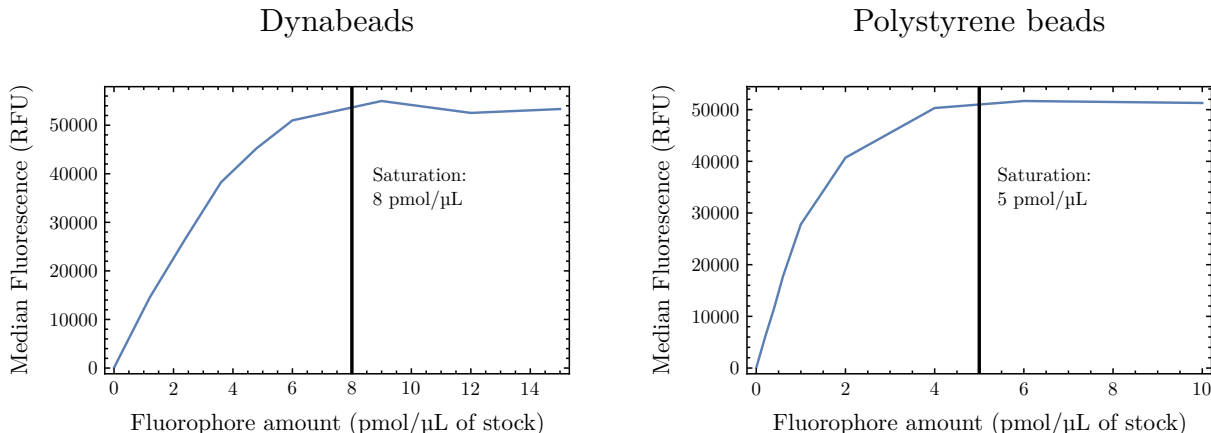


Figure 2.13: Measurement of the oligonucleotide binding capacity of the two types of $1 \mu\text{m}$ streptavidin-coated particles. One microliter of Dynabeads stock solution can carry up to 8 pmol of oligonucleotides, while the saturation of polystyrene particles is of 5 pmol/ μL of stock solution. RFU values are not directly comparable because fluorescence measurements were realized with different cytometry settings.

code exchange could decrease the number of distinguishable particles subpopulations, thus lowering the multiplex ability of the method. We however decided to use streptavidin-coated particles for the development of the method.

The oligonucleotide binding capacity of the streptavidin-coated Bangs particles and Dynabeads was then measured by adding increasing amounts of fluorescent biotinylated DNA strands and measuring the resulting fluorescent signal by flow cytometry. The results are shown on figure 2.13. The binding capacity of Dynabeads is approximately 8 picomoles (pmol) of oligonucleotides per μL of beads stock solution. The capacity of Bangs Laboratories polystyrene beads is lower, at 5 pmol/ μL of stock solution.

Finally, the resistance of the coupling in emulsion was investigated. As explained in section 1.2.1, our multiplex detection method relies on the partitioning of beads in microdroplets, during which our team already observed loss of DNA in other projects. We thus functionalized the two types of particles with fluorescent oligonucleotides (30% of saturation) and analyzed their fluorescent intensity by FC before and after a microfluidic encapsulation in $10 \mu\text{m}$ droplets. Figure 2.14 compares the fluorescent distributions before and after encapsulation for both types of particles. While for Dynabeads the particle fluorescence distribution was barely modified by the encapsulation, only a small fraction of polystyrene beads displayed the same fluorescence before and after partitioning, suggesting that oligonucleotides are released from the particles during the process. This makes polystyrene beads unusable in our detection method. We therefore used streptavidin-coated Dynabeads with $1 \mu\text{m}$

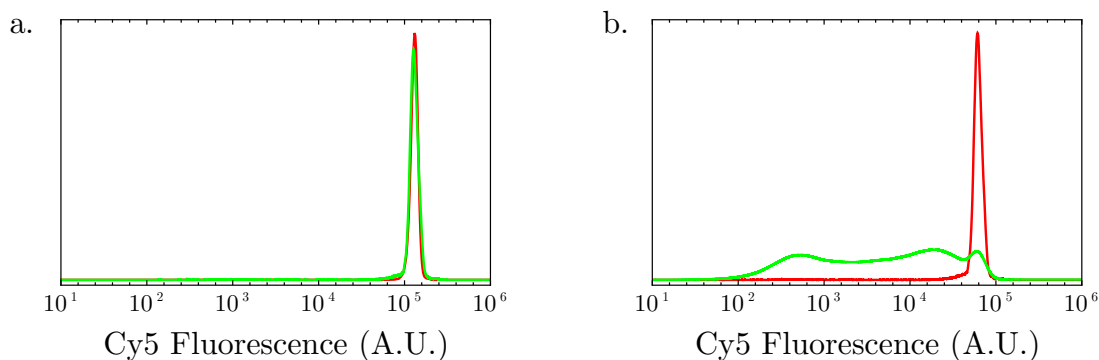


Figure 2.14: Distribution of particle fluorescence before and after encapsulation. a: Dynabeads: The fluorescent distributions before and after are almost identical, indicating that no fluorescent oligonucleotides were lost during encapsulation. b: Polystyrene beads: Most of the fluorescent oligonucleotides were lost during the partitioning in microdroplets, resulting in a heterogeneous fluorescence distribution.

diameter for the rest of this study.

Particle type	Bangs particles	Dynabeads
Material	Polystyrene	Polystyrene and iron oxide
Density	1.06	2.0
Saturation (pmol/ μ L stock)	5 pmol/ μ L	8 pmol/ μ L
Saturation (oligo/bead)	170000 oligo/bead	480000 oligo/bead
Resistance to encapsulation	Poor	Excellent

Table 2.1: Summary of beads characteristics

2.2.3 Particle barcoding



Particle barcoding is the key to our detection method: The multiplex capacity of the assay is indeed directly determined by the number of distinguishable subpopulations we are able to generate. For this project, fluorescence appeared to be the most efficient barcoding strategy. Indeed, fluorescent dyes are low-cost, and can easily be coupled to biotin and grafted on the streptavidin-coated microparticles we used. Moreover, fluorescent barcodes can be read by flow cytometry, allowing the high-throughput analysis of beads.

Our assay relies on fluorescence for both barcoding and readout. A fluorescent channel is therefore reserved for reporting. In this project we chose the dye FAM as a reporter. Absorption and emission spectra of FAM are shown on figure 2.15a as well as the 490 nm

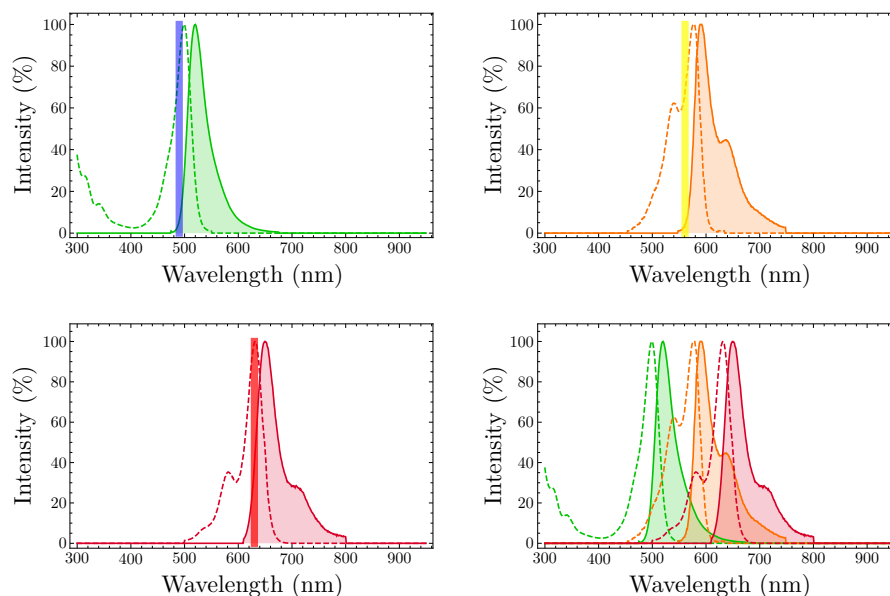


Figure 2.15: a: Absorption (dashed) and emission spectra of FAM (a), Cy3.5 (b) and Cy5 (c). The lines at 490 nm, 561 nm and 630 nm indicate the wavelength of the corresponding excitation laser. d: Overlay of the 3 emission spectra. There is a slight overlap between Cy3.5 and Cy5 spectra, which could produce fluorescence spillover.

excitation laser. Another limitation is related to the cytometer used and fluorescence readout: For this project, we used a flow cytometer equipped with three lasers, for excitation at 490 nm, 561 nm and 630 nm. Based on these constraints, we designed a barcoding system composed of two dyes: Cy3.5 (excitation at 561 nm, fig 2.15b) and Atto633 (630 nm, fig 2.15c). The emission spectra of all 3 fluorophores are overlaid on figure 2.15: There is a slight overlap between Cy3.5 and Cy5 emissions, which might result in fluorescence spillover.

The oligonucleotide binding capacity of the particles is 8 pmol/ μ L of particles stock solution. The converter templates occupy about 0.1% of this capacity, and the reporters 15%, 85% of the streptavidin sites are therefore available for barcoding. Using this 85% of slots, we managed to create 20 distinguishable combinations, as shown on figure 2.16. This number was achieved by using 5 different levels of Cy5 dye (0%, 0.6%, 2.5%, 11% and 35% of the streptavidin sites) and 4 levels of Cy3.5 dye (0%, 2.5%, 12.5% and 50% of the sites). The fluorescence histograms of both channels are also displayed on figure 2.16. Due to saturation, the 35% Cy5 - 50% Cy3.5 subpopulation is slightly less fluorescent in both channels than its unsaturated counterparts. One can also note that, as figure 2.15d suggested, the Cy5-Cy3.5 spectral overlap generates a slight crosstalk between both channels. This is particularly evidenced by the 4 subpopulations that did not receive any Cy5 dye (leftmost clusters): The Cy5 fluorescent signal slightly increases when more Cy3.5 dye is added.

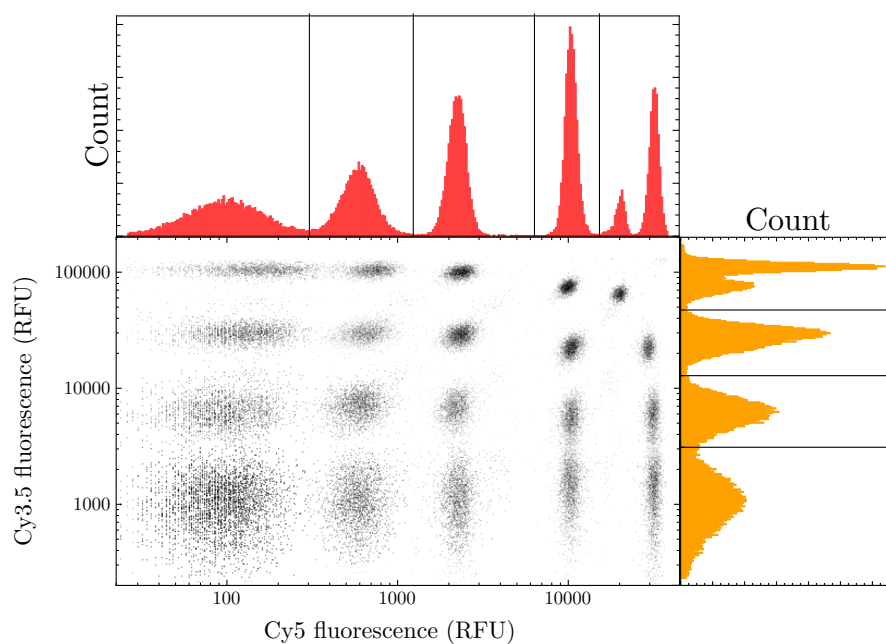
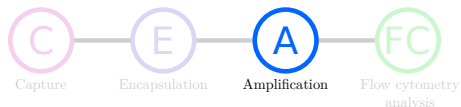


Figure 2.16: Flow cytometry Cy5 vs Cy3.5 fluorescence diagram of a mix containing 20 subpopulations of barcoded particles. The fluorescence distributions of Cy5 (top) and Cy3.5 (right) are also displayed. Due to the saturation of the streptavidin sites on their surface, the particles of the cluster in the top-right corner did not capture all the available fluorescent oligonucleotides. Consequently, this subpopulation is slightly less fluorescent than expected in both channels, although it can still be easily clustered.

2.3 On-particle detection of DNA analogs of miRNAs

2.3.1 On-bead converter template



Our multiplexing strategy, presented in section 1.2.1, requires the grafting of the converter and reporter templates on particles. We will first focus on the design and testing of on-bead cTs. In this process, we used a DNA analog of Let7a as a target. All cTs presented in this section are therefore designed for the detection of Let7a. The sequence of the cT used for our singleplex methods is presented in Table 2.2 (Non biotinylated cT).

Converter type	Sequence (5'→3')
Non biotinylated cT	TGCAGTCCAGAA-GTTTGACTC- AACTATAACAACCTACTACCTCA
Biotin cT	TGCAGTCCAGAA-GTTTGACTC- AACTATAACAACCTACTACCTCA-Biotin
Biotin T7 cT	TGCAGTCCAGAA-GTTTGACTC- AACTATAACAACCTACTACCTCA-TTTTTTT-Biotin
A15 cT	TGCAGTCCAGAA-GTTTGACTC- AACTATAACAACCTACTACCTCA- AAAAAAAAAAAAAAAAA
A30 cT	TGCAGTCCAGAA-GTTTGACTC- AACTATAACAACCTACTACCTCA- AAAAAAAAAAAAAAAAAAAAAAAAAAAAAAAAA

Table 2.2: Sequences of the potential on-bead converters. Green regions: Complementary of the trigger sequence. Violet: Nt.Bst.NBI recognition site. Red: Let7a-specific sequence. Blue: Spacer. Orange: Region allowing coupling to the particle.

In order to be grafted on streptavidin-coated particles, oligonucleotides need to present a biotin on one of their ends. The basic design is therefore to add a biotin on the 3' end of our non biotinylated cT. This design is referred to in Table 2.2 as biotin cT. The immobilization of the cT on the surface of a 1 μm -particle could prevent or interfere with the miRNA hybridization of the miRNA and the action of the polymerase and nicking enzyme on the cT once the target miRNA has been captured. We therefore designed a biotin T7 cT, whose sequence is the same as the biotin cT with the addition of a spacer of 7 thymine residues between the biotin and the miRNA binding site. Alternatively, we designed poly(A) (A15 and A30) cTs. These cTs are not biotinylated, but can hybridize to a T30-biotin oligonucleotide grafted to the particle. This reversible binding allows the release of the cTs once the particle has been encapsulated in a droplet, preventing any interference of the

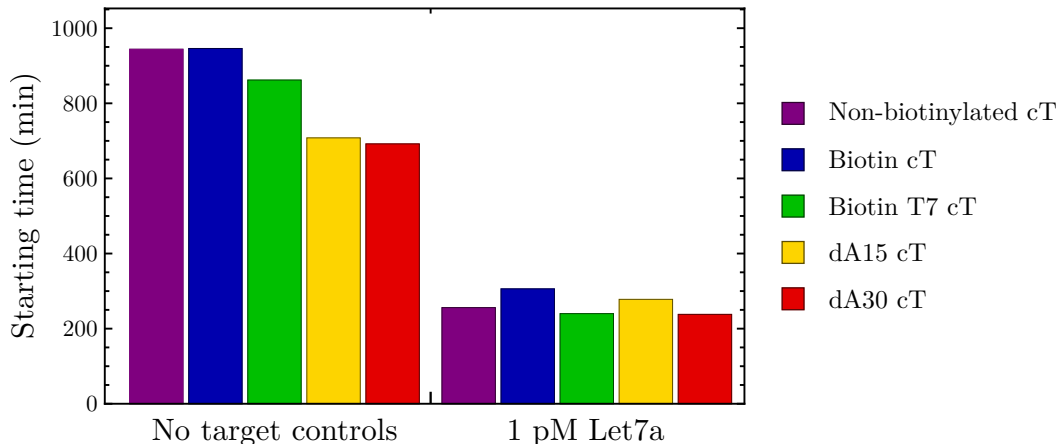


Figure 2.17: Comparison of the on-bead cT designs.

particle in the enzymatic conversion of the miRNA in trigger molecule. These designs were tested by replacing the cTs by cT-carrying beads in a bulk detection. Figure 2.17 compares the incubation time required to trigger amplification for all 4 on-bead designs and the non biotinylated cT when mixed with 1 pM of Let-7a DNA analog. A no target control was also performed to assess the leak-proneness of the cTs.

All designs allowed the detection of the miRNA and display similar amplification times for the Let7a-containing samples. We also notice that both poly(A) designs appear to be more prone to unspecific trigger production than the biotinylated cTs. In order to choose the best cT design, we calculated a score taking into account the speed of conversion and the leakiness:

$$\text{Score} = \frac{\text{Amplification time of the 1 pM sample}}{\text{Amplification time of the no target control}} \quad (2.7)$$

The scores of all designs are presented in Table 2.3. The biotin T7 cT displays the highest score and is therefore the design used in further on-bead experiments.

Converter type	Score
Non biotinylated cT	3.7
Biotin cT	3.1
Biotin T7 cT	3.6
A15 cT	2.5
A30 cT	2.9

Table 2.3: Comparison of the on-bead cTs scores, as defined by equation 2.7

A similar experiment was then performed to optimize the cT concentration. Particles were grafted with 3 different amounts of biotin T7 cT so the final cT concentration in the reaction mixture is 0.5 nM, 2 nM or 8 nM. A no cT control was also performed. Increasing the

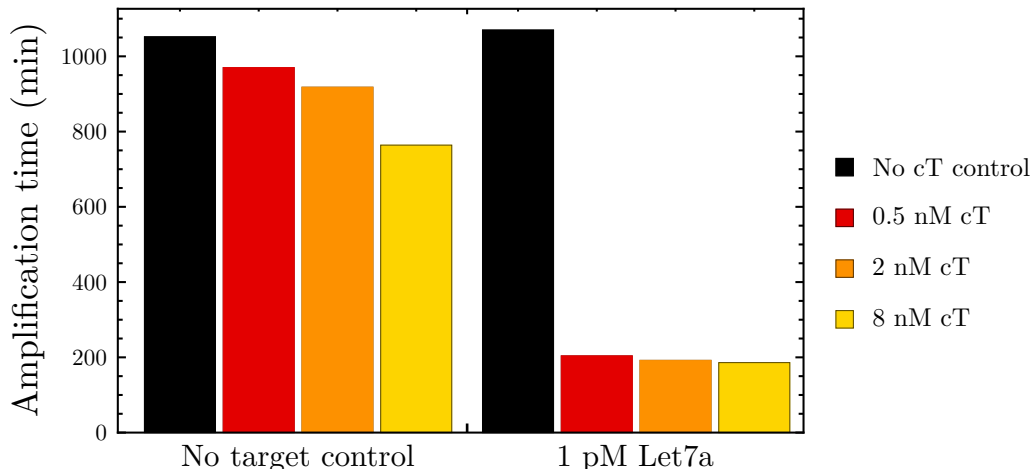


Figure 2.18: Optimisation of the biotin T7 cT concentration. Increasing the cT concentration accelerates both the detection of 1 pM Let7a and the self-start of the system.

cT concentration allows faster detection of 1 pM of Let7a, but slightly increases non-specific trigger production and self-start, as shown on figure 2.18. The 3 concentrations displayed similar scores. We chose a cT concentration of 0.5 nM for further experiments.

As a first step towards multiplex detection, we decided to perform a singleplex detection using immobilized cTs. The rest of the molecular program (aT, pT, rT) remains in solution. This experimental design is similar to that of our previously reported singleplex detection method, the only difference being that the cT is not free in the solution. Since beads do not carry reporter templates, the readout will not be performed by flow cytometry, but by fluorescence imaging of the droplets after the incubation at 50°C. Results are shown on figure 2.19.

First, we observe that part of the particle-containing droplets display red fluorescence, thus indicating that a miRNA was successfully converted and the amplification was consequently triggered. Noteworthy, no droplet containing no particle appears to be positive, which was expected since these droplets should not contain any cT. Algorithmic analysis of the microscopy images shows that 57% of particle-containing droplets were positive, which is equivalent to a concentration of 1,13 pM Let7a, very close to the expected concentration of 1 pM. On-bead conversion therefore appears to be fully functional (at least for DNA versions of the miRNA sequences).

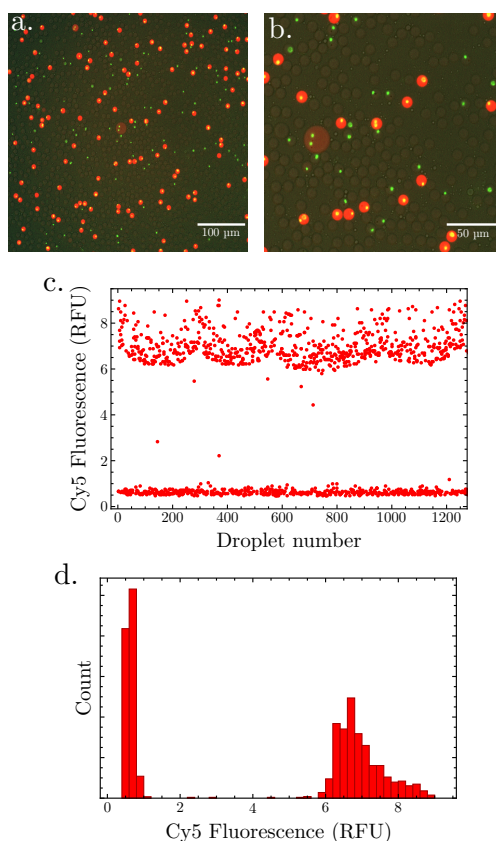


Figure 2.19: Singleplex digital detection of 1 pM Let7a using on-bead biotin T7 cTs. a. and b. Fluorescence microscopy images. The green spots are the particles. c. and d. Fluorescence analysis of the particle-containing droplets. 57% of bead-containing droplets were found to be positive, which is in accordance with the 1 pM Let7a in the original sample (expected: 53%). The variation of fluorescence of positive droplets observed on c. is caused by heterogeneous background light.

2.3.2 Capture time optimization



The conditions of the capture step were also optimized. Since the capture mixture contains all the enzymes and molecular program templates required for amplification, the capture temperature needs to be significantly lower than the amplification temperature (50°C) to avoid triggering the amplification before sample partitioning. We decided to perform the capture at 30°C. Since Dynabeads tend to sediment quickly, the reaction was stirred at 2000 rpm. In order to determine the optimal duration of the capture step, the singleplex digital detection of 1 pM Let7a was performed using various capture durations. The results indicate

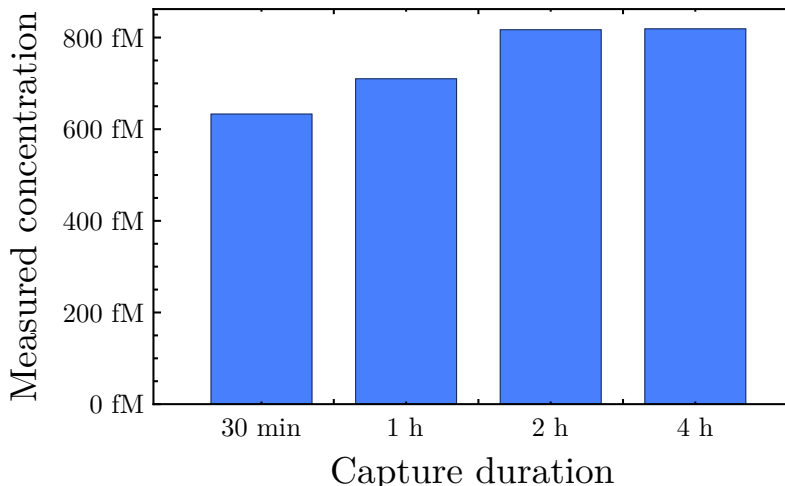
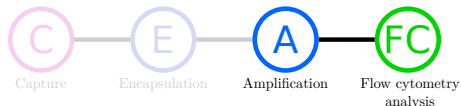


Figure 2.20: Capture step kinetics. A capture duration of 2 hours appears to be optimal, but the differences are small (from 38% positive beads after 30 min to 46% after 4h) and might not be significant.

that a capture step duration of 2 hours appears to be optimal (figure 2.20)

2.3.3 On-bead reporting



The second module of the molecular program that we immobilized on-particle is the rT. The aim is to switch from a fluorescence microscopy readout to a flow cytometry readout. Flow cytometry allows a much higher analysis throughput, as tens of thousands of particles can be analyzed in a few minutes. Flow cytometry is also less expertise-demanding, since the percentage of positive particles is readily available whereas fluorescence microscopy requires the use of complex image analysis algorithms.

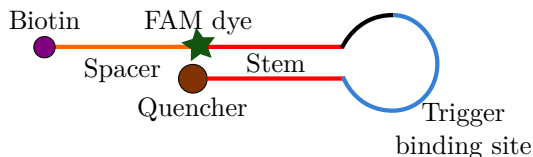


Figure 2.21: Generic scheme of a biotinylated rT. The regions are colored accordingly to Table 2.4. The biotin can either be at the 5' or 3' end.

As the rT is designed to hybridize to the amplified trigger, it is likely that it reroutes a fraction of trigger, therefore inhibiting the autocatalysis. Also, the enzymatic machinery

rT designation	Sequence (5'→3')
rT 1	Biotin-TTTTTTTTTT-FAM- GTGAGAATGCAGTCCAGAATGTCTCAC-BHQ2
rT 2	Biotin-TTTTTTTTTT-FAM- TGTGAGAATGCAGTCCAGAATGTCTCACA-BHQ2
rT 3	Biotin-TTTTTTTTTT-FAM- GTGAGAATGCAGTCCAGAATGTCTCAC-BHQ1
rT 4	Dabcyl-GTGAGAATGCAGTCCAGAATGTCTCAC-FAM- TTTTTTTTTT-Biotin

Table 2.4: rT designs sequences. Color code: Orange: Biotin; Purple: T10 spacer; Green: dT FAM; Red: Stem region; Blue: Trigger binding site; Brown: Fluorescence quencher. Designs 1, 2 and 3 carry the biotin on their 5' end, whereas rT 4 is biotinylated on its 3' end. Design 2 possesses a slightly longer stem region to increase stability of the closed conformation. rT 1 and 3 only differ by their fluorescence quencher.

may be sensitive the dye used. For instance, it as been shown that the FAM fluorophore strongly inhibit the amplification reaction (data not shown). We designed 4 different rTs, displaying slight variations (e.g. the length of the stem, the quencher, etc). The sequences of the rT designs are presented in table 2.4. The reaction-inhibiting effect of each design has been tested by an on-bead bulk detection of 10 pM Let7a. The results are shown on fig 2.22. The rT 4 displays the lowest reaction-inhibiting effect of all designs, followed by the rT 1 design.

The other major factor for the choice of the rT design is the fluorescent signal difference between rTs in closed and open configurations. A high ON signal/OFF signal ratio allows a clearer separation between positive and negative particles, which avoids false-positive events. The ON/OFF ratio of each design was tested by flow cytometry. Results are displayed in table 2.5.

rT design	ON/OFF ratio
rT1	8.2
rT2	2.3
rT3	6.0
rT4	6.6

Table 2.5: ON/OFF fluorescence signal ratios of on-particle rT designs

Based on our experimental data, rT1 and rT4 are the most promising rT designs: rT4 has the lowest reaction-inhibiting effect and an acceptable ON/OFF ratio, while rT1 displays the highest ratio but slows down the reaction. We chose the rT1 design in order to reduce the amount of rT required for a clear negative/positive separation, which leaves more streptavidin

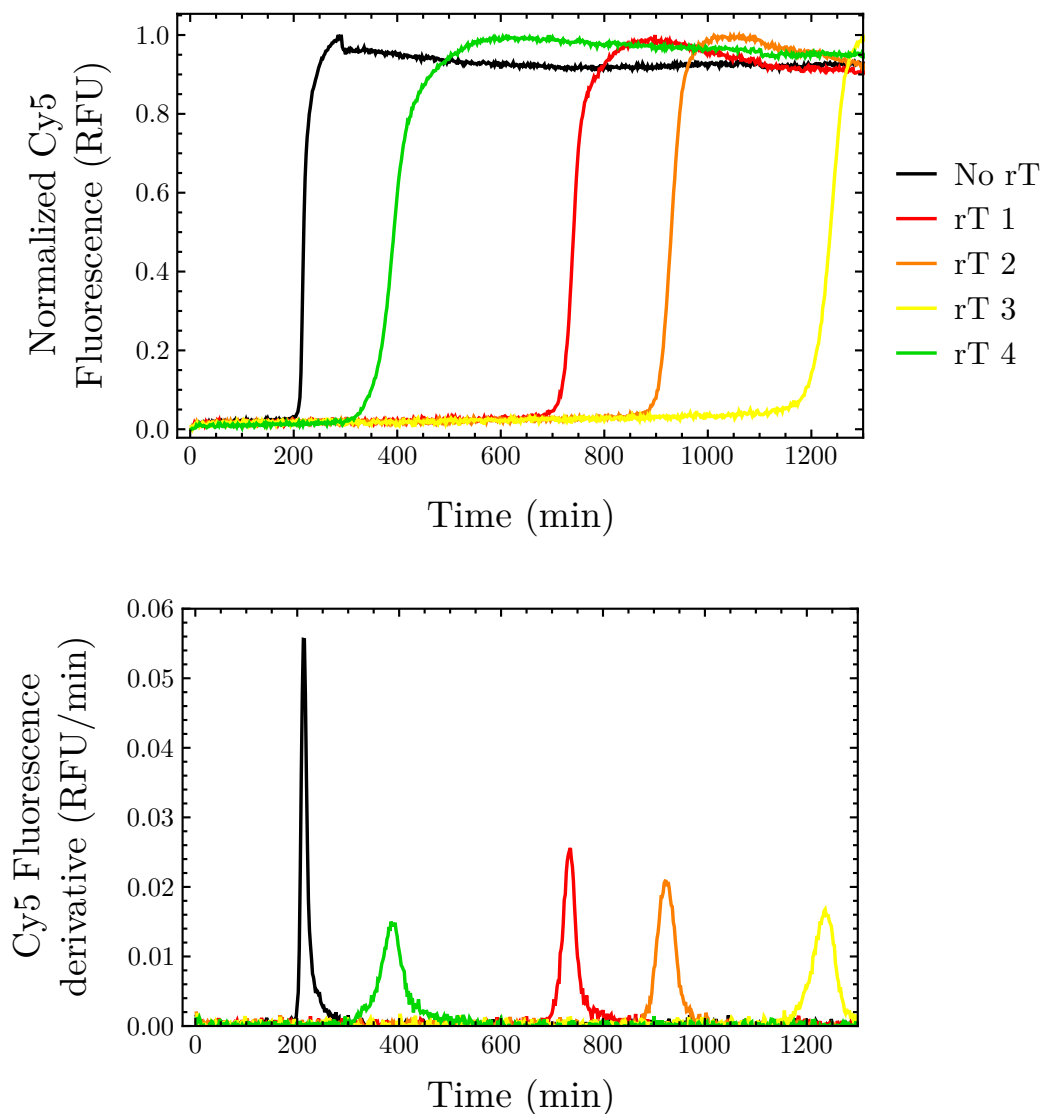


Figure 2.22: Comparison of the reaction-inhibiting effects of rT designs. a. Fluorescence monitoring over time. All 4 rT designs delay the amplification of the bulk reaction. rT4 appears to be the least amplification-delaying design by a large margin, followed by rT1, rT2 and rT3. The shown fluorescent signal is from an orthogonal reporter in solution. b. Fluorescence derivative over time. Although rT4 displays a lower inhibiting effect, the probe opening process appears to be slower than for the 3 other designs.

sites available for particle barcoding and therefore increases the multiplexing potential of the method.

2.3.4 Multiplex detection of DNA versions of miRNAs

We so far showed that our design was functional for the digital singleplex detection of the DNA analog of a miRNA. On-particle cTs are still able to convert the target into trigger strands, and immobilized rT enable the high-throughput readout of the reaction by flow cytometry. Additionally, we demonstrated in section 1.2.3 that we were able to distinguish multiple beads subpopulations using fluorescent oligonucleotides.

As a proof of concept, we therefore performed a 3-plex detection of the DNA analogs of Let7a, miR 92a and miR 203a. Four samples were prepared for analysis:

- A no target control
- A sample containing 1 pM Let7a (DNA)
- A sample containing 1 pM miR 92a (DNA)
- A sample containing 1 pM miR 203a (DNA)

Figure 2.23b compares the reporter fluorescence distributions of the three beads subpopulations for the Let7a-containing sample. As predicted, the proportion of positive Let7a particles was significantly higher than the proportion of positive miR 92a and miR 203a particles. We however notice a strong false positive signal. This is confirmed by the analysis of the no target control (Figure 2.23c). MiR 92a particles were particularly prone to non-specific amplification, with more than 11% false positive particles, which corresponds to a concentration of 150 fM. The LOD of the method therefore appears to be insufficient for the detection of miRNAs at physiologically relevant concentrations, that are usually comprised between a few pM and a few fM[27, 30]. The coencapsulation of particles is a probable promoter of false positive, as the particles tend to aggregate before being encapsulated, resulting in non-poissonian particle distribution. The false positive levels measured in the no target controls were subtracted to the percentage of positive particles in the miRNA samples (Figure 2.23d). Although the detected concentrations are lower than the expected levels (1 pM), in each sample the beads population corresponding to the present miRNA presented a significantly higher percentage of ON particles than the two other populations. The working principle of the method thus enables the multiplex detection of DNA analogs of miRNAs.

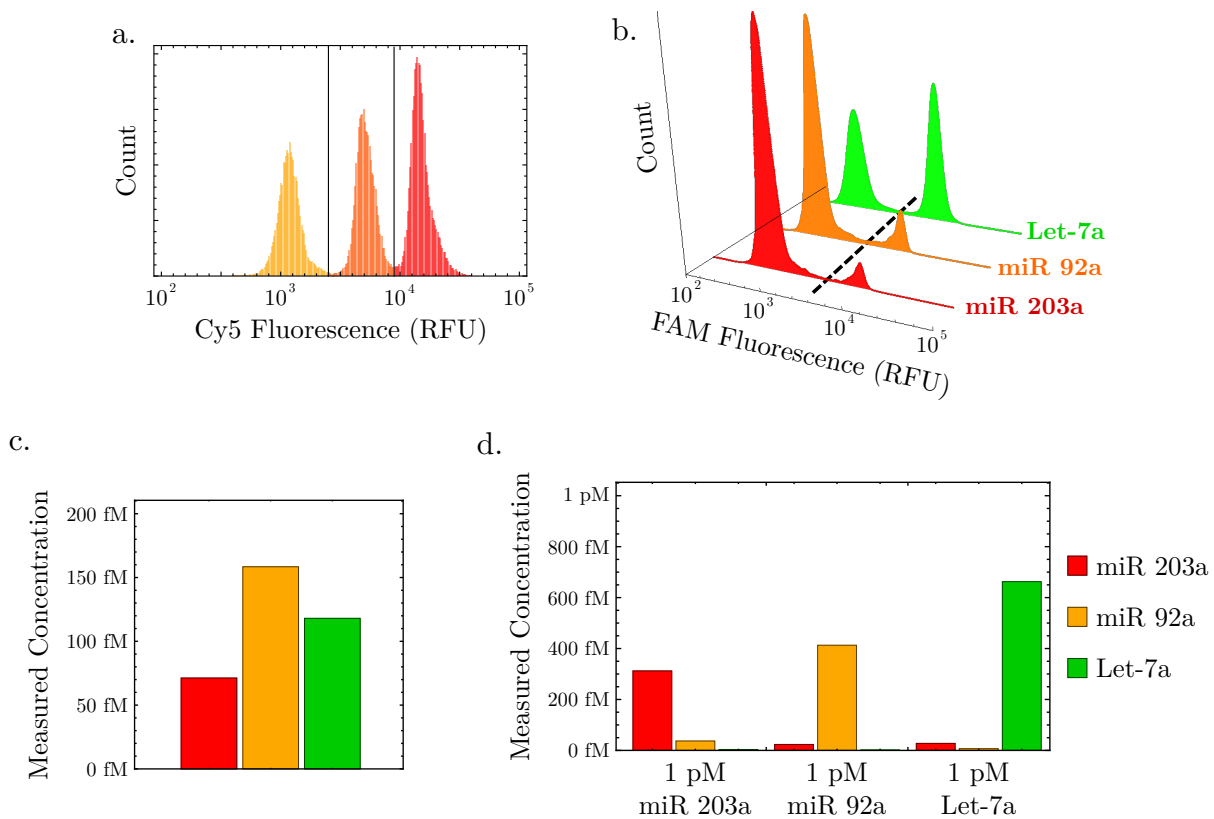


Figure 2.23: Simultaneous detection of 3 DNA analogs of miRNAs. a. Fluorescence histograms of the barcode fluorescence (Cy5). The 3 barcoded subpopulations are clearly distinguishable. b. Reporter fluorescence histograms of all 3 subpopulations in the sample containing 1 pM Let7a. The Let7a-targeting subpopulation has a much higher positive particles proportion. c. Detected concentrations in the no-target control. d. Measured concentrations in the 3 miRNA-containing samples. The false positive percentage from the no-target control was subtracted. Although the detected concentrations are lower than the expected concentrations, in each sample the beads population corresponding to the present miRNA presented a significantly higher percentage of ON particles than the two other populations.

2.4 Chapter summary

Very few of the reported miRNA detection methods combine absolute quantification and high multiplex ability (see chapter 1). The main aim of this project was to develop such an highly sensitive, digital and multiplex approach.

Here, we validate our method for the multiplexed and absolute quantification of DNA analogs of miRNAs commonly dysregulated in cancers. This was achieved using a noise-reducing amplification chemical network composed of 4 tailored DNA templates, based on the PEN DNA toolbox. This molecular program was successfully applied to singleplex or low-multiplex absolute miRNA quantification. The immobilization of part of these DNA templates on functionalizable microparticules, divided in subpopulations targeting one miRNA sequence each, greatly enhanced the multiplexing potential of the method.

In order to perform on-bead miRNA detection, preliminary tests were required. First, the particles were selected and characterized. The best candidates were streptavidin-coated 1 μm magnetic beads. The multiplex potential of these particles was assessed by optimizing the number of barcoded subpopulations. We reached a maximum of 20 particle populations with our equipment, thus setting the maximal multiplicity of the assay at 20 miRNAs, which is much higher than most multiplexed approaches reviewed in chapter 1.

We then designed and characterized converters and reporters adapted to on-bead detection. We first performed on-bead converting, using solution reporters and a microscopy readout, before immobilizing the rT as well and transitioning to a high-throughput flow cytometry readout. Finally, a 3-plex detection of DNA analogs of miR 92a, miR 203a and Let7a was successfully performed as a proof of concept.

This preliminary result on synthetic DNA now needs to be confirmed for the detection of RNA, first in synthetic conditions and then in biological samples. Technical limitations also need to be tackled, most notably the coencapsulation of particles, that generates false positive signal. This problem could be tackled by diluting the particles after the capture step, as presented in chapter 3.

Chapter 3

Particle enzyme scavenging

3.1 Discovery of the effect

The detection process developed in chapter 2 enables the multiplex detection of DNA analogs of miRNA sequences, but still suffers of serious limitations, especially its high percentages of false positive particles, which greatly limits the sensitivity of the technique. This high limit of blank may be caused by two independent effects:

- Non-specific amplification reaction: In spite of the presence of the noise-reducing pseudo template, the chemical amplification network can be non-specifically triggered due to *ex nihilo* polymerization, as is also observed in bulk experiments (see section 2.1.2.). The particle contained in a droplet in which non-specific amplification takes place is detected as positive during flow cytometry analysis. Our main path to reducing non-specific amplification is increasing the concentration of pT, which comes at the cost of reaction speed.
- Particle coencapsulation: As explained in chapter 2, the encapsulation of a non-miRNA-bound particle in the same droplet as a miRNA-bound particle results in the activation of the rTs attached to both particles. The non-miRNA-bound particle is therefore wrongly counted as positive during flow cytometry analysis. This effect is for example evidenced on the experiment presented on fig 2.23, in which the false positive rate is significantly higher for all particles in samples containing any target. The probability of coencapsulation can in theory be decreased by lowering the concentration of particles during the encapsulation step.

Diluting the particles prior to the encapsulation step appears to be the most efficient way to reduce the noise without lowering reaction speed. We therefore decided to implement a post-capture washing/dilution step.

3.1.1 Addition of a washing step

The addition of the washing step presents two main advantages:

- First, this washing should remove any product present in the capture mix that could be toxic to the reaction or promote the self-start of the system. This also may improve the specificity of the system by preventing the partial hybridization of a miRNA to a cT designed for the detection of another microRNA of highly homologous sequence. The washing step is particularly important for the analysis of biological samples, which may contain inhibitors and nucleases.
- Second, it allows to modify the concentration of particles between the capture step and the partitioning step. As explained in chapter 2, both steps follow a Poisson distribution, whose parameters are linked to the concentration of particles (Equations 2.2 and 2.6). Lowering the concentration of particles is beneficial to the encapsulation step, as it theoretically reduces the risk of coencapsulation. Beads dilution can however be detrimental to the quantitativity of the assay, since a very high miRNA-per-particle ratio will result in nearly 100% of the particles being positive, which does not allow accurate quantification. Without a pull-down/resuspension step, the concentration of particles is identical in the capture and partitioning step, forcing us to find a trade-off concentration, which is not optimal for either step. The procedure presented in fig 3.1 allows us to use particles at their optimal concentration for capture, wash and resuspend them in a larger volume to reduce coencapsulation.

The updated procedure is presented on figure 3.1. Contrary to the workflow presented in figure 2.9, the reaction mixture assembly was performed in two steps. First, the detection particles and the miRNA-containing sample were mixed in a preliminary mix, referred to as the capture mix. The capture step was then performed as described in chapter 2. Following capture, a washing step was added. The particles were magnetically gathered and the rest of the capture mix was discarded. The beads were then washed by supernatant discarding/resuspension cycles in the beads storage buffer. The particles were finally resuspended in storage buffer. The final reaction mixture was finally assembled by mixing the resuspended particles with the molecular program and the reaction enzymes. The rest of the procedure was identical to the one presented in chapter 2.

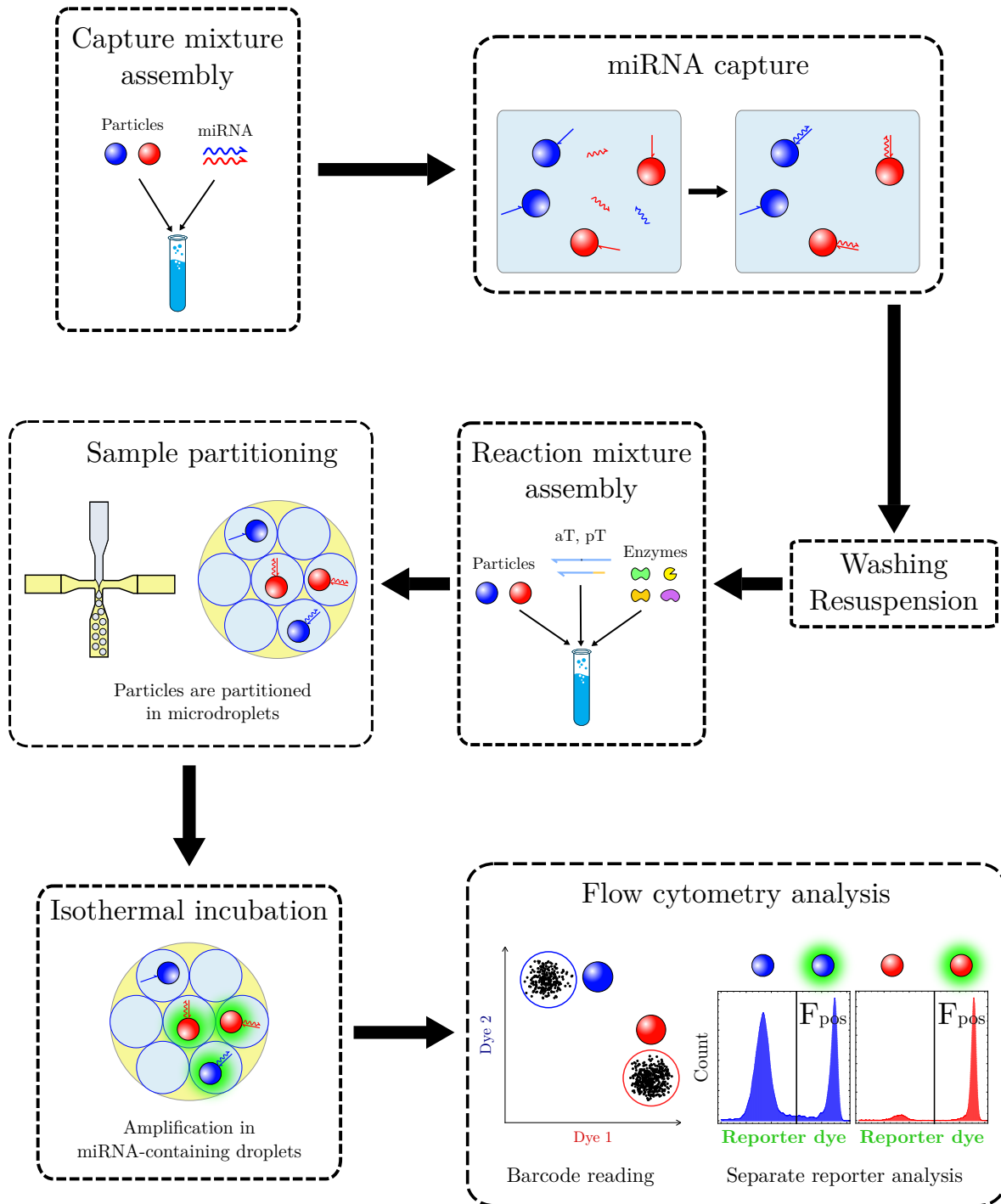


Figure 3.1: Updated workflow with a post-capture washing step. Contrary to the previous chapter, the capture mixture is composed of the miRNAs and the particles only. The enzymes, aT and pT are added once the particles were washed and resuspended. The resuspension of the particles allows us to dilute them in order to avoid coencapsulation. The rest of the procedure is identical to that of chapter 2.

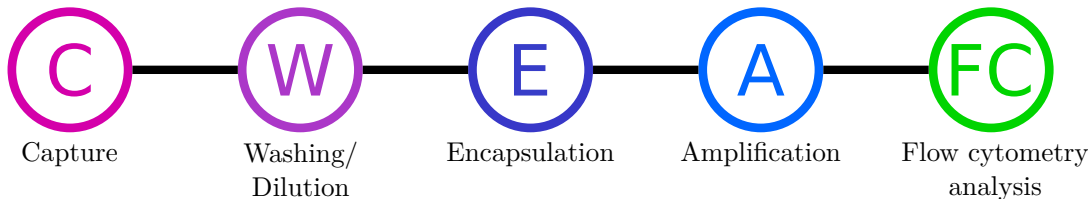


Figure 3.2: Updated summarized workflow

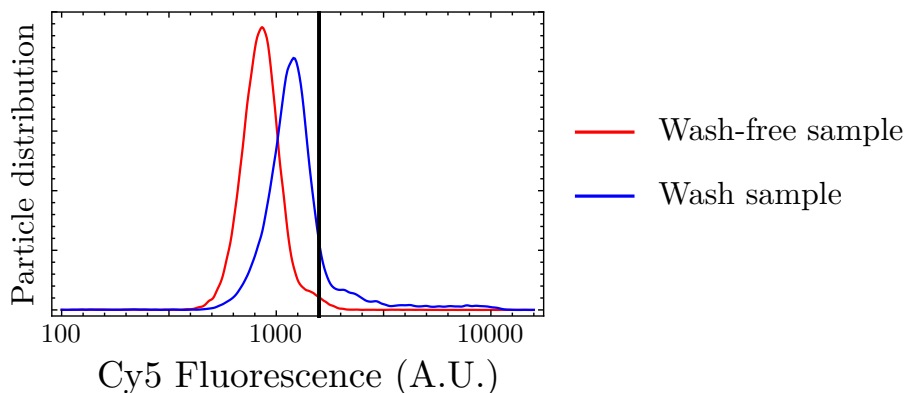


Figure 3.3: Comparison of the reporter fluorescence distribution for particles in no-target controls that underwent, or not, the washing/dilution step. The vertical bar shows the usual limit between positive and negative particles. The proportion of particles in the positive region is much higher among particles that underwent the washing step.

3.1.2 Effect of particles dilution



In order to assess the efficiency of the washing step, we performed the detection of 1 pM of Let7a (DNA version) with and without washing/resuspension. In samples in which the washing was implemented, the particles were finally resuspended in a larger volume to reach a particle-per-droplet ratio of 0.04 for 10 μ m droplets, which theoretically reduces the probability of particle coencapsulation to 0.08%. Figure 3.3 compares the results with and without washing. Surprisingly, the percentage of false positive particles in the no target control is much higher if the particles were washed (10% in the washed sample, 1% in the wash-free sample). The addition of the washing step appears to promote nonspecific amplification.

This effect was further studied by investigating the reaction kinetics whether a washing is performed or not. The results are shown of figure 3.4. In the samples containing 1 pM Let7a, the amplification is triggered faster in the washed sample. After 2 hours of incubation, 19% of the washed particles are positive, whereas only 1% of the beads are positive in the sample

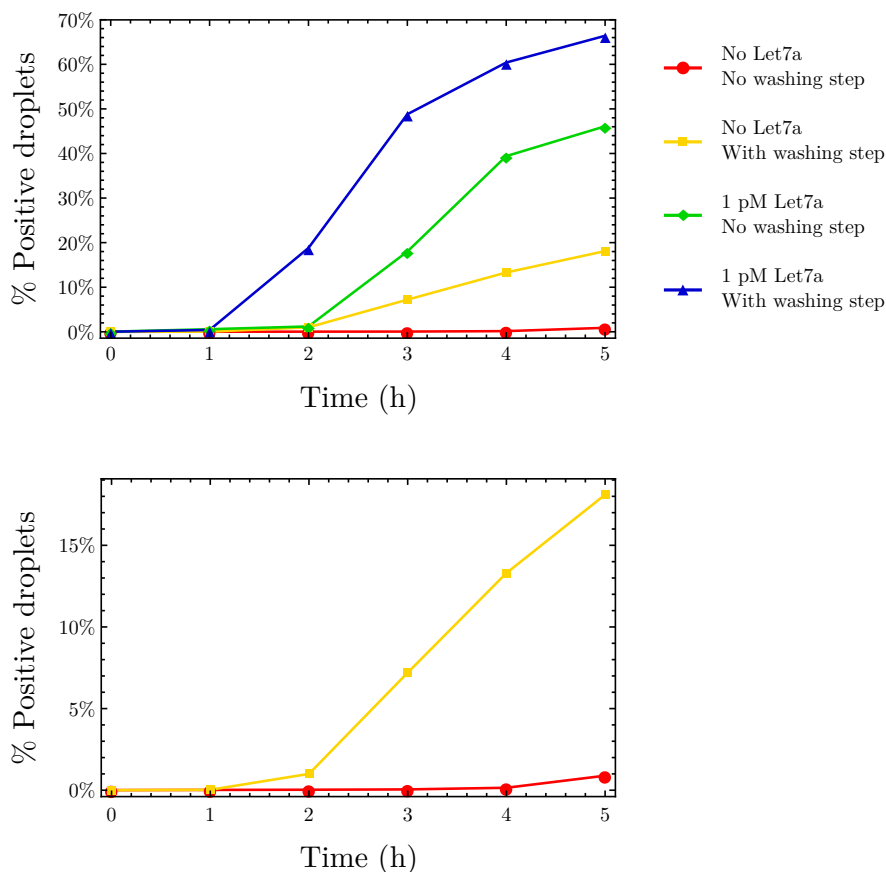


Figure 3.4: Amplification kinetics in samples in which the washing/dilution step was implemented. In the washed samples the amplification is triggered significantly sooner, and the plateau positive rate is higher than washing-free samples.

without washing step. After 5 hours, the percentages tend to stabilize at different levels: 66% with the washing step, 46% without. In these experimental conditions, the expected percentage for 1 pM is 53%. The excess of positive particles in the washed sample is in accordance with the analysis of the no target controls: After 5 hours, 18% of the washed beads turned on, while less than 1% of unwashed particles are positive. The amount of false positive beads in the washed sample appears to increase linearly. An endpoint measurement was realized after an overnight incubation: 59.8% of the particles of the washed sample were positive. The proportion was only 9.6% in the unwashed sample.

As explained earlier, washing the particles consists in gathering the particles, removing the supernatant and resuspending the beads in their storage buffer. It appears very unlikely that the washing itself would promote nonspecific reactions. The final resuspension, however, was so far always used to dilute the particles in order to avoid coencapsulation. If we compare the final reaction mixtures in the procedures described in figures 2.9 and 3.1, their composition

is identical, with the exception of the concentration of particles, that is lower when the washing/dilution step is implemented. Our hypothesis was that reducing the concentration of particles, and thus of cT and rT, while the concentrations of enzymes, aT and pT remained the same would explain the higher rate of nonspecific reactions. We therefore investigated the influence of particles dilution by comparing the percentage of false positive particles in two samples that underwent a washing step, but were resuspended in different volumes.

3.2 Effect characterization: Enzyme depletion experiments

During encapsulation, the content of a solution is theoretically randomly distributed. For the enzymes and in-solution DNA templates, the molecule per droplet ratio is very high (typically 8000 for aT, 1000 for pT), resulting in very similar levels in all droplets. For particles, the ratio is in favor of the droplets (typically 0.1), meaning that most droplets contain either 0 or 1 particle. The concentration of cT and rT is proportional to the number of particles in the droplet. According to this model, the content of bead-containing and non-bead-containing droplets is not modified by the concentration of particles in the pre-encapsulation mix, as can be seen of figure 3.5. This theory is however contradicted by the observations discussed in section 3.1.2.

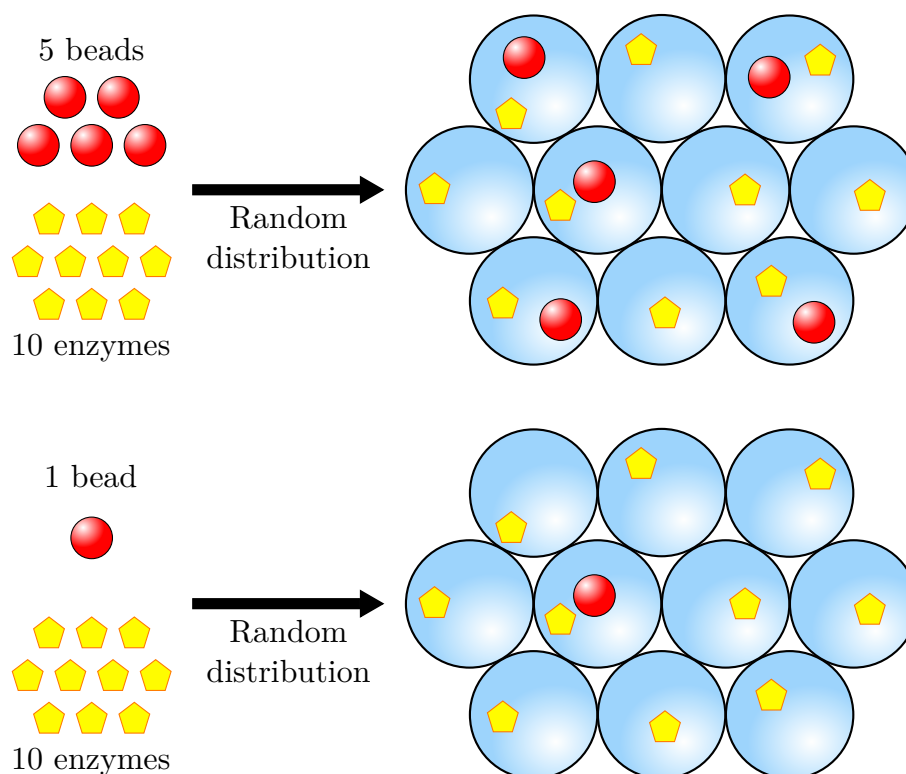


Figure 3.5: Theoretical distribution of enzymes in droplets. The enzymes are equally distributed in bead-containing and empty droplets.

The most probable explanation to the effect of particle dilution is that enzymes and/or free DNA templates distribution is influenced by the presence of a particle in the droplet. Based on the observations of section 3.1.2, our hypothesis was that some of the enzymes used

by the molecular program are attracted and trapped on the surface of the particles, resulting in enzyme overconcentration in bead-containing droplets. If the concentration of particles is lowered, each particle can trap even more enzymes, amplifying the enzyme overconcentration in bead-containing droplets (fig 3.6).

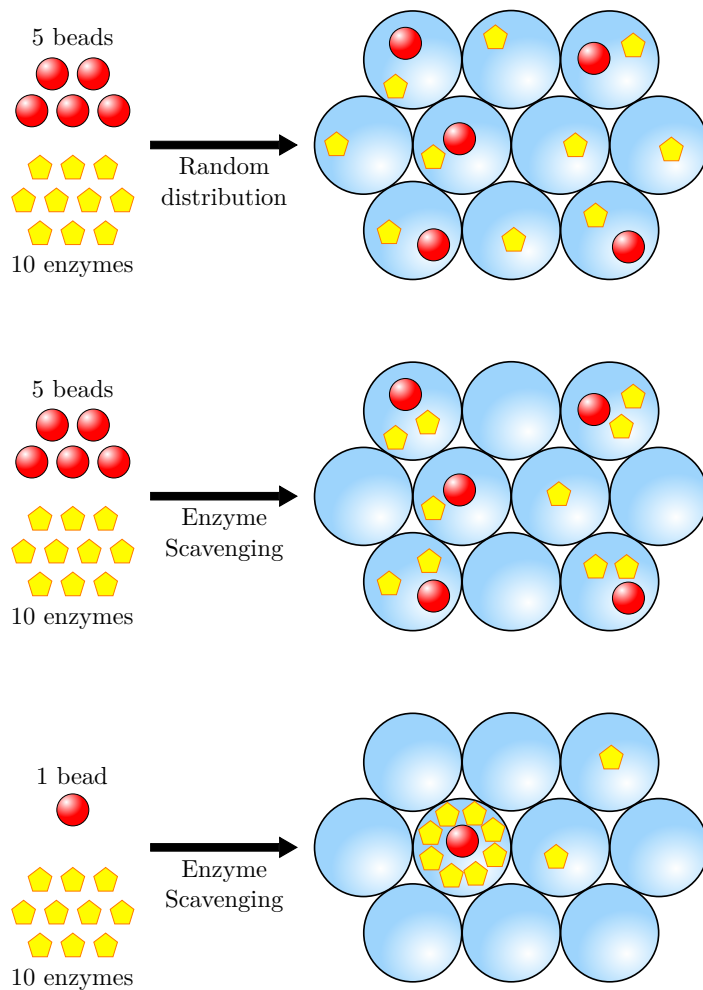


Figure 3.6: Schematic representation of the enzyme scavenging effect. a. Random distribution. b. Enzyme-scavenging effect: Enzymes are preferentially distributed in bead-containing droplets. c. Effect of particle dilution: Less concentrated particles means that one particle can scavenge more enzymes than in undiluted samples. The enzyme concentration in particle-containing droplets is further increased, promoting nonspecific reactions.

In order to validate this hypothesis, the following experiment was designed: A mixture containing all enzymes used by the chemical network at their usual concentrations was assembled and splitted in 3 tubes. One tube was left untouched as a control, while raw particles were introduced in the second tube and rT-coupled (30% of streptavidin sites) particles in the third. All three tubes were incubated at room temperature for an hour, as would typically

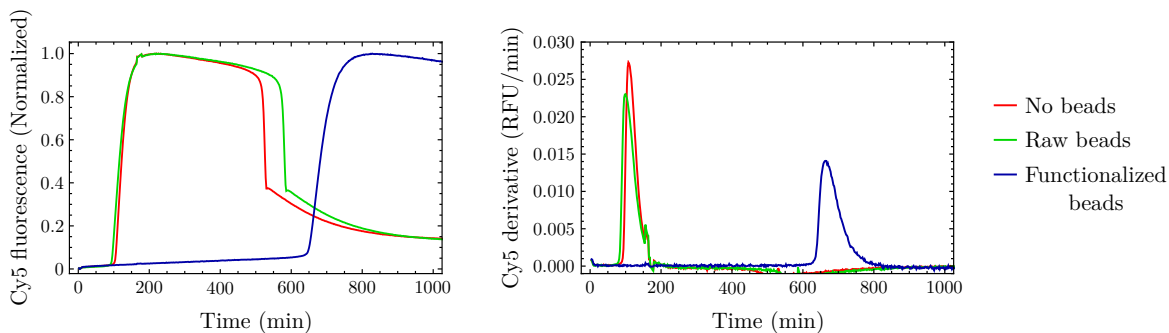


Figure 3.7: Enzyme depletion experiment. a. Fluorescence monitoring over time. The enzyme mixture in which functionalized particles were introduced is not as efficient for detection as enzyme mixtures in which raw particles or no particles were introduced. b. Derivative of the fluorescence. In addition of being late, the functionalized beads sample displays a lower amplification sharpness, also indicating that the sample is enzyme-depleted.

be the case for a reaction mixture awaiting to be encapsulated. After this incubation, the particles are removed. The supernatants were used as an enzyme mix for the bulk detection of 1 pM of Let7a. If the particles indeed trap enzymes on their surface, the supernatant should be depleted in enzymes, and amplification should therefore be delayed or shut down. The results of the experiment are shown on figure 3.7.

The amplification is triggered at the same time in the no particles control and the unfunctionalized particles sample. The amplification is however severely delayed if rT-coupled particles were introduced in the enzyme mix. The enzymes are not captured by the particles themselves, but are trapped by interacting with the on-bead rTs. This is also evidenced by the analysis of the fluorescence derivative (fig 3.7b), that shows a softer amplification in this third sample. The influence of barcodes, that are T5 oligonucleotides coupled to biotin on the 5' end and a fluorophore on the 3' end, was also tested (fig 3.8). The composition of the particles is described in table 3.1.

Particles	rT amount	Barcode amount
rT only	15%	0%
rT and barcode	15%	30%

Table 3.1: Composition of the particles mentioned in fig 3.8

The barcode oligonucleotides also trap the enzymes, which is all the more worrying, given that barcodes can occupy up to 85% of the streptavidin sites of a particle. The effect of converters was not investigated, as cTs are far less numerous than rTs and barcodes (**0.1% of sites**).

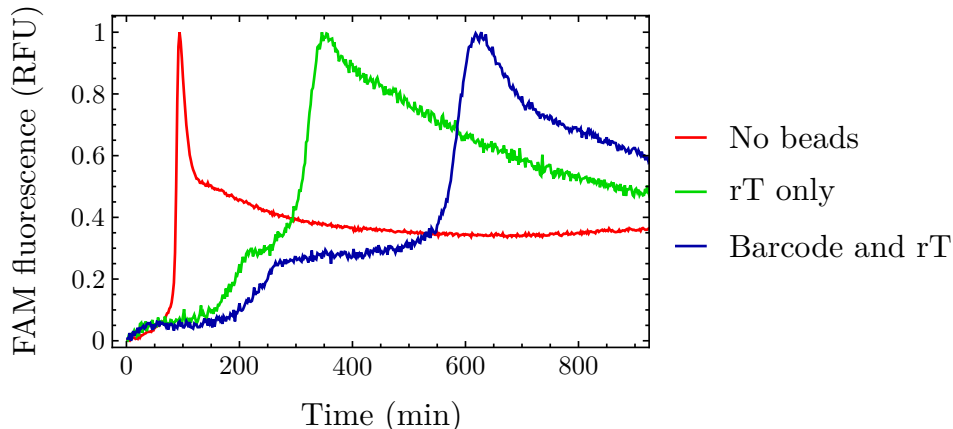


Figure 3.8: Identification of the oligonucleotides responsible for the scavenging of enzymes. Reporter templates and florescent barcodes appear to be equally responsible for enzyme scavenging.

3.3 Proposed solutions

As explained in the previous section, the concentration of particles relatively to the enzymes is of crucial importance. In order to implement the dilution step, which reduces the absolute concentration of particles, without triggering more nonspecific reactions, the obvious solution would be to reduce the concentration of enzymes accordingly. This solution is however highly inconvenient, since the enzymes levels would need to be adjusted depending both on particles concentration and functionalization. This would require extensive crossed calibration for both parameters. We thus investigated 1/ the addition of "neutral" particles, only used to keep a constant particle concentration and not for detection, and 2/ the addition of a second water phase inlet to the encapsulation microfluidic device so enzymes and particles can be introduced separately.

3.3.1 Addition of "neutral" particles



Based on our previous observations, diluting detection particles inevitably results in an increase of the false-positive rate. This may however be avoided by introducing another particle population, not dedicated to miRNA detection, to maintain the overall concentration of particles constant while lowering the detection particle concentration. These particles could therefore act as "enzyme lures", maintaining an enzyme-per-particle ratio that limits the non-specific reaction rates in an acceptable range. The base principle of this approach is pre-

sented of figure 3.9. This class of particles, only dedicated to limiting the enzyme trapping on detection beads, are referred to as neutral particles/beads. Since enzymes are not trapped by the beads themselves but by the oligonucleotides immobilized on their surface, neutral particles were functionalized with the same amount of rT than regular detection beads (figure 3.10).

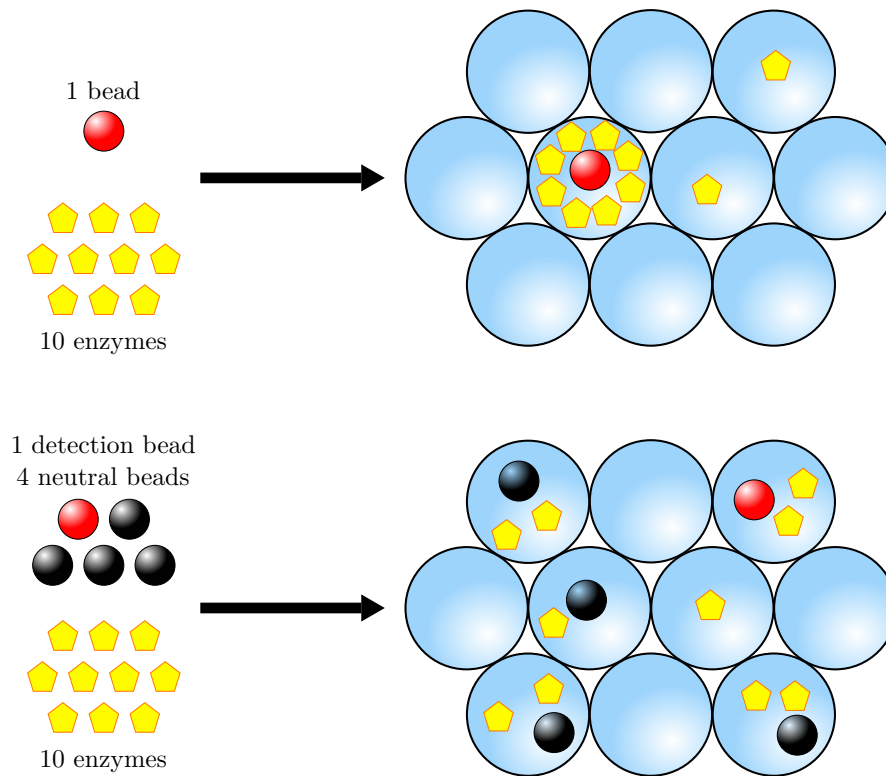


Figure 3.9: Principle of neutral beads. The addition of neutral beads increases the overall particle concentration without modifying the concentration of miRNA detection particles. This maintains an acceptable enzyme-per-particle ratio while also preventing the coencapsulation of detection particles.

In order to determine the optimal amount of neutral particles for noise reduction, a singleplex detection of Let7a was performed with reaction mixtures containing various amounts of neutral particles. The concentration of detection particles was 100.000 beads/ μL in all samples. As observed on fig 3.11, adding neutral particles does indeed reduce the proportion of false positive particles. From 5% of false positive beads without neutral particles, the proportion falls to 0,8% with a concentration of 1.000.000 particles/ μL . This background noise reduction comes however at the cost of severely reducing the reaction speed. The NP-free reaction is completed after 5 hours of incubation only, whereas with 900.000 NP/ μL , the amplification requires an incubation of more than 8 hours.

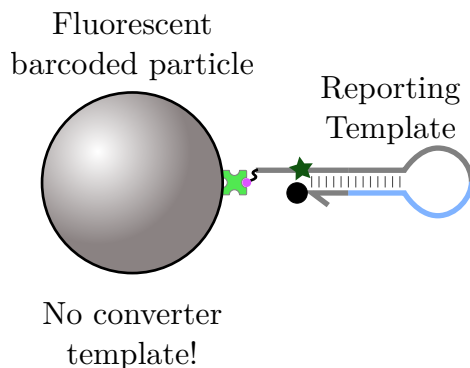


Figure 3.10: Representation of a neutral particle. The only difference between detection particles and neutral particles is that neutral particles do not carry converters.

Although we observed a noise-reducing effect of NP, this effect was too limited to be a realistic strategy. At 300.000 particles/ μL , the false positive rate is slightly below 1%, which was our objective, but the amplification requires approximately 10 hours to complete. In addition, the use of 100.000 detection particles/ μL and 200.000 NP/ μL triples the consumption of particles compared to using detection particles alone. Both of those factors encouraged us to explore alternative solutions to the enzyme scavenging effect.

3.3.2 Modification of the encapsulation microfluidic device



A possible solution to avoid any trapping of enzymes on the surface of the particles is to mix particles and enzymes only a few seconds before sample partitioning. Doing so would allow to optimize once the experimental conditions and use this set of conditions with any particle concentration and functionalization. This also lowers the consumption of particles compared to the "neutral beads" approach.

Assembling the reaction mix right before beginning the amplification is however not sufficient, since the microfluidic partitioning of a typical 25 μL sample requires around 30 minutes, during which enzymes can be captured at the surface of the particles. In order to bring enzymes and particles together shortly enough before encapsulation, the microfluidic system needs to be adapted.

The microfluidic device so far used for the generation of 10 μm is shown on figure 3.12. The device is based on the flow focusing technique. At the nozzle, the pinching of the convergent oil flows forms monodisperse droplets of the water phase (*ie* the sample in our case). This setup possesses a single sample inlet, thus requiring the reaction mixture to

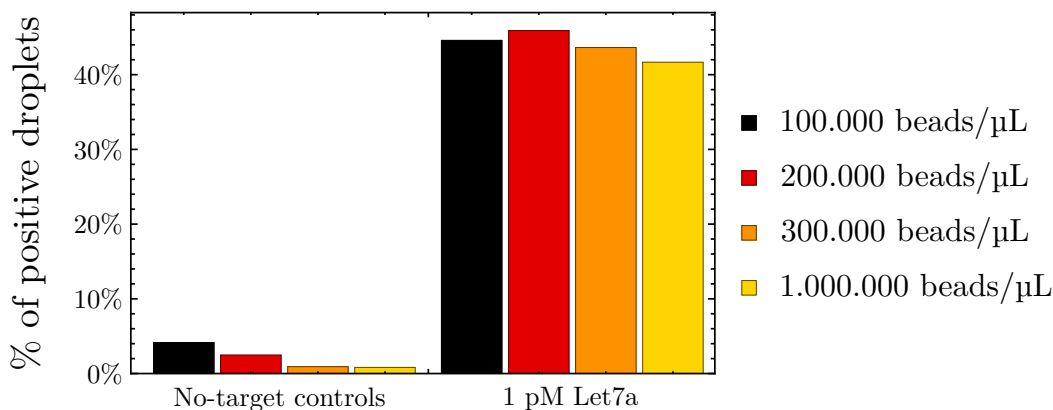


Figure 3.11: Results of the neutral particle range. The concentration of Let7a detection particles is 100000 particles/ μ L in all samples. The concentration of neutral particles in the samples are therefore 0, 100.000, 200.000 and 900.000 beads/ μ L respectively. The false positive rate is lowered by the use of neutral particles, without significantly modifying the positive percentage in the 1 pM samples. Increasing the concentration of particles however slows down the amplification reaction, from 5 hours in the 100000 particles/ μ L to more than 24 hours in the 1000000 particles/ μ L. The false positive rate is much lowered compared to those of section 3.1.2 due to an increase of the amount of on-bead rT, which also slowed the reaction.

be assembled beforehand. Based on the same principle, we designed a microfluidic device displaying 2 water inlets (fig 3.13). This allows the mixing of enzymes and particles at the very moment of encapsulation by splitting the reaction mixture in two pre-mixes, one containing the enzymes, the other the particles and the free DNA templates. The Reynolds number being very low in microchannels, the two converging water flows do not mix before encapsulation, preventing any trapping of enzymes. Additionally, the time interval between flow convergence and encapsulation is very small (less than 1s). This hydrodynamic effect is evidenced by fig 3.14.

This modification of the microfluidic setup came with a reoptimization of the concentrations of the bistable switch templates. The previous set of concentrations was indeed optimized for a reaction in which enzymes were overconcentrated by the enzyme trapping effect. With this effect removed, the rate of specific and non-specific trigger-producing reaction has decreased. The amplification-inhibiting strength therefore needs to be lowered. To that end, the final concentration of pT was adjusted at 8 nM (12 nM previously).

A 3-plex assay was realized using the updated settings. Results are displayed in fig 3.15. The false-positive rates for all 3 miRNAs in the no-target control are low, ranging from 0,6% for miR 16 particles to 1,0% for Lin 4 particles. These low levels were obtained even though the washing/dilution step was implemented, meaning that 2-water inlet microfluidics is a

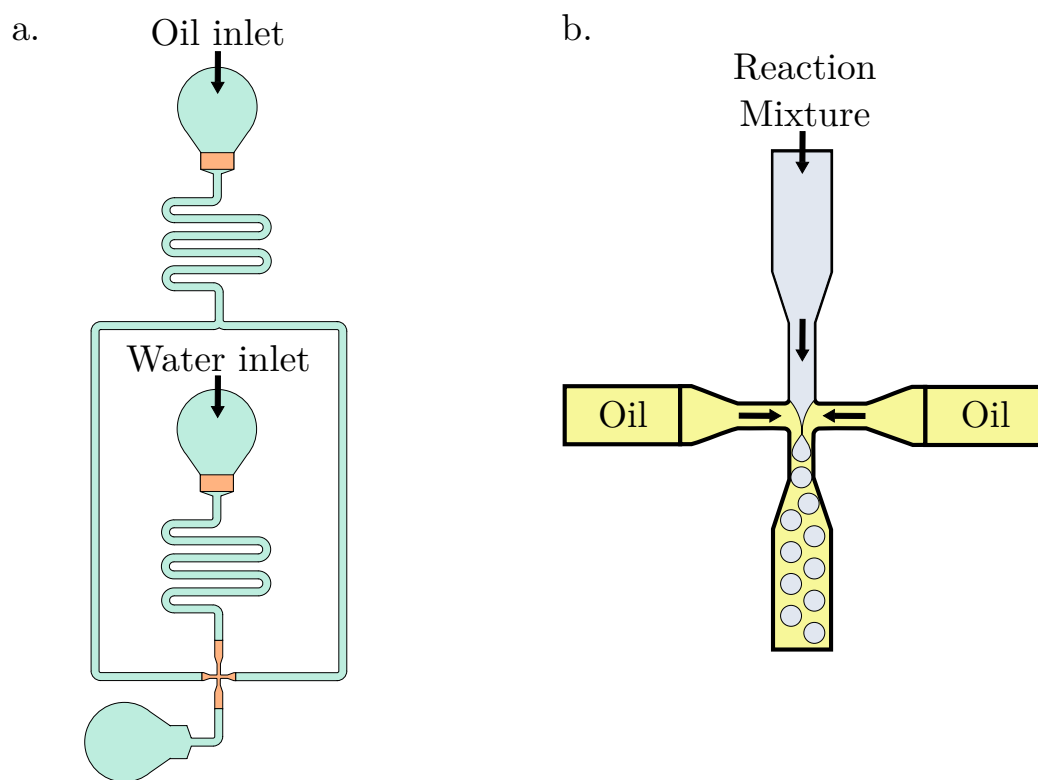


Figure 3.12: Single water inlet microfluidic device. a. View of the whole device. Green parts correspond to a height of $30\ \mu\text{m}$ and orange parts (filters and nozzle) have a height of $7\ \mu\text{m}$. b. Zoom on the nozzle of the device. The water phase, coming from the top, is pinched from both sides by the oil phase, composed of fluorinated oil mixed with supernatant.

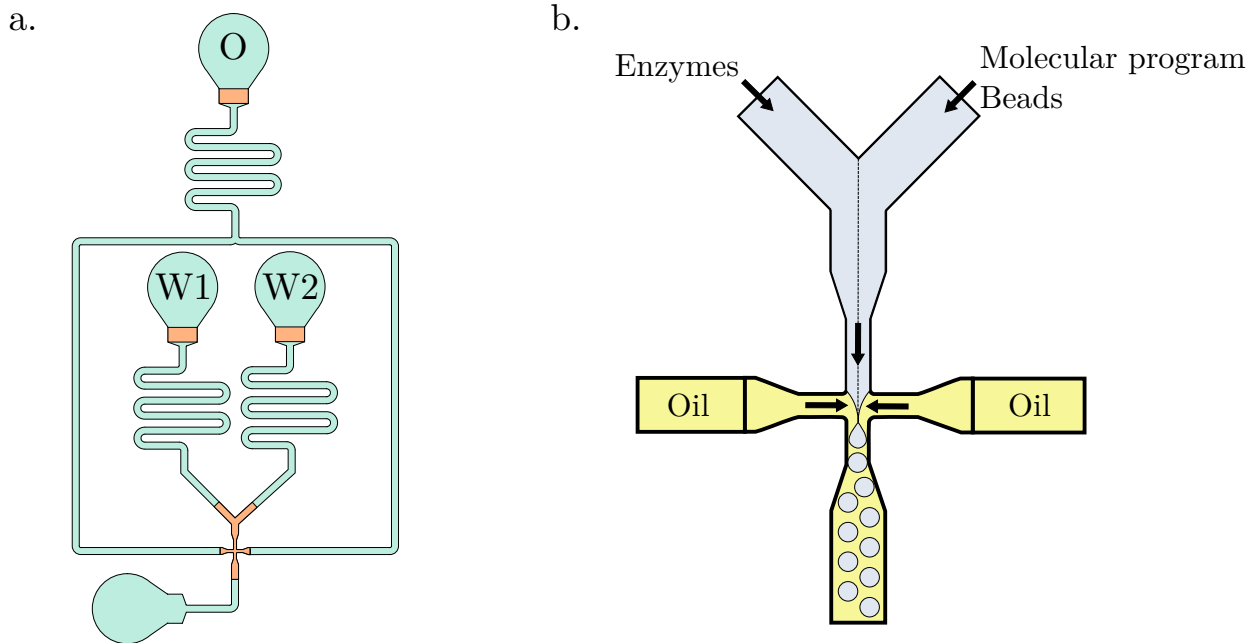


Figure 3.13: Co-flow microfluidic device. a. View of the whole device. As in figure 3.12, green parts are $30\ \mu\text{m}$ high and orange parts are $7\ \mu\text{m}$ high. O corresponds to the oil inlet, and W1 and W2 are the two water inlets. b. Zoom on the nozzle.

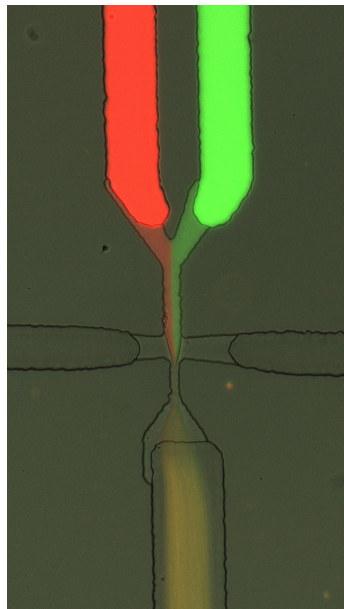


Figure 3.14: Fluorescence microscopy image of the nozzle of the co-flow microfluidic device. Both water phases contained a fluorescent dye. The two incoming water flows do not mix at the channel intersection due to the low Reynolds number in the system, forming a straight interface. The water phases only mix after encapsulation, as evidenced by the orange color of the produced droplets

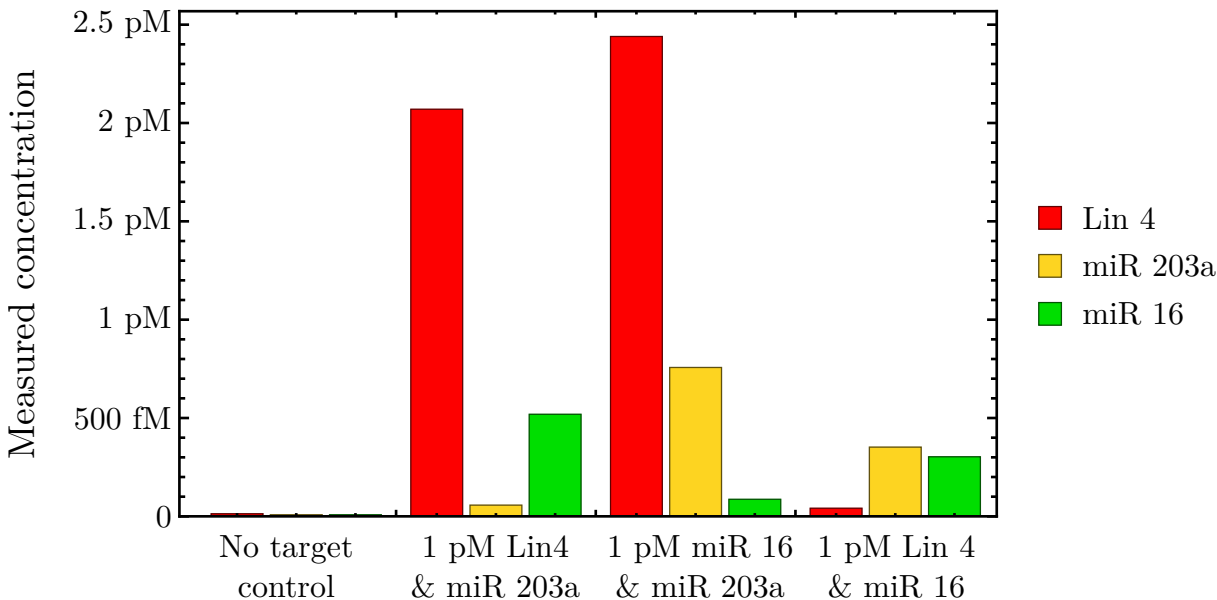


Figure 3.15: Implementation of 2-water inlet microfluidics for miRNA detection. The no-target control displays low false positive rates, from 0,6% for miR 16 particles to 1,0% for Lin 4 particles. Detected concentrations are different from the expected levels, but there is no tendency shared by all miRNAs: Measured concentrations of Lin 4 are above the expected 1 pM in both Lin 4-containing samples, while miR 203a and miR 16 levels are under the expected concentration. This could mean that the differences between expected and measured concentrations are caused by experimental errors rather than inaccuracy of the detection system. This experiment was realized by Alexis Moravic during his internship.

satisfactory solution to the enzyme-scavenging effect. In terms of accuracy, the detected levels are different from the expected levels by factors around 2. The observed differences are however not of the same nature for all miRNAs: Detected amounts of Lin 4 are above 1 pM in both Lin 4-containing samples, while miR 203a and miR 16 levels are below the expected concentrations in relevant samples. This could mean that those differences are caused by experimental errors rather than by an inaccuracy of the system.

3.4 Chapter summary

In this chapter, we introduced an additional washing and dilution step following capture. The objectives of this new step are two-fold:

- Washing the particles following the capture is an important step towards detection from biological samples, which may contain components impeding the detection, for example by destroying targets or inhibiting the reaction.
- The dilution of the particles prior to sample partitioning may reduce the prevalence of coencapsulated particles, therefore lowering the false positive rate.

The introduction of the post-capture washing/dilution step unexpectedly increased the false positive rate. This increase was found to be related to the dilution of the particles, and not by the washing itself. The underlying cause appears to be the scavenging of free enzymes by oligonucleotides immobilized on the surface of particles. We indeed demonstrated that the introduction and removal of functionalized particles in an enzyme-containing solution significantly lowered the enzyme concentration in the solution. Due to this enzyme scavenging effect, enzymes were overconcentrated in bead-containing droplets, disturbing the fine balance of the molecular program and resulting in an increased rate of nonspecific reactions.

This effect was first tackled by compensating the dilution of detection particles with the introduction of neutral particles, only dedicated to maintaining a constant particle concentration. This approach indeed allowed the reduction of the false positive rate, but at the cost of reaction speed and particle consumption.

We therefore elected to suppress the enzyme-trapping effect by not mixing enzymes and particles before the encapsulation. To that end, a new microfluidic device, allowing the separate introduction of enzymes and particles, was designed. Thanks to this device, enzymes were not brought into contact with the particles before the formation of the droplet. This new encapsulation strategy efficiently prevented enzyme distribution heterogeneity, reducing the false positive rate without slowing down the reaction.

Chapter 4

From DNA to miRNA detection

We presented in chapter 2 the multiplex detection of DNA analogs of miRNAs. In this chapter, we present the transition towards the detection of synthetic miRNAs spiked in buffer.

4.1 Introduction: Inaccurate quantification of RNA

The multiplex detection of synthetic miRNAs was implemented using the optimized conditions from chapters 2 and 3. Unless specified otherwise, all the expected concentrations are determined based on ID3miR quantification of the stock aliquots.

Initially, we simply applied these experimental conditions to the 5-plex detection of synthetic miRNAs in their RNA version. During the assay, 5 samples were analyzed, each containing 1 pM of one of the 5 miRNAs. Let7e was introduced in its DNA version instead of RNA in the corresponding sample. The results are presented on fig 4.1.

Close to no miRNA-detection was observed in the samples containing miR 16, Let7c and miR 92a. This is inconsistent with the results obtained with their DNA versions. The system appears unable to detect the RNA versions of these miRNAs. Considering the Let7a-containing sample, contrary to the previous 3 samples, the detected levels of Let7a and Let7e clearly stand out from the background noise. We can thus suspect a specificity problem concerning Let7a and Let7e, since the Let7a strands appear to have been captured indifferently by Let7e and Let7a particles. The combined concentration of Let7a+Let7e is however still significantly lower than the expected 1 pM concentration. This specificity problem appears to be reciprocal, as in the Let7e-containing sample, miRNA strands were captured in similar proportions on Let7a and Let7e particles. In this sample, the Let7a+Let7e concentration is close to the expected level of Let7e. As mentioned earlier, the DNA version of Let7e was introduced instead of its RNA version, which may confirm the observation made for miR 16,

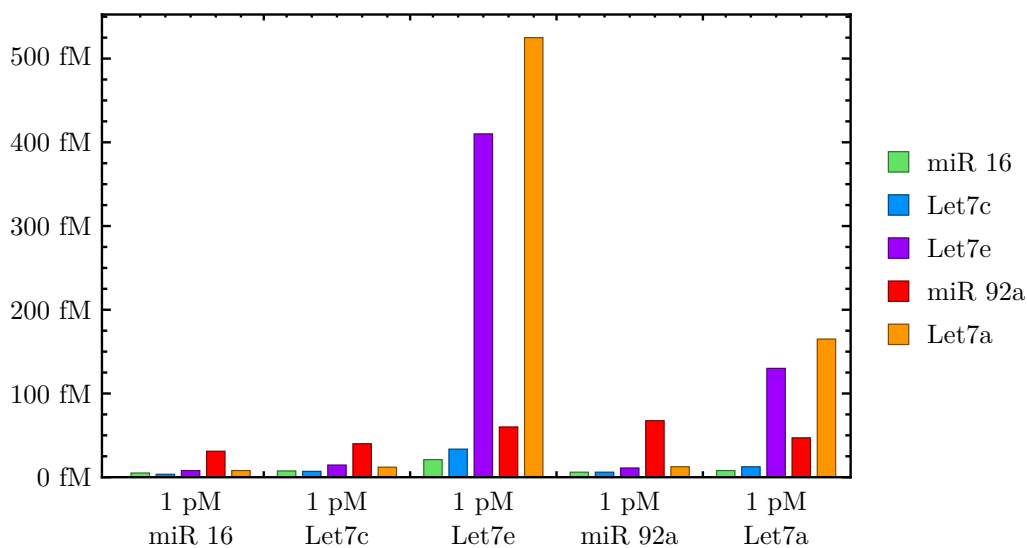


Figure 4.1: Results of the 5-plex assay on RNA versions of miRNAs. The DNA version of Let7e was introduced instead of its RNA version. We observe that in the samples containing Let7c, miR 16 and miR 92a, very low amounts of miRNAs were measured. The system appears to be unable to detect these 3 miRNAs in their RNA version. The detection of the DNA versions of these 3 miRNAs was however accurate. The concentrations detected in the Let7a-containing sample are also lower than the expected level, but stand out from the background noise, contrary to the 3 previously discussed samples. One can note that the system appears to be unable to differentiate Let7a and Let7e. The Let7e-containing sample is the only one displaying a combined Let7e+Let7a concentration that is close to the expected Let7e concentration

miR 92a and Let7c samples that the system does not work as efficiently when detecting RNA instead of DNA.

This hypothesis was tested by performing three singleplex quantifications of both RNA and DNA versions of Let7a. Fig 4.2 clearly shows the discrepancy of the measured concentrations between RNA and DNA versions of Let7a. The detected concentrations of the DNA version are consistent with the expectation, while the concentration of the RNA version is consistently underestimated by the method. The measured concentration of RNA is on average 40% of the expected concentration.

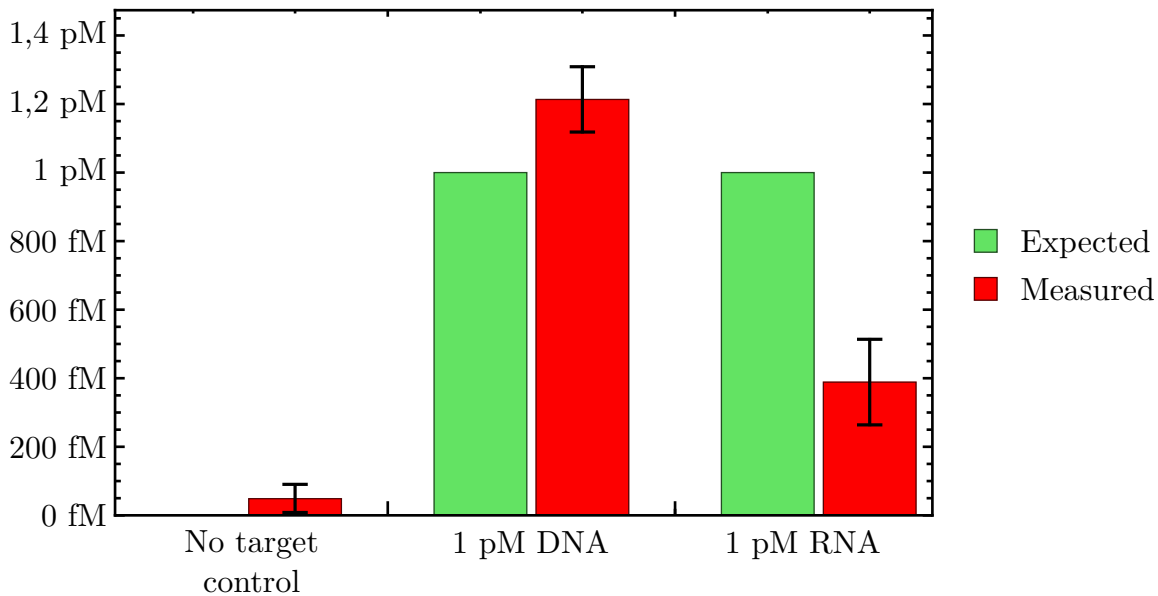


Figure 4.2: Digital detection of Let7a in its DNA and RNA versions. The measured concentration of the DNA version is close on average (1.2 pM) to the expected. The concentration of the RNA version, however, is consistently underestimated, around 400 fM on average. The measured concentrations shown are the average of 3 technical replicates. The error bars represent the standard deviation based on the 3 measurements.

To explain the RNA-specific nature of the lack of quantitativity of the method, our first hypothesis was the presence of RNA-specific nucleases, such as RNase H, that specifically degrades RNA-DNA duplexes. Such miRNA degradation by RNases was already observed during the development of the ID3miR method (Roberta Menezes' PhD). Another possible explanation, based on supplier information, is that the Vent polymerase used for signal amplification elongates RNA primers less efficiently than DNA primers.

We first tried to determine if our experiments were contaminated by RNases. We therefore carried out an on-bead capture step with murine and placenta RNase inhibitors, recovered the particles and performed by a bulk detection reaction. The results, shown on fig 4.3, confirm the observations made previously on digital detection of a lower performance of the system

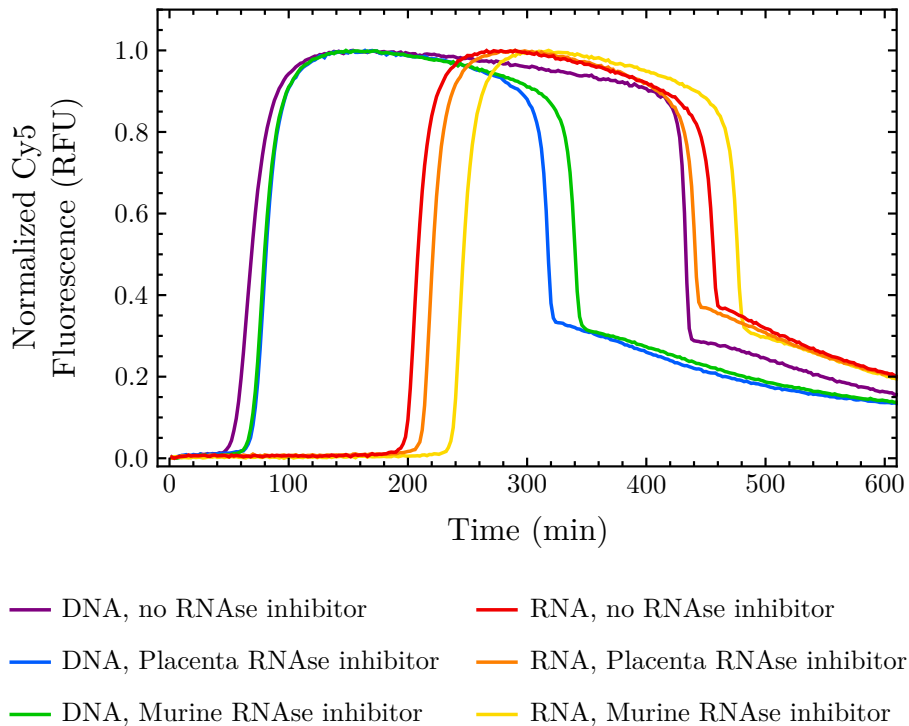


Figure 4.3: Results of the addition of RNase inhibitors during capture. A capture step integrating either murine or placenta RNase inhibitors was performed by a bulk detection reaction. We first observe that RNA samples are overall significantly slower to amplify than DNA samples, which confirms our previous observations. The addition of either RNase inhibitor does not appear to significantly influence the amplification time, indicating that the lower performance of the system towards RNA targets is probably not caused by a contamination by RNases. The sudden drop of fluorescence observed after the first plateau of all curves is caused by the closing of rTs once all dNTPs have been expanded. Adding BsmI to the reaction mixture suppresses the drop by irreversibly cleaving the rTs, as is for example the case on fig 2.6

when quantifying RNA targets. The addition of RNase inhibitors did not decrease the time required for amplification. RNases do not appear to be responsible for the underestimation of RNA targets concentrations.

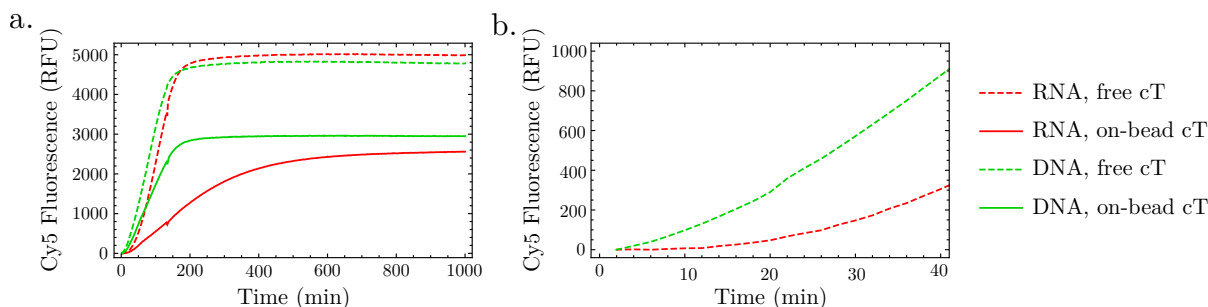


Figure 4.4: Comparison of on/off-bead trigger production rates of cTs when converting DNA or RNA targets. Free cTs and on-bead cTs are mixed with their target sequence, either in its RNA or DNA version, in the presence of Vent polymerase and Nt.BstNBI. A free rT is also introduced to report on the production of trigger. Since there is no aT in the mix, all triggers are produced by the cTs. The variation of fluorescence is therefore directly correlated to the production rate of the cTs. a. Overview of the fluorograms. Free cTs appear to produce trigger from RNA and DNA targets at the same rate. On-bead cTs produce trigger molecules at a lower rate, especially when the target is made of RNA. b. Zoom on the first minutes of the reaction. Although for free cTs the average production rate is the same for RNA and DNA targets, the initiation of the reaction appears to be slower in the RNA sample. This could indicate that the first polymerization, that uses the captured target as a primer, is slowed by the RNA nature of said primer.

4.2 Trigger production rate

The main polymerase used by our team for miRNA detection reactions is the Vent(exo-) polymerase from New England Biolabs (NEB). Although this enzyme worked fine for fully in-solution miRNA detection, the supplier does not recommend the use of Vent polymerase to elongate RNA primers, as is the case in our miRNA detection chemical network. A reduction of the efficiency of the polymerase could very well explain the differences observed between detection of DNA and RNA versions of a miRNA sequence. This hypothesis was tested by the following experiment: Converter templates (either free or particle-bound) are introduced with an excess of miRNA sequence (DNA or RNA version). Vent(exo-) polymerase and Nt.Bst.NBI are added to the mix to allow trigger production from the cTs. Trigger production is reported using trigger-specific rTs. The production rate of trigger sequence is therefore directly accessed by monitoring the rT fluorescence. In order to ensure the production rate is limited only by the efficiency of Vent polymerase, Nt.BstNBI is introduced at higher levels than in typical miRNA detection experiments. Figure 4.4 shows the result of this experiment.

We observe that the slope during the increase phase is significantly reduced when cTs are immobilized on particles, suggesting that cT immobilization slows down the trigger production by the polymerase down. Trigger production rate appears to be further reduced when

the detected primer is made of RNA. When the cT is in solution, however, this reduction is no longer observed. Focusing on the very first minutes of the experiment for both free-cT samples still reveals a slower start to the trigger production for the RNA target, even though the maximal rates in solution are similar for RNA and DNA. This could be interpreted to be caused by a slower first elongation of a RNA target. In order to perform the first elongation, the polymerase uses the captured target as a primer, whereas for the subsequent elongations the primer is composed of the target and the 9 bases of the Nt.BstNBI cutting site, which are made of DNA.

These observations support the hypothesis of a lower efficiency of the Vent polymerase when working from RNA primers. This reduction of the productivity of Vent appears to be mild and limited to the first elongation reaction when the cT is in solution, which explains why this characteristic was not causing quantitativity issues to the ID3miR system. The effect appears to be severely enhanced and affects both initiation and further polymerization cycles when cTs are immobilized on particles, resulting in the underestimation of the concentration of RNA targets.

4.3 Proposed solutions

4.3.1 Addition of Klenow polymerase



A possibility to solve the lower efficiency of Vent polymerase when working on RNA primers is to use another polymerase better suited to the elongation of RNA primers. DNA pol I, large Klenow fragment (referred to as Klenow polymerase in the rest of this thesis) appears as a promising polymerase to complement Vent(exo-). This enzyme is derived from *Escherichia coli*'s DNA pol I, and retains polymerase activity while lacking the exonuclease activity of the original enzyme. According to the supplier (NEB), Klenow polymerase elongates RNA as well as DNA primers, which is the main feature we are looking for. Its optimal working temperature being 37°C, and its half-life at 50°C is approximately 60 minutes. Klenow polymerase is therefore not a suitable solution for fully replacing Vent polymerase, which is perfectly stable at 50°C. Klenow can however efficiently complement Vent by accelerating the initiation of the reaction.

This decay of Klenow polymerase at 50°C can be used to our advantage. The main objective of Klenow is indeed to perform the conversion of the miRNA to trigger molecules more efficiently than Vent. Once the amplification is triggered, Klenow loses its usefulness, as Vent polymerase can perform the exponential amplification on its own. During the amplification, Klenow could even be detrimental to the detection since it is more prone to nonspecific reactions than Vent. If its concentration is tuned correctly, the decay of Klenow could theoretically improve the speed and specificity of the system, by rapidly triggering the amplification in miRNA-containing droplets while its degradation prevents Klenow from contributing to late, nonspecific amplification.

In order to assess the effectiveness of Klenow polymerase to increase the production rate, a similar experiment as the one presented on fig 4.4 was performed with part of the Vent polymerase substituted by Klenow polymerase. Results of this experiment are presented on fig 4.5.

We observed that the addition of Klenow polymerase increased the trigger production rate of the cTs, even when converting a RNA target. The production rate from RNA in the Klenow-containing sample is even higher than the no-Klenow rate for DNA. This observation implies that the addition of Klenow polymerase should restore the quantitativity of the assay for RNA targets. Klenow however appears to also increase the production rate in the no-target control, which may increase the false positive particles rate. It is also worth noting that Klenow polymerase does not remove the delay observed in RNA samples caused by the

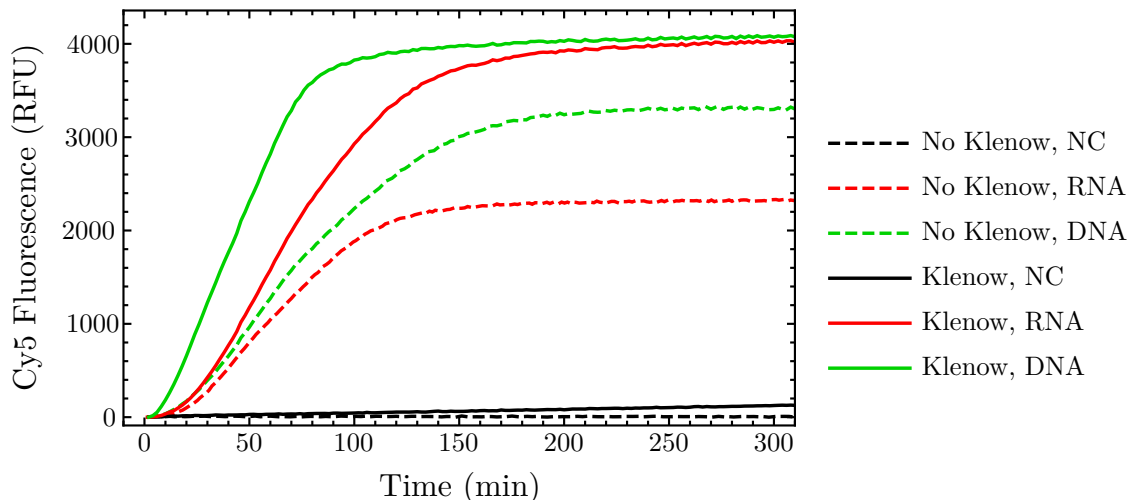


Figure 4.5: Comparison of the trigger production rates from RNA and DNA with or without Klenow polymerase. NC stands for negative control, meaning no target was introduced. Klenow significantly increases the slope, and thus the production rate, for both DNA and RNA targets. Noteworthy, the delay of production from RNA observed in fig 4.4 and attributed to a slow first elongation is still observed. In no-target controls, the production rate in the Klenow-containing sample is much higher than in its no Klenow counterpart. Klenow polymerase could therefore cause an increase of the false positive rate.

first target elongation.

We then assessed the optimal concentration of Klenow polymerase to maximize the reaction rate while maintaining a low background noise. An on-bead bulk detection was performed, integrating different concentrations of Klenow polymerase: 0% (v/v), 0,25% (12,5 units/mL), 0,5% (25 units/mL) and 1% (50 units/mL) were introduced. The results are presented on figure 4.6. As expected, increasing the concentration of Klenow polymerase increases the rate of the reaction, as observed in the sample containing 1 pM Let7a. This acceleration comes at the cost of also increasing the non-specific reaction rate: The two highest Klenow concentrations triggered amplification in the no-target control. Noteworthy, the effect described previously, relying on Klenow’s decay to accelerate the specific amplification without triggering non-specific amplification, may be responsible for the huge difference observed in the no-target controls between amplifying (amplification before 300 minutes) and not amplifying (nothing after 2000 minutes) samples.

We then tested the effect of Klenow polymerase in digital detection reactions. The result of this experiment is presented on figure 4.7. The detected amount of Let7a (RNA version) in the 1 pM sample without Klenow polymerase is about 50 % of the detected amount with 0,25 % of Klenow, which is consistent with the expected/measured differences observed on fig 4.2.

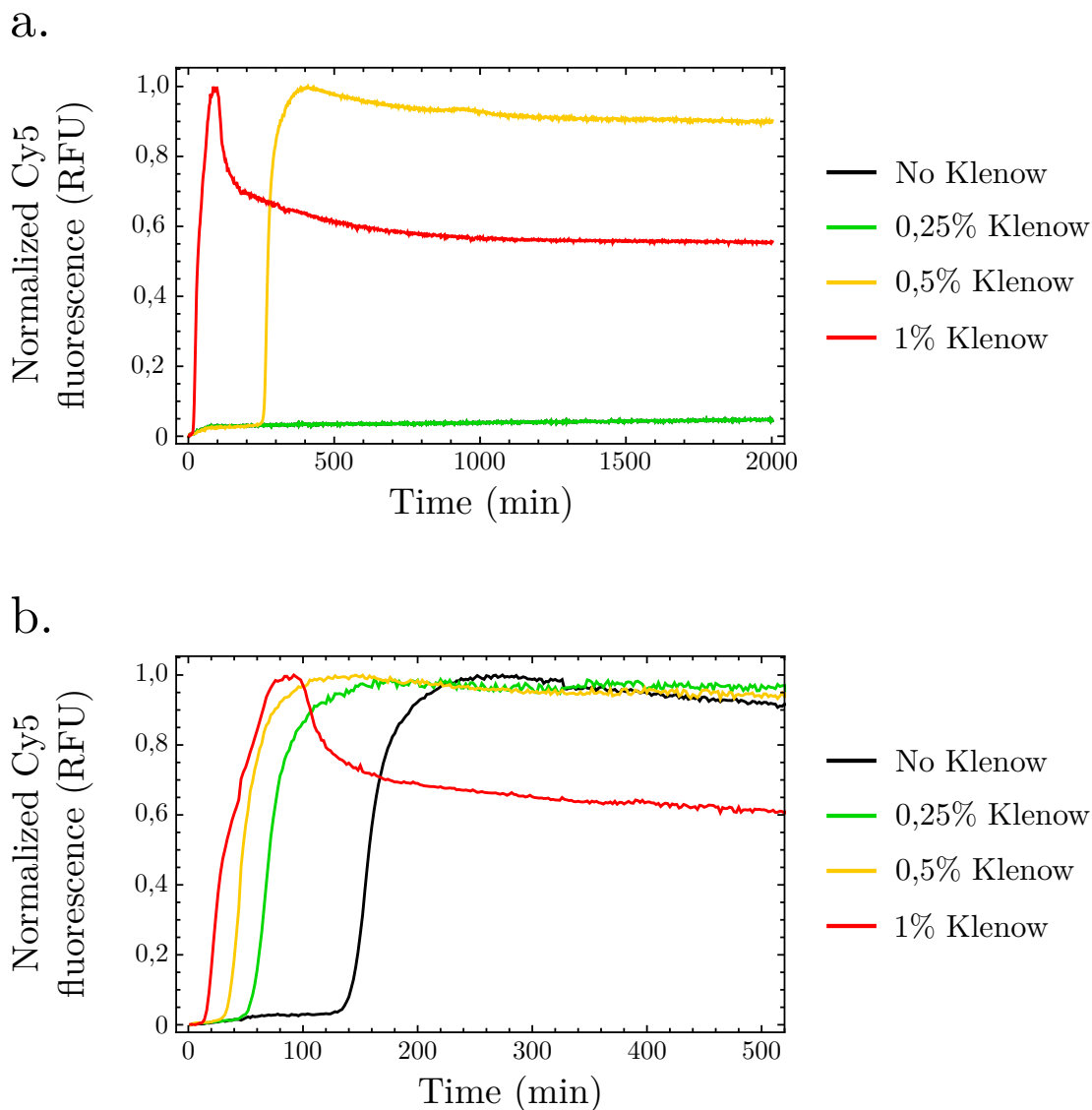


Figure 4.6: Range of Klenow polymerase in bulk detection reactions. a. No target controls. Non-specific amplification was observed for the two highest Klenow percentages. b. Samples containing 1 pM Let7a. The addition of Klenow polymerase indeed increases the reaction speed. The optimal concentration appears to be 0,25% (12,5 units/mL). Percentages are volume-per-volume percentages.

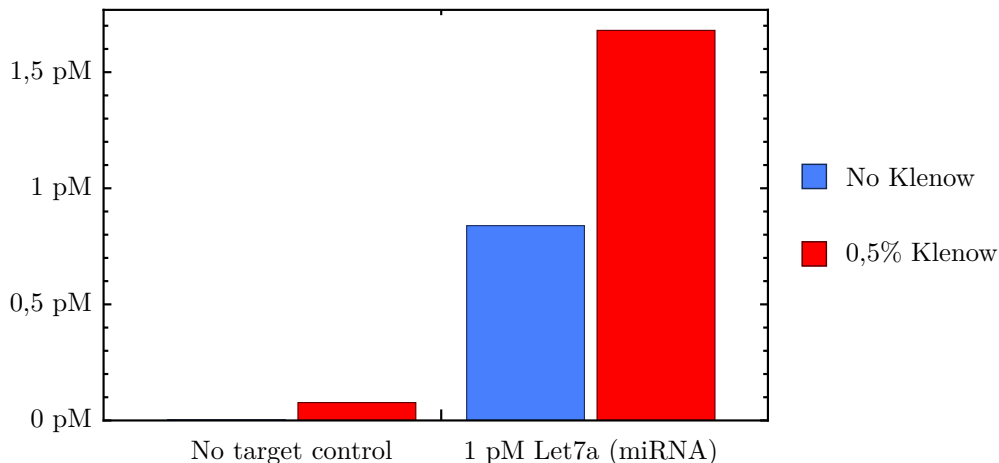


Figure 4.7: Effect of Klenow polymerase during the amplification step. The detected concentration in the Let7a-containing sample is indeed higher, but at the cost of a much higher rate of false positive particles.

4.3.2 1 dNTP capture step



As already discussed, the first elongation of the capture miRNA appears to require much more time than subsequent elongations. Consequently, we tried to introduce the Klenow polymerase during the capture step only. Klenow would then be removed during the washing/resuspension step, which would prevent the Klenow-induced nonspecific reactions. Since Klenow polymerase optimal working temperature is 37°C, the capture temperature was adjusted accordingly, from 30°C to 40°C.

Even when introduced only during the capture step, Klenow polymerase increases the false positive rate. Our hypothesis is that Klenow polymerase manages to "load" cTs *ex nihilo*. A "loaded" cT will act exactly the same as a miRNA-bound cT.

In order to circumvent the *ex nihilo* synthesis by Klenow polymerase on cTs, a new class of converters are designed, displaying a poly(T) spacer between the miRNA binding site and the Nt.BstNBI recognition site. These cTs would be employed in a capture mix containing only dATPs instead of all 4 dNTPs. In the absence of the target miRNA, *ex nihilo* polymerase reactions can only generate poly(A) strands, the length of which is equal to the length of the poly(T) spacer. A short spacer would therefore generate short poly(A) strands, with a melting temperature well below the capture temperature of 40°C. These short strands would thus melt away of the converter, preventing nonspecific reactions. On the other hand, if the miRNA is indeed captured, it will be extended, strengthening the hybridization to the

converter. Moreover, the first elongation might be favored, since the Vent polymerase will not extend the miRNA directly, but the poly(A) spacer. The efficiency of this new design was first tested in a production rate experiment. A capture step was performed in presence of Klenow polymerase and particles functionalized with cTs presenting poly(T) spacers of various lengths. Particles were then recovered, washed and incubated with Vent polymerase, Nt.BstNBI and a free rT. Results are presented on fig 4.8. The experiment shows that the addition of a poly(T) spacer as short as 5 nucleotides increases the trigger production rate of the converter when compared to the no-spacer cT. The length of the spacer, from 5 to 20 bases, does not modify the production profile nor the maximal production rate. The poly(T) spacer cTs may be a solution to the lower efficiency of Vent polymerase when working from RNA targets.

The poly(T) cT designs were then implemented in an on-bead digital detection. The results of the digital detection of 1 pM of Let7a (RNA version) are shown on fig 4.9. The detected concentrations for the T5 and T15 designs are in good accordance with the expected 1 pM Let7a, while the T10 cT reports a Let7a concentration of just over 300 fM. Although surprising, this underestimation of the concentration by the T10 cT was observed in several further experiments (data not shown). Looking at the no-target control, there is a clear difference between the false positive rates observed for T5 and T10 cTs (0,88% and 0,90% respectively) and the rate for the T15 cT (3,39%). This can possibly be explained by the melting temperatures of poly(A)/poly(T) duplexes of 5, 10 and 15 base pairs. The melting temperature of a 15-base pair duplex is around 30°C, and the capture step is set to be performed at 40°C, but the actual temperature is most reasonably comprised between 35°C and 40°C. A small portion of the poly(A) produced *ex nihilo* by Klenow polymerase may therefore not melt away and are still present during the 50°C amplification step, triggering the amplification in the droplets containing them. This is not the case for 5- and 10-base pair duplexes, which display lower melting temperatures and/or priming efficiency. The converter design with a 5 bases-long poly(T) spacer appears to be the best candidate for accurately quantifying a miRNA in its RNA version while maintaining a low background noise level. This design is the one used in all further experiments.

The same experiment was realized on miR 21 instead of Let7a to confirm that the observations made for Let7a can be translated to other miRNAs. Fig 4.10 shows the results of the experiment, that are almost identical to those of fig 4.9. The optimal cT design for miR 21 detection also appears to be the T5 design.

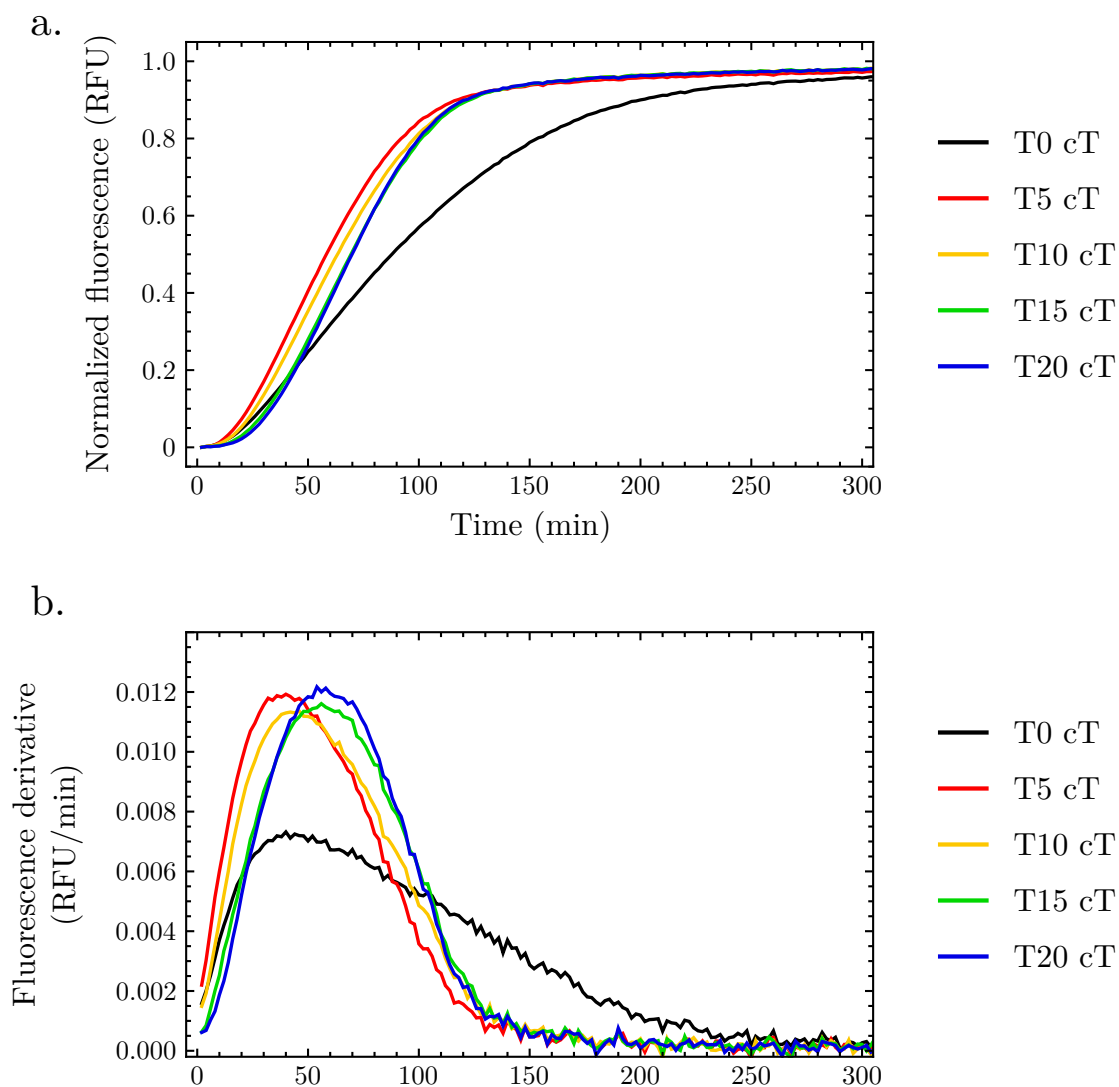


Figure 4.8: Evaluation of the trigger production rate by poly(T) spacers cTs after Klenow capture. a. Evolution of the fluorescence during incubation. All cT designs integrating a poly(T) spacer display similar profiles of trigger production, with rates significantly higher than the no-spacer design. The addition of just 5 bases between the miRNA-binding spot and the Nt.BstNBI cutting site appears sufficient to facilitate the Vent-only conversion of RNA targets. b. Time derivative of the fluorescence. The maximal rates are almost identical for all poly(T) cTs, almost twice as high as the T0 cT.

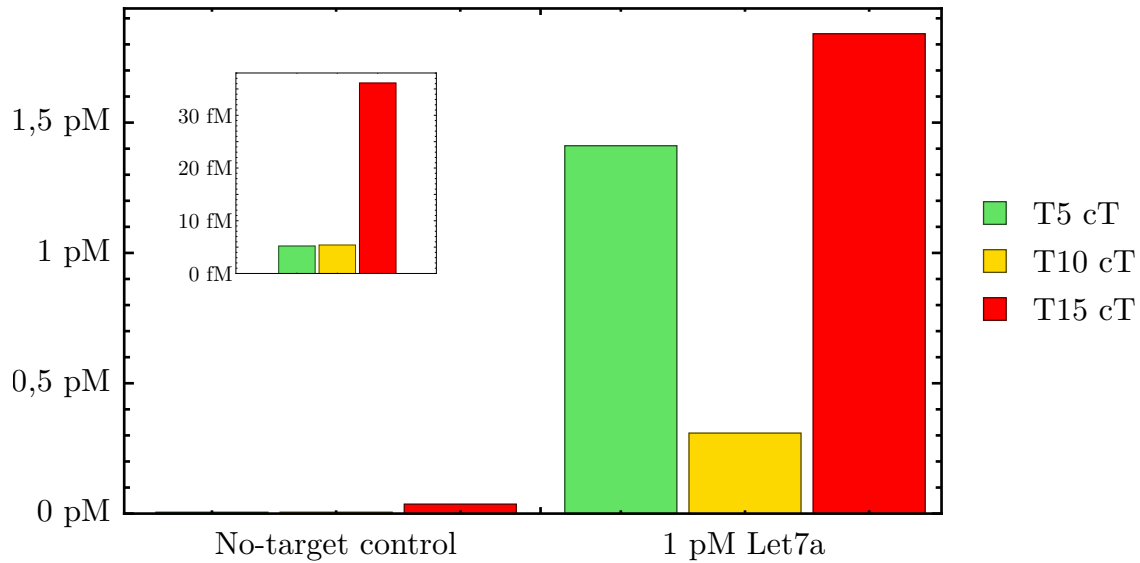


Figure 4.9: Evaluation of poly(T) cTs for the singleplex detection of Let7a (RNA version). The T5 and T15 cTs report concentrations even higher than the expected 1 pM, probably indicating that the actual concentration of the sample was above 1 pM. Surprisingly, the concentration detected by the T10 cT is much lower. Insert: Zoom on the no-target controls. The T15 design displays a much higher false positive rates than the T5 and T10 cTs

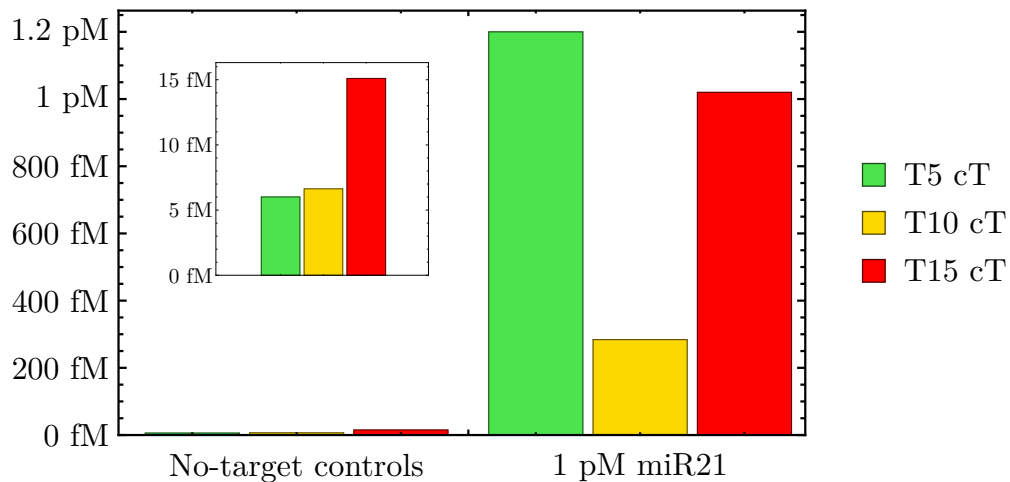


Figure 4.10: The experiment presented on fig 4.9 was also performed on miR 21 instead of Let7a, for similar results. As for Let7a, the T5 design appears to be the optimal cT for RNA detection

4.3.3 Post-capture particle washing



As experienced in chapter 3, the oligonucleotides bound to the surface of the particles tend to trap enzymes displaying a high affinity towards DNA. For the amplification step, this effect was suppressed by mixing particles and enzymes right before encapsulation thanks to 2-water inlet microfluidics. The new conditions of the capture step, developed in the previous section, could however lead to scavenging of Klenow polymerase on the surface of the beads, probably increasing the false positive particle rate. The post-capture washing step conditions need to be adapted to the new capture procedure.

The washing step was so far composed of 2 resuspension/supernatant discarding cycles in the buffer used for particles storage (for composition, see chapter 6). We designed a more stringent washing procedure (referred to as "hard" washing procedure), composed of 2 resuspension/ultrasound sonication/supernatant discarding cycles in a salty buffer (see chapter 6) followed by 2 resuspension/supernatant discarding cycles in the storage buffer to restore salts concentrations compatible with the molecular program. The average (3 technical replicates) percentage of positive particles in the no-target controls and the standard deviations are presented in table 4.1. The false positive rate is reduced by a 3-fold when the hard washing procedure is implemented, probably indicating that trapped Klenow molecules were removed from the surface of the particles. These stringent conditions did not significantly modify the detected concentrations from miRNA-containing samples (data not shown).

Procedure	False positive %	Standard deviation
Storage buffer washing	1,04%	0,29%
"Hard" washing	0,32%	0,14%

Table 4.1: Comparison of the false positive rates measured for the 2 proposed washing procedures. The "hard" washing procedure reduces the percentage of positive particles in the no-target control by 3-fold. This decrease of the false positive rate is probably caused by the removal of Klenow polymerase molecules trapped on the surface of the particles.

Procedure	False positive rate	RNA detection quantitativity
Vent only amplification	+	-
RNase inhibitors	+	-
Vent + Klenow amplification	- - -	+ + +
Klenow capture only	-	+ + +
Klenow capture 1 dNTP only	+ +	+ + +
Klenow capture 1 dNTP only Hard wash	+ + +	+ + +

Table 4.2: Summary of the effect of the tested optimization procedures. In the false positive column, "- - -" means the false positive rate is high, while "+ + +" indicates a very low false positive rate. In the "RNA detection quantitativity" column, "+ + +" indicates that the detection of RNAs is quantitative.

4.4 Dynamic range of the method

Our method relies on the hypothesis that the number of miRNAs captured by a particle follows a poissonian distribution. As discussed in chapter 2, the concentration of miRNAs in the capture mix is computed from the percentage of positive particles F_{pos} and the concentration of particles $C_{\text{particles}}$ as follows:

$$C_{\text{miRNA}} = -\ln(1 - F_{\text{pos}}) \cdot C_{\text{particles}} \quad (4.1)$$

The variation of the percentage of positive particles depending on the target concentration for a given concentration of particles is presented on figure 4.11. The curve displays a linear region, comprised between 15% and 95%, and 2 plateaus outside of the corresponding concentration range. In the two flat regions of the curve, a small, non-significant variation of F_{pos} results in a wide difference of measured concentration, which may lead to inaccuracies in the quantification.

The percentage of positive particles observed in no-target controls with the conditions optimized in section 4.3.3. is 0,32% with a standard deviation of 0,14%. The limit of detection (LOD) is often defined in the litterature as the average blank plus 3 standard deviations. In the case of our method, the LOD is thus the miRNA concentration corresponding to 0,74% of positive particles. This percentage defines the lower limit of the dynamic range of the

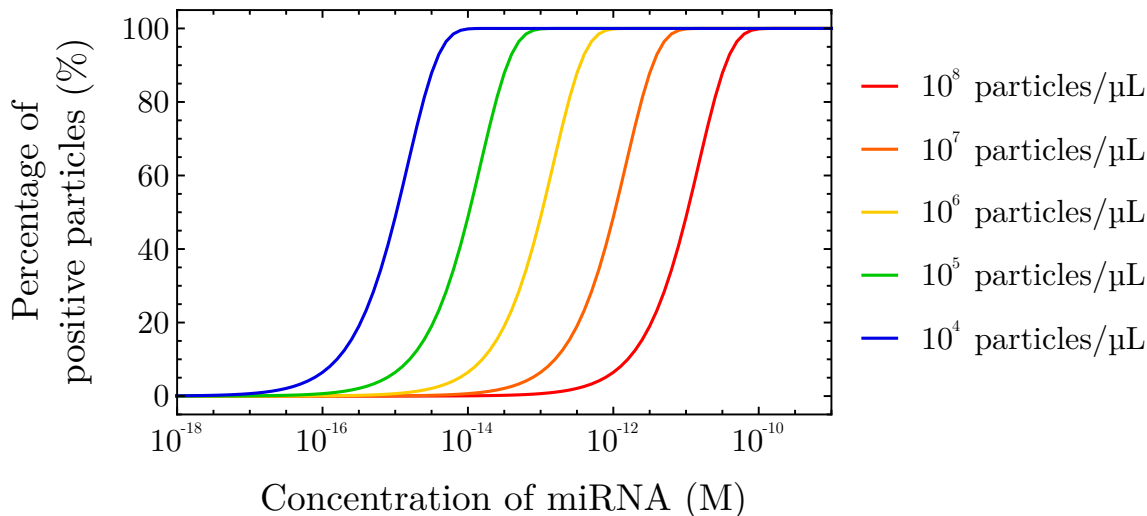


Figure 4.11: Theoretical curves of the percentage of positive particles depending on the concentration of particles and miRNA. The curves are S-shaped, with a linear range from approximately 10% to 95% positive particles and plateaus at percentages under 10% and above 95%.

method. At high positive percentages, where the turn from the linear to the plateau region is very sharp, quantification accuracy dramatically decreases above 95% of positive particles. For an example $C_{\text{particles}}$ of 10^9 particles/mL, the upper limit of the quantification range is approximately of 5 pM, and the LOD is 12 fM. For a given $C_{\text{particles}}$, the span of the dynamic range covers between 2 and 3 orders of magnitude, which is relatively narrow compared to other miRNA detection methods, such as RT-qPCR (8 orders of magnitude).

The dynamic range of the method can however be tuned by modifying the concentration of particles during the capture step. According to equation 4.1, the measured concentration of miRNAs varies linearly with $C_{\text{particles}}$. Hence, lowering $C_{\text{particles}}$ by a factor 10 theoretically shifts the dynamic range to concentrations 10 times lower, as shown on fig 4.11.

In order to verify the accuracy of the system and to assess its dynamic range, we performed a quantification of a range of standard samples of known concentrations for 2 different $C_{\text{particles}}$. The experimental results (Fig. 4.12) are in accordance with the theoretical curves. This experiment confirms that the dynamic range can be tuned by modifying $C_{\text{particles}}$. This feature extends the relatively low span of the dynamic range for a given $C_{\text{particles}}$.

Based on the only two $C_{\text{particles}}$ we considered for these experiments, we accurately quantified Let7a for concentrations comprised between 10 pM and 3 fM. Although it is still relatively narrow, this dynamic range appears adequate for the detection of miRNAs in bodily fluids, as the concentrations of a miRNA in plasma is in the fM-pM range. Lower $C_{\text{particles}}$ have not been investigated yet, but may allow the sensing of even lower miRNA concentrations.

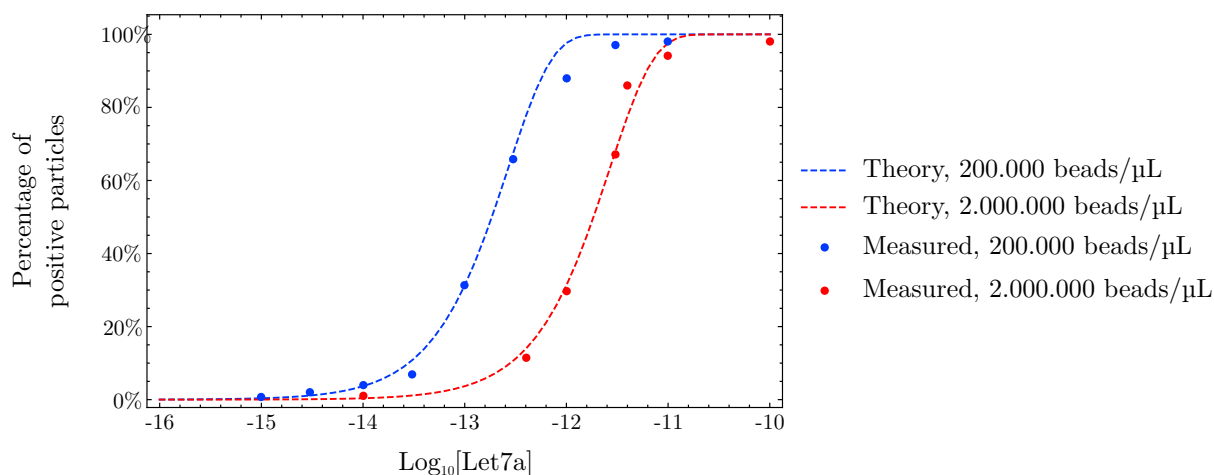


Figure 4.12: Comparison of the measured percentages of positive particles with the theoretical result at 2 different concentrations of particles. The expected results are computed using equation 4.1

4.5 Specificity of the method

Specificity is a major challenge for miRNA detection methods, due to the short sequences of miRNAs and the high level of homology found within some miRNA families, such as the Let7 family. In this miRNA family, miRNAs only vary from one another by one or two nucleotides, making it ideal for studying the specificity of a detection method. The sequences of the miRNAs of the Let7 family are presented in table 4.3.

MicroRNA	Sequence (5'→3')
Let7a	UGAGGUAGUAGGUUGUAUAGUU
Let7b	UGAGGUAGUAGGUUGUGUGGUU
Let7c	UGAGGUAGUAGGUUGUAUGGUU
Let7d	AGAGGUAGUAGGUUGCAUAGUU
Let7e	UGAGGUAGGAGGUUGUAUAGUU
Let7f	UGAGGUAGUAGAUAUAGUU
Let7g	UGAGGUAGUAGUUUGUACAGUU
Let7i	UGAGGUAGUAGUUUGUCUGUU

Table 4.3: Sequences of the members of the Let7 family. The sequence of Let7a is taken as reference for comparison with the other members of the family. Nucleotides are marked green if identical to the nucleotide in the same position in Let7a, and red if different.

As presented at the beginning of the chapter, the results of a 5-plex experiment indicated that the system might not be able to efficiently differentiate Let7a and Let7e. As presented in table 4.3, these two miRNAs differ by a single nucleotide. Let7c is another member of the

Let7 family that shares all but one nucleotides with Let7a. To assess the specificity of our detection method, we performed duplex digital detection experiments with Let7a and Let7c or Let7e as follows:

- Detection particles targeting 2 different miRNAs are introduced in the capture mix.
- Only one of the 2 targeted miRNAs is introduced.
- The MultimiR procedure is performed as usual.
- After flow cytometry analysis, the positive particles in both populations are counted. The results are presented as the proportion of each subpopulation among the pool of positive particles.

The results of these specificity experiments are presented on fig 4.13. The data shows that although the system shows some specificity between Let7a and Let7c, no specificity was observed between Let7a and Let7e, as the capture of Let7a targets was reported in similar proportions by Let7a and Let7e particles, and vice-versa.

This difference of specificity between two miRNA pairs sharing all but one nucleotide can be explained by the position of the lone mismatched base. In the case of the Let7a-Let7c pair, the differing base is located close to the 3' of the miRNA. During the conversion, this very 3' end is extended to produce a trigger strand. Improper hybridization of the 3' end of the miRNA to the cT could hinder the action of the polymerase, reducing the production rate of trigger, preventing the initiation of amplification in some droplets. The Let7a-Let7e pair, on the other hand, presents a mismatch further from the 3' end, which would not hinder elongation by the polymerase if a miRNA is captured by the wrong cT.

Even in the case of the Let7a-Let7c pair, the mechanism proposed above implies that the specificity observed is not caused by the capture, but by the conversion. We can therefore assume that when targeting very highly homologous sequences, the detected amounts are underestimated due to non-specific capture, even if that capture did not trigger amplification.

Several strategies to improve the specificity of miRNA detection methods were discussed in chapter 1. The implementation of a ligation step, during which the cT is assembled upon miRNA hybridization, might be particularly effective to discriminate miRNAs differing only by their 3' end. The use of modified residues, such as LNA, also produced good results in the literature. The relevance of trying to discriminate members of the Let7 family is however yet to be assessed. As discussed in chapter 1, the main mechanism for miRNA-induced silencing involves only the binding of the miRNA "seed", comprised between positions 2 and 7, which are shared by all members of the Let7 family (see table 4.3).

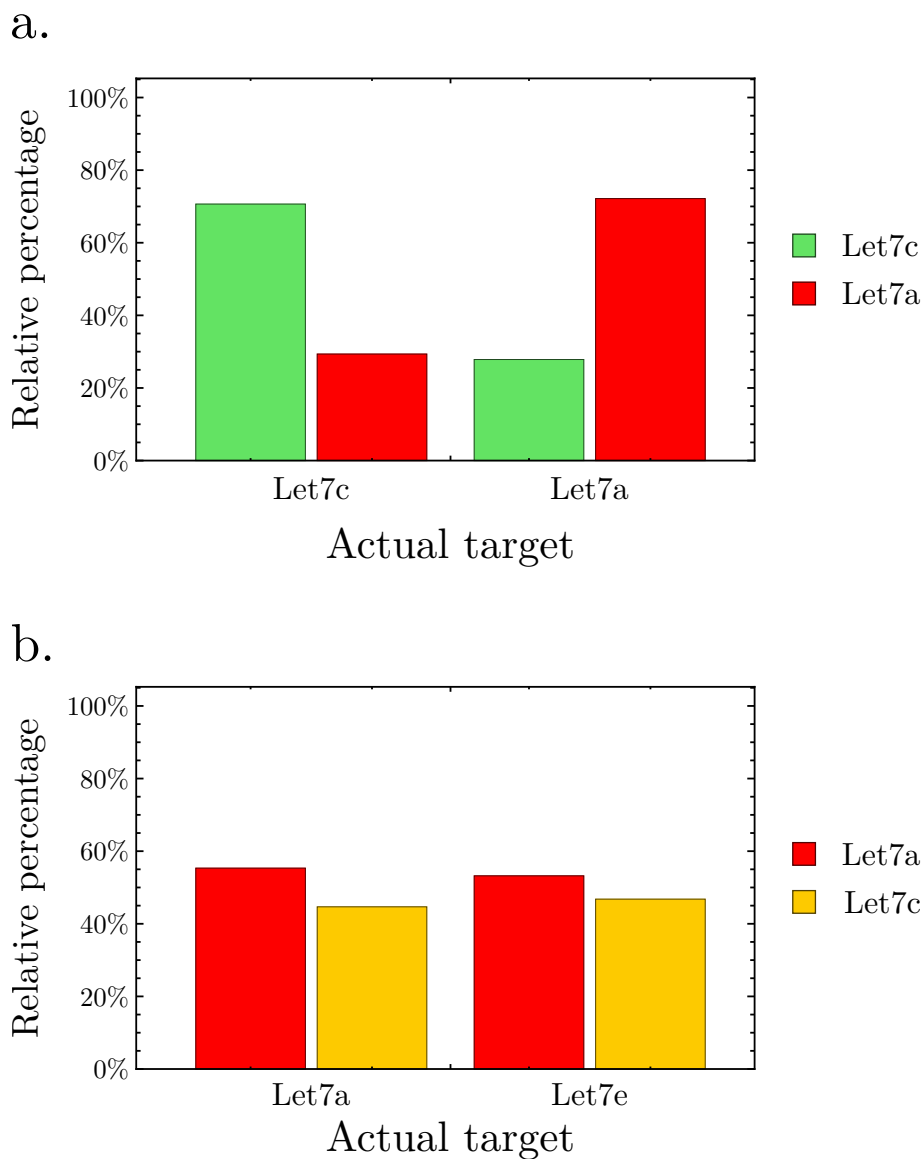


Figure 4.13: Specificity experiments. The bars indicate the proportion of each population among the pool of all positive particles. a. Let7a vs Let7c specificity. The data indicates that, when Let7c was the introduced target, approximately 70% of positive particles after amplification were Let7c detection particles and the other 30% were Let7a particles, and vice-versa. The system exhibits some single-nucleotide specificity between Let7a and Let7c. b. Let7a vs Let7e specificity. Contrary to a., the pool of positive particles is composed of 50% Let7a and 50% Let7e particles independantly of the actual target, which confirms the observations of fig 4.1. The system therefore appears to be completely unable to differentiate Let7a from Let7e and conversely.

4.6 Multiplex detection of synthetic miRNAs

We have seen in section 4.4. that our system was able to accurately quantify a single miRNA. In this section, we present a proof of concept 6-plex quantification of synthetic miRNAs spiked in buffer in their RNA versions.

The target miRNAs for this 6-plex assay were miR 21, Let7a, miR 10a, miR 16, miR 203a (human miRNAs) and Lin4, from *Caenorhabditis elegans*. Two different mixes of these miRNAs were prepared, each mix containing all 6 miRNAs either at high (500 fM) or low (10 fM) concentration. The two miRNA mixes were submitted to a capture step as described in section 4.3.2., after which the particles were washed following the "hard" washing procedure (see section 4.3.3.). A multiplex digital detection was then performed as described in chapter 3. The used experimental conditions were as follows:

- Particles functionalization: 300 cT and 300000 rT/particle
- $C_{\text{particles}}$: 556 fM of each subpopulation (3.33 pM total)
- Capture buffer: dATP-only miRNA detection buffer 1X
- Capture conditions: 2 hours at 40°C, 2000 rpm
- Klenow concentration during capture: 50 units/mL
- Enzymes concentrations during amplification: Nb.BsmI: 200 u/mL; Nt.BstNBI: 10 u/mL; Vent(exo-): 80 u/mL; ttRecJ/140: 23 nM; BsmI: 50 u/mL
- Templates concentrations during amplification: aT: 50 nM; pT: 8 nM
- Droplet incubation time: 10 hours

The results for both miRNA mixes are presented on fig 4.14.

miRNA	mix A	mix B
Lin4	500 fM	10 fM
miR 21	10 fM	500 fM
Let7a	500 fM	500 fM
miR 10a	10 fM	10 fM
miR 16	500 fM	500 fM
miR 203a	10 fM	500 fM

Table 4.4: Composition of the 2 miRNA mixes

Measured concentrations are overall close to the expected values. The average relative error on the concentration is of 30%. The concentration of some of the tested miRNAs, in

particular Lin4, are still significantly underestimated, which may indicate that the problem of lowered efficiency of the molecular program when detecting RNA targets is not completely solved for all miRNAs yet. In this study, we mostly relied on Let7a as our model miRNA for the development of the detection technique, thus assuming that other miRNAs would display similar responses. Custom sequence optimization of the cT might however be required for each miRNA individually, as our molecular network is prone to sequence-dependant effects that are still poorly understood. This was evidenced in this very chapter by the unpredicted and still unexplained lower conversion efficiency of the T10 cT. Similarly, spacers of different lengths or sequences might be more efficient than the T5 design for other miRNAs than Let7a.

This 6-plex assay is nonetheless a satisfactory proof of concept of the system we developed for the multiplex detection of miRNAs, as it allows the unambiguous discrimination of microRNA patterns.

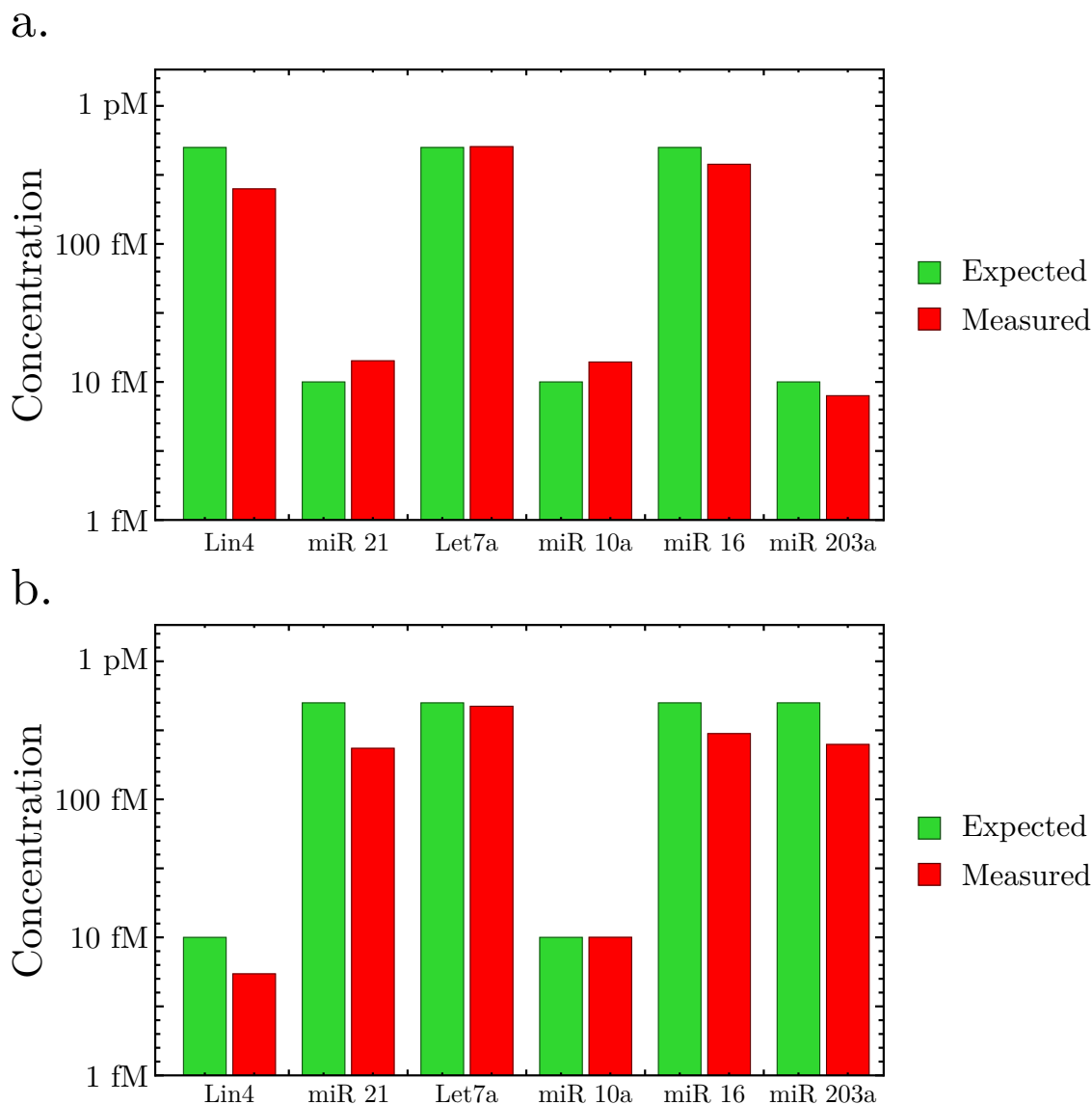


Figure 4.14: 6-plex detection of miRNAs in their RNA version. The targeted miRNAs are Lin4, miR 21, Let7a, miR 10a, miR 16 and miR 203a. Two different miRNA mixes (a. and b.) were analyzed. The results show good accordance between expected levels and the measured concentrations for both patterns. The average relative error on the concentration is of 30%. The concentration of some of the tested miRNAs, in particular Lin4, are still significantly underestimated, which may indicate that the problem of lowered efficiency of the molecular program when detecting RNA targets is not completely solved for all miRNAs yet. It is possible that the T5 cT design, which is the best fit for the quantification of Let7a, is not optimal for the detection of other miRNA sequences.

4.7 Conclusion

In this chapter, we demonstrated the transition from a system optimized for the detection of DNA analogs of miRNAs to a technique adapted to the quantification of actual miRNA targets. The process was not as straightforward as expected due to a lowered efficiency of the used DNA polymerase (Vent polymerase) when extending RNA primers, such as miRNAs. This reduced efficiency lowered the trigger production rate of the activated cTs. In a large part of miRNA-containing droplets, the trigger production rate was too low to exceed the trigger threshold concentration required to initiate the isothermal amplification, resulting in a significant underestimation of the miRNA concentration.

Our first approach to solving this problem was substituting part of the introduced Vent polymerase for a more RNA-friendly DNA polymerase, the Klenow polymerase. This enzyme indeed increased the trigger production rate from RNA targets, but also increased the non-specific reaction rate, lowering the sensitivity. Even when introduced only during the capture step, Klenow polymerase was able to "load" cTs without prior hybridization of the target miRNA, also increasing the false positive particle rate.

A compromise was found by designing new cTs presenting a poly(T) spacer between the miRNA binding site and the Nt.BstNBI recognition sequence. Instead of introducing the Klenow polymerase and all 4 dNTPs during the capture step, only dATPs were introduced: Upon hybridization, the miRNA is still extended by Klenow, facilitating the work of Vent during amplification; If the miRNA is absent, however, Klenow can only "load" cTs with poly(A) strands too short to stay hybridized to the cT at capture temperature. A T5 spacer was found to be the most effective design for the detection of Let7a and allowed its accurate detection in its RNA version.

Based on these conditions, the dynamic range of the system was assessed. For a given concentration of particles during capture, the span of the dynamic range was found to be comprised between 2 and 3 orders of magnitude, which is relatively narrow compared to other miRNA detection methods such as RT-qPCR (8 orders of magnitude). The dynamic range can however be extended by adapting the concentration of particles during capture to the concentration of the target. Using 2 different particles concentrations, we demonstrated the accurate detection of Let7a at concentrations ranging from 3 fM to 10 pM. Such dynamic range appears to be adequate for the detection of miRNAs in the bloodstream (concentrations comprised between a few fM and a few hundreds of fM). Lower concentrations of particles are still to be tested, but have the potential to lower the LOD of the system even more.

Experimental results suggested that the method was not completely specific when trying to detect highly homologous miRNAs, in particular towards the Let7a/Let7e pair. Fur-

ther experiments showed that the MultimiR method could indeed not differentiate between Let7e and Let7a, that only differ by one nucleotide. Similar experiments performed on the Lat7a/Let7c pair (1 mismatch also) indicated that mismatches near the 3' end of the miRNA were easier to discriminate for the method than 5' end mismatches. Adding a preliminary ligation step, during which the cT is assembled upon miRNA binding, could increase the specificity of the method towards miRNAs presenting identical 3' end but different 3' ends. Alternatively, modifying the cTs using LNA residues could also be a solution to improve specificity.

Finally, a 6-plex proof of concept assay was performed, producing satisfactory results. The quantification was not as accurate for all miRNAs as it was for our model miRNA, Let7a, probably indicating that the modified experimental conditions, in particular cT sequence, are not yet optimal for all miRNAs, and may require individualized optimization efforts.

Chapter 5

Conclusion

MiRNAs are promising new biomarkers for numerous diseases, such as cancers and neurodegenerative diseases. The aim of this PhD project was to design a multiplex and digital miRNA quantification method.

The current standard methods for miRNA detection are RT-qPCR and microarrays. These methods display symmetrical strengths and weaknesses: RT-qPCR is extremely sensitive, but is limited to 4-5 miRNAs in terms of multiplexing, while microarrays are highly multiplexable but their sensitivity is too low for miRNA detection from bodily fluids. Both methods only provide a relative quantification of their targets.

Our group designed a droplet-based technique providing absolute quantification of a miRNA. The method relied on an exponential amplification chemical network based on the PEN DNA toolbox. This approach was however more suited to singleplex or low-multiplex detection.

Building from this technique, we immobilized part of the chemical network on particles to increase the multiplexing potential of the method. Particles were "programmed" to capture a particular miRNA and report its capture by grafting tailored DNA templates on their surface. Fluorescent barcodes were also immobilized on the surface to indicate the miRNA target of each particle. This transition from a fully in-solution reaction to a supported format allowed us to increase the throughput of the method by replacing the fluorescence microscopy readout by a high-throughput flow cytometry readout. The maximal multiplexing potential of the method is determined by the number of barcoded subpopulations of particles that can be simultaneously distinguished by flow cytometry. In the current configuration of the used flow cytometer, the multiplexing potential was found to be 20 miRNAs quantified simultaneously, but similar approaches have been demonstrated with 100 populations (xMAP technology, Luminex Corporation). The detection procedure is composed of a first incubation of the reaction mixture at 30°C, during which miRNAs are captured by the particles, followed by

the microfluidic encapsulation of the mixture in microdroplets and a second incubation at 50°C during which the chemical network is activated if the miRNA is present. As a proof of concept, we realized a 3-plex assay detection of the DNA analogs of 3 miRNAs. Non-specific reactions were however a problem in this assay, in part due to the coencapsulation of particles.

A washing step was added to the procedure after the capture step in prevision of detection from more complex samples, such as cell extracts or plasma. This washing was coupled to a dilution of the particles in order to reduce the probability of particle coencapsulation. The dilution of particles however revealed an unexpected effect increasing the non-specific reaction rate and reducing the sensitivity: The enzymes used by the molecular program could be trapped by the DNA oligonucleotides attached to the surface of the particles. Diluting the particles increased the enzyme-per-particle ratio, resulting in an overconcentration of enzymes in the bead-containing droplets, which increases the non-specific reaction rate. We solved this problem by modifying our microfluidic device in order to mix the particles and the enzymes at the very last moment.

The transition from detecting DNA targets, as was the case at early stages of development of the method, to RNA targets, turned out to be more difficult than expected because of the lower efficiency of the Vent polymerase when extending RNA primers. This effect, which did not cause any disruption to our in-solution detection schemes, was enhanced by the on-bead format. Consequently, the production rate of trigger strands by the on-bead converters was lower when the miRNA sequence was made of RNA instead of DNA. This resulted in an underestimation of the concentration of RNA targets observed for all tested miRNAs. The quantitativity of the assay towards RNA targets was restored by modifying the cT design to increase the distance between the miRNA binding site and the trigger coding region, where the polymerase action is required. A 6-plex assay was successfully performed on actual miRNAs spiked in buffer, which constitutes a nice proof of concept of our detection method.

No specificity issues were detected for miRNAs outside of the Let7 family. The analysis of the Let7a-Let7c and Let7a-Let7e pairs, that share the same sequence except for one nucleotide, showed that the position of the mismatch was important. The specificity was indeed better for the Let7a-Let7c pair, which presents a mismatch near the 3' end, than for the Let7a-Let7e pair, the mismatch of which is located in the middle of the sequence. This specificity however appears to be determined by the conversion step, as a mismatch near the 3' end would reduce the efficiency of the polymerase for extension, and not by the capture. A miRNA (miR X) could therefore be captured by a cT designed for a homologous miRNA without being converted, which would lead to the underestimation of the concentration of miR X.

So far, we demonstrated the accurate quantification of miRNAs for concentrations ranging from 3 fM to 10 pM, which is a suitable dynamic range for miRNA detection in the blood. We additionally demonstrated that the dynamic range could be tuned by modifying the concentration of particles during the capture step. Lowering $C_{\text{particles}}$ might enable the detection of even lower concentrations, which is yet to be tested.

Perspectives

Significant developments efforts still remain necessary to increase the potential of this detection method. First, the range of detectable miRNAs needs to be extended. Although the theoretical multiplexing limit is defined by the number of distinguishable subpopulations of barcoded particles, we do not currently have working cTs for 20 different miRNAs. The functioning of a converter is sequence-dependent, and this dependency follows mechanisms that we do not fully understand yet. Due to that dependency, cT designs can not always be generalized to all miRNAs, some requiring individualized sequence optimisation efforts.

The method appears nonetheless to be working for some miRNA sequences spiked in buffer. The natural next step of development would be to detect multiple miRNAs from biological samples to assess the therapeutic potential of the method. We first intend to analyze cell extracts from healthy and tumor samples. More challenging, detecting miRNAs from plasma, first with an extraction step and then directly, would be a great step towards miRNA-based liquid biopsy.

In parallel, our team is currently working on the use of the same noise-reducing amplification network for the detection of other targets than nucleic acids, such as proteins or cells. The implementation of our multiplex detection system for multi-target appears extremely promising for diagnostics applications.

On the longer term, the developed procedure would need to be adapted to an industrial scale to actually be implemented for clinical purposes. Kits of pre-mixed particles subpopulations, allowing the quantification of an application-specific miRNA panel, would need to be prepared. This particle kit would only need to be introduced in the sample to analyze, capturing all targeted miRNAs, and would then be recovered for analysis. Enzymes and molecular pre-mixes would also be prepared, simplifying the reaction mixture assembly. The most operator time-consuming step of the MultimiR procedure is sample partitioning, since it requires constant monitoring from the operator to avoid any clogging and maintain a proper balance between both water flows. Using the current setup, the microfluidic encapsulation of a 25 μL samples requires up to 1 hour. The automation of this step using an integrated platform is thus essential for routine use. Some commercial platforms already enable the

generation of such small droplets, but the use of aggregation-prone microparticles and the 2-water inlet device make this step even more challenging. The other steps, namely capture, washing, amplification and flow cytometry analysis, are much less operator time-consuming: Capture and amplification are incubation steps and do not require any monitoring; The washing step and emulsion breaking only require 5 minutes each per sample, and could easily be automated; Flow cytometry analysis does not require monitoring and automated sample changers are already commercially available.

Overall, the MultimiR method proved to be a powerful tool for the multiplex detection of miRNAs. Its limit of detection and dynamic range are adequate for clinical applications. Much of its potential remains to be explored, but the method holds great promise.

Chapter 6

Materials and methods

6.1 General material and methods

Oligonucleotides were purchased from Biomers (Germany). The sequences were purified by HPLC and checked by matrix-assisted laser desorption/ionization mass spectrometry. Template sequences are protected from the degradation by the exonuclease using phosphorothioate modifications at the 5' end of each template. The sequences of the oligonucleotides used in this study are presented in tables 6.1 and 6.2.

Nb.BsmI, Nt.BstNBI, Vent(exo-) and Klenow large fragment DNA polymerases and BSA were purchased from New England Biolabs (NEB). A 10-fold dilution of Nt.BstNBI prepared by dissolving the stock enzyme in diluent A (also from NEB) supplemented 0.1% (v/v) Triton X100.

Oligo name	Sequence (5'→3')	Function
α	CATTCTGGACTG	Trigger
ato α	C*A*G*T*CCAGAATGCAGTCCAGAA p	aT
pT α	T*T*T*T*TCAGTCCAGAATG p	pT
Free rT α	Atto633 *A*T*TCTGAATGCAGTCCAGAAT BHQ2	free rT
OB rT 1	Biotin *T*T*T*TTTTTTT FAM GTGAG- -AATGCAGTCCAGAATGTCTCAC BHQ2	On-bead rT
OB rT 2	Biotin *T*T*T*TTTTTTT FAM TGTGA- -GAATGCAGTCCAGAATGTCTCACA BHQ2	On-bead rT
OB rT 3	Biotin *T*T*T*TTTTTTT FAM GTGAG- -AATGCAGTCCAGAATGTCTCAC BHQ1	On-bead rT
OB rT 4	Dabcyl *G*T*G*AGAATGCAGTCCAGAAT- -GTCTCAC FAM TTTTTTTTTT Biotin	On-bead rT
Let7ato α	TGCAGTCCAGAAGTTTGACTCAAA- -CTATAACAACCTACTACCTCA p	free cT
Let7ato α biot	TGCAGTCCAGAAGTTTGACTCAAA- -CTATAACAACCTACTACCTCA Biotin	On-bead cT
Let7ato α T7 biot	TGCAGTCCAGAAGTTTGACTCAAACCTATA- -CAACCTACTACCTCATTTTTTTT Biotin	On-bead cT
Let7ato α T15	TGCAGTCCAGAAGTTTGACTCAAACCTATA- -CAACCTACTACCTCATTTTTTTTTTTTTTTTTT	On-bead cT
Let7ato α T30	TGCAGTCCAGAAGTTTGACTCAAA- -CTATAACAACCTACTACCTCA- -TTTTTTTTTTTTTTTTTTTTTTTTTTTTTTTTTTT	On-bead cT
A30 Biotin	Biotin AAAAAAAAAA- -AAAAAAAAAAAAAAAAAAAAA	Connector
Let7ato α T5 T7 Biotin	TGCAGTCCAGAAGTTTGACTCTTTTTAACT- -ATACAACCTACTACCTCATTTTTTTT Biotin	On-bead cT
Let7ato α T10 T7 Biotin	TGCAGTCCAGAAGTTTGACTCTTTTTT- -TTTTTAACTATAACAACCTACTACC- -TCATTTTTTTT Biotin	On-bead cT
Let7ato α T15 T7 Biotin	TGCAGTCCAGAAGTTTGACTCTTTTTT- -TTTTTTTTTTTAACTATAACAACCTA- -CTACCTCATTTTTTTT Biotin	On-bead cT
Let7ato α T20 T7 Biotin	TGCAGTCCAGAAGTTTGACTCTTTTTT- -TTTTTTTTTTTTTTTTTAACTATAACA- -ACCTACTACCTCATTTTTTTT Biotin	On-bead cT
miR21to α T5 T7 Biotin	TGCAGTCCAGAAGTTTGACTCTTTTTTCAA- -CATCAGTCTGATAAGCTATTTTTTTT Biotin	On-bead cT
miR21to α T10 T7 Biotin	TGCAGTCCAGAAGTTTGACTCTTTTTTTTTT- -TTCAACATCAGTCTGATAAG- -CTATTTTTTTT Biotin	On-bead cT

Table 6.1: Sequences of the oligonucleotides used in this study

Oligo name	Sequence (5'→3')	Function
miR21toα T15 T7 Biotin	TGCAGTCCAGAAGTTTGACTCTTTTTTTTTT- -TTTTTTTTCAACATCAGTCTG- -ATAAGCTATTTTTTTT Biotin	On-bead cT
miR21toα T20 T7 Biotin	TGCAGTCCAGAAGTTTGACTCTTTTTTTTTT- -TTTTTTTTTTTTTCAACATCA- -GTCTGATAAGCTATTTTTTTT Biotin	On-bead cT
miR16toα T5 T7 Biotin	TGCAGTCCAGAAGTTTGACTCTTTTTTCGCC- -AATATTTACGTGCTTTTTTTT Biotin	On-bead cT
Let7ctoα T5 T7 Biotin	TGCAGTCCAGAAGTTTGACTCTTTTTTAACC- -ATACAACCTACTACCTCATTTTTTTT Biotin	On-bead cT
miR10atoα T5 T7 Biotin	TGCAGTCCAGAAGTTTGACTCTTTTTTCACA- -AATTCGGATCTACAGGGTATTTTTTTT Biotin	On-bead cT
miR203atoα T5 T7 Biotin	TGCAGTCCAGAAGTTTGACTCTTTTTTCTAG- -TGGTCCTAAACATTTCACTTTTTTTT Biotin	On-bead cT
Lin4toα T5 T7 Biotin	TGCAGTCCAGAAGTTTGACTCTTTTTTTCAC- -ACTTGAGGTCTCAGGGATTTTTTTT Biotin	On-bead cT
Let7etoα T5 T7 Biotin	TGCAGTCCAGAAGTTTGACTCTTTTTTAAAC- -TATACAACCTCCTACCTCA Biotin	On-bead cT
Let7a	UGAGGUAGUAGGUUGUAUAGUU	miRNA
Let7c	UGAGGUAGUAGGUUGUAUGGUU	miRNA
Let7e	UGAGGUAGGAGGUUGUAUAGUU	miRNA
miR 16	UAGCAGCACGUAAAUAUUGGCG	miRNA
miR 21	UAGCUUAUCAGACUGAUGUUGA	miRNA
miR 10a	UACCCUGUAGAUCCGAAUUUGUG	miRNA
miR 203a	AGUGGUUCUUAACAGUUCAACAGUU	miRNA
Lin4	UCCUGAGACCUCAAGUGUGA	miRNA

Table 6.2: Sequences of the oligonucleotides used in this study

6.2 Buffers

6.2.1 miR Buffer

MiR Buffer is the custom buffer our group optimized for miRNA detection using molecular programming. The composition of this buffer is presented in table 6.3.

Component	Concentration
Tris HCl ph 7.9	20 mM
(NH ₄) ₂ SO ₄	10 mM
KCl	40 mM
MgSO ₄	10 mM
dNTP	50 μ M each
Synperonic F 104	0.1% (w/v)
Netropsin	2 μ M

Table 6.3: Composition of the 1X miRNA detection buffer

6.2.2 Binding and washing buffer

As indicated by its name, the binding and washing (B&W) buffer is used for washing the particles and functionalizing them.

Component	Concentration
Tris-HCl ph 7.5	20 mM
NaCl	1 M
EDTA	1 mM
Tween 20	0.2% (v/v)

Table 6.4: Composition of the binding and washing buffer

6.2.3 Particles storage buffer

Component	Concentration
Tris-HCl ph 7.5	5 mM
NaCl	50 mM
EDTA	500 μ M
MgSO ₄	5 mM

Table 6.5: Composition of the storage buffer

6.3 Particles functionalization

The selected particles were streptavidin-coated MyOne Dynabeads from ThermoFisher. Prior to functionalization, particles are washed 3 times using B&W buffer, and are also resuspended in B&W buffer. Particles are then introduced in a tube containing the oligonucleotides to be grafted. The mix is vortexed for 30 seconds to prevent heterogeneous functionalization. The particles are incubated for 30 minutes at room temperature. A first wash is performed, again with B&W buffer, followed by 2 washes in storage buffer in order to lower the salt concentration, as the NaCl concentration is not compatible with the molecular program.

6.4 MultimiR reaction mixture

All reactions of the chemical network are performed in miR buffer 1X (see table 6.3). The typical enzymes compositions are displayed in table 6.6. Unless stated otherwise (when Klenow polymerase is added), these enzyme mix is the one used for all miRNA detection experiments.

Enzyme	Composition
Nb.BsmI	200 u/mL
Nt.BstNBI	10 u/mL
Vent(exo-)	80 u/mL
ttRecJ	23 nM
BsmI	50 u/mL

Table 6.6: Typical enzymes concentrations for miRNA detection

The concentration of DNA templates varied during the project. The only concentration kept constant was the concentration of aT, which was 50 nM. The concentrations optimized for the detection of RNA targets, and used for the proof of concept 6-plex assay of chapter 4, were 50 nM aT and 8 nM pT. On-bead templates concentrations were 300 cT (0,015% of saturation) and 300.000 rT (15% of saturation) per bead.

The miRNA targets were serially diluted in Tris-EDTA buffer (Sigma-Aldrich) using low DNA retention tips from Eppendorf.

6.5 Capture step

The conditions of the capture step varied during the course of the project. The initial scheme was to assemble the reaction mixture prior to the capture step. The capture was performed

at 30°C in a ThermoMixer C from Eppendorf. The stirring was set at the maximum speed, 2000 rpm, to avoid biases caused by particle sedimentation. The optimal capture time was found to be 2 hours.

Once the washing step was implemented, the composition of the capture mix was modified. Instead of assembling the whole reaction mixture prior to the capture step, the capture mix was only composed of the detection particles and the miRNA-containing sample. The capture buffer was miR buffer 1X.

Finally, the capture step was again adapted in order to detect RNA targets. Klenow polymerase was added to the capture mix at a concentration of 1% v/v. The capture temperature was changed to 40°C in order to favor the action of Klenow polymerase, whose optimal working temperature is 37°C. The capture buffer was slightly modified by removing all dNTPs with the exception of dATPs to avoid non-specific "loading" of the cTs by Klenow polymerase.

6.6 Post-capture particles washing

As described in chapter 3, a post-capture washing step was added to the protocol.

6.6.1 "Soft" washing procedure

1. The particles are gathered using a magnet.
2. The supernatant is discarded.
3. The particles are resuspended in storage buffer. (Same volume as capture mix)
4. Magnetic particle gathering.
5. Supernatant discarding.
6. Resuspension in storage buffer. (Same volume as capture mix)
7. Magnetic particle gathering.
8. Supernatant discarding.
9. Resuspension in storage volume. (Free volume)

6.6.2 "Hard" washing procedure

1. Magnetic particle gathering.
2. Supernatant discarding.
3. Resuspension in B&W buffer. (Same volume as capture mix)
4. Ultrasound bath sonication.
5. Magnetic particle gathering.
6. Supernatant discarding.
7. Resuspension in B&W buffer. (Same volume as capture mix)
8. Ultrasound bath sonication.
9. Magnetic particle gathering.
10. Supernatant discarding.
11. Resuspension in storage buffer. (Same volume as capture mix)
12. Magnetic particle gathering.
13. Supernatant discarding.
14. Resuspension in storage buffer. (Same volume as capture mix)
15. Magnetic particle gathering.
16. Supernatant discarding.
17. Resuspension in storage buffer. (Free volume)

6.7 Microfluidics

6.7.1 Microfluidics material

The microfluidic setup was composed of a 4-channel MFCS-EZ pressure pump controller from Fluigent and an Eclipse-TI microscope from Nikon. The used tubings were 200 μm -diameter PTFE tubing from C.I.L.. The oil phase of the generated microemulsions is fluorinated oil Novec 7500 from 3M supplemented by Fluosurf surfactant from Emulseo.

6.7.2 Microfluidic devices preparation

6.7.2.1 Soft lithography

Microfluidic molds preparation was performed by soft lithography. A thin layer SU-8 photosensitive resin (MicroChem Corp., USA) was homogeneously deposited on a 4-inch silicon wafer by spin-coating. The thickness of the SU-8 layer can be adjusted by choosing the viscosity of the resin and the spin-coating speed. The covered wafer was then selectively exposed to UV light through a photolithography mask. After exposition, the wafer was introduced in a developer solvent (PDMEA) bath in order to remove all unreticulated resin.

6.7.2.2 PDMS chip preparation

40 g of a 10:1 (w/w) mix of PDMS resin/curing agent was poured on the mold. The mold was placed in a vacuum chamber in order to remove all dissolved gas from the PDMS mix. The PDMS was then baked in an oven at 70°C for 2 hours for crosslinking. The crosslinked PDMS was then peeled from the mold.

6.7.2.3 Plasma cleaning

The PDMS chip was irreversibly bound to a 1mm-thick glass slide thanks to a plasma cleaner. In order to avoid clogging of the microfluidic channels by dust, the procedure was realized in a clean room. The chip and the glass slide were introduced in the plasma oven, that was then placed under vacuum. Three vacuum/O₂ flushing cycles were performed to remove all other gases than O₂ from the chamber. Finally, the O₂ pressure is fixed around 300 mTorr and a plasma is generated for 60 seconds in the chamber. The vacuum is then broken, and the surfaces that were exposed to the plasma are brought together for bonding.

6.7.2.4 Hydrophobic treatment

In order to produce microdroplets, the microfluidic chip needs to be hydrophobic, which is not initially the case. The chip is baked at 200°C for 5 hours.

6.7.3 Single water inlet microfluidics

The original chip design used to generate microdroplets is presented on fig 6.1. The colors indicate the height of the microchannels. Green regions have a height of 30 μm , while orange parts are 7 μm parts. The oil phase is introduced from the top inlet, and the water phase from the bottom inlet. The oil flow is split in half, and pinches the water flow at the nozzle to generate droplets. Filter regions, in which the height is the same as in the nozzle region,

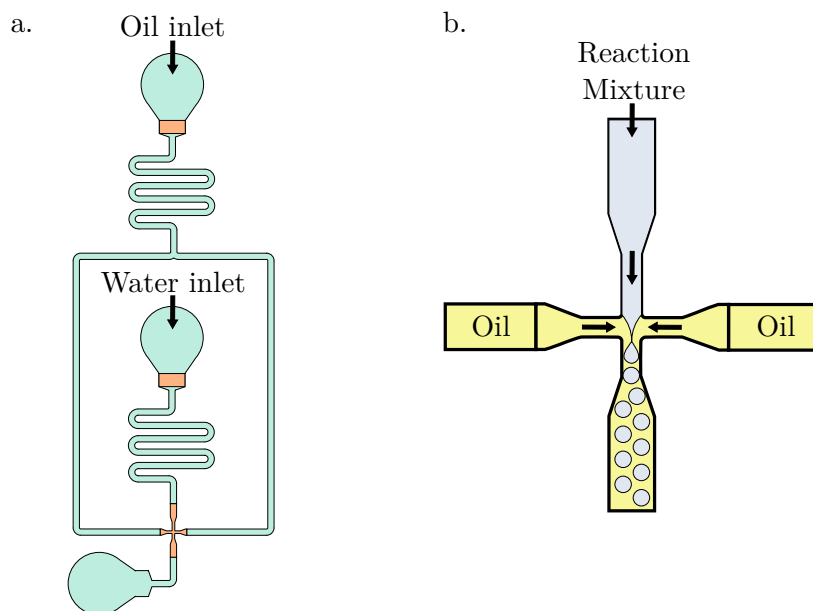


Figure 6.1: Single water inlet microfluidic chip

are placed after both inlets to prevent the clogging of the nozzle. This device allows us to generate droplets with a diameter of $9\ \mu\text{m}$.

6.7.4 2-water inlet microfluidics

The design of the microfluidic device was modified to counter the enzyme scavenging effect presented in chapter 3. The new chip is presented on fig 6.2. A second water phase inlet is added to introduce particles and enzymes separately. Both water phases meet right before the nozzle, preventing any enzyme scavenging by the particles. Channel heights are identical to those of the single water inlet device.

6.8 Amplification step

The amplification step was performed at 50°C , in a CFX96 Touch qPCR thermocycler from Biorad. The rT fluorescence is measured in real time. The aim is to stop the incubation when the fluorescence reaches plateau, indicating that the amplification took place in all miRNA-containing droplets. For MultimiR experiments, however, the amplitude of the variations of the rT fluorescence is very low, which makes the determination of the optimal time to stop amplification difficult. In practice, the produced emulsion was split in several tubes stopped at different times to find the optimal incubation stopping time. At the conditions used for the 6-plex miRNA detection of chapter 4, the incubation time was approximately 10 hours.

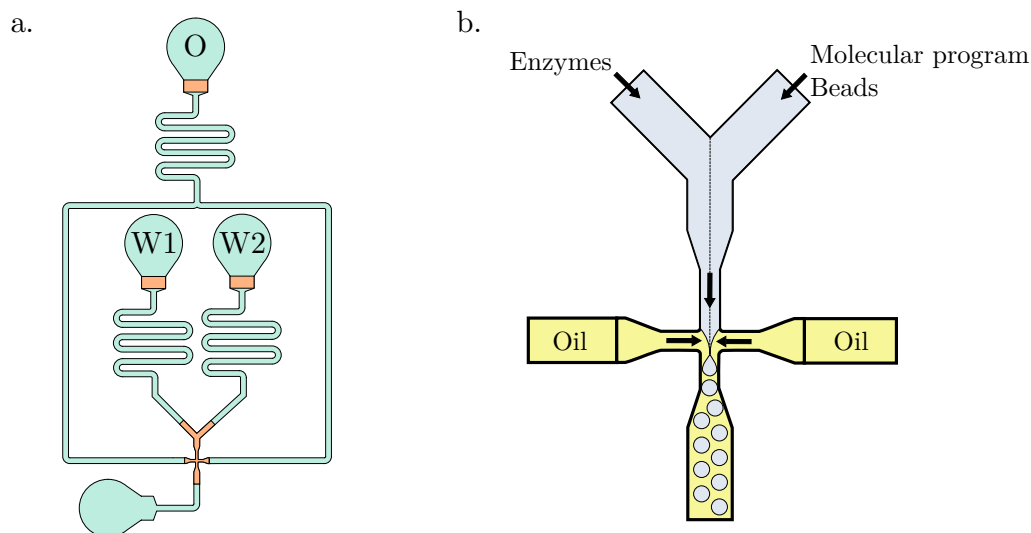


Figure 6.2: Double water inlet microfluidic chip

6.9 Flow cytometry analysis

The flow cytometer used in this study is a Attune NxT from ThermoFisher, equipped with three lasers, emitting at 490 nm, 561 nm and 630 nm. The optical configuration of the flow cytometer is presented in table 6.7. The particles were first sorted from the dusts using a FSC vs SSC plot. The barcode fluorescence of the particles was then analyzed using detectors YL-3 (Cy3.5) and RL-1 (Atto633). Finally, rT fluorescence was measured using the BL-1 detector (Atto488 fluorescence). The optical configuration of the flow cytometer used for this study is presented in table 6.7.

Detector name	Laser	Center	Bandwidth
BL-1	Blue	488 nm	10 nm
BL-2	Blue	530 nm	30 nm
BL-3	Blue	590 nm	40 nm
BL-4	Blue	695 nm	40 nm
YL-1	Yellow	585 nm	16 nm
YL-2	Yellow	620 nm	15 nm
YL-3	Yellow	695 nm	40 nm
YL-4	Yellow	780 nm	60 nm
RL-1	Red	670 nm	14 nm
RL-2	Red	720 nm	30 nm
RL-3	Red	780 nm	60 nm

Table 6.7: Configuration of the detectors of the used flow cytometer

6.10 ID3miR

Isothermal Digital Droplet Detection of miRNAs (ID3miR) is the singleplex miRNA detection method MultimiR is based on. In this technique, the full reaction mixture is assembled as described in section 6.4. The mix is encapsulated using a single water inlet microfluidic device into 10 μm -diameter droplets. The distribution of the miRNA targets into the droplets follows a Poisson law. The droplets are incubated at 50°C in a qPCR thermocycler. The fluorescence of the rT is monitored in real time. The incubation of the droplets is stopped once the rT fluorescence reaches a plateau. At that point, droplets are placed in microscopy chambers composed of two glass slides and sealed by epoxy glue. The glass slides were treated to be hydrophobic by dipping them in Novec 1720 (3M) and heating them. Polymer particles with a diameter of 10 μm are spotted on the surface of the glass slide to maintain a minimal distance of 10 μm between the glass slides in order to prevent droplet compression. Fluorescence images were captured using an epifluorescence microscope Nikon Eclipse Ti equipped with a motorized XY stage (Nikon), a camera Nikon DS-Qi2, an apochromatic 10X and a CoolLed pE-4000 illumination source. Microscopy images are analyzed thanks to a Mathematica software (Wolfram) algorithm.

6.11 Production rate experiments

The production rate protocol is a variation of the bulk detection protocol. The aim of this kind of experiment is to assess the efficiency of the conversion step. To that end, only cTs and rTs are introduced in the mix. The only necessary enzymes are the polymerase and Nt.BstNBI. The reaction buffer is miR buffer 1X. Experimental conditions for production rate experiments are presented in table 6.8. Nt.BstNBI is introduced in excess compared with miRNA detection experiments in order to make sure that polymerisation is the kinetic-limiting process.

Component	Concentration
cT	0,5 nM
rT	25 nM
Polymerase	Various
Nt.BstNBI	20 u/mL
Let7a	1 nM

Table 6.8: Reaction mixture for production rate experiments

6.12 Enzyme depletion experiments

Enzyme depletion experiments allowed us to evidence the enzyme-scavenging effect in chapter 3. In this kind of experiment, the enzymes are pre-mixed, and particles are introduced. The concentrations in the enzyme pre-mix are 10 times higher than in the miRNA detection mixture. The enzyme-particles mix is incubated for 30 minutes at 25°C with a 2000 rpm stirring in a ThermoMixer (Eppendorf). After incubation, particles are gathered in the bottom of the tube using a magnet, and 1 μ L of the supernatant is pipetted and introduced instead of the separate enzymes in a miRNA detection mixture.

Bibliography

- [1] R. C. Lee, R. L. Feinbaum, and V. Ambros. The *C. elegans* heterochronic gene *lin-4* encodes small RNAs with antisense complementarity to *lin-14*. *Cell*, 75(5):843–854, December 1993.
- [2] Robin C. Friedman, Kyle Kai-How Farh, Christopher B. Burge, and David P. Bartel. Most mammalian mRNAs are conserved targets of microRNAs. *Genome Research*, 19(1):92–105, January 2009.
- [3] Andrew Fire, SiQun Xu, Mary K. Montgomery, Steven A. Kostas, Samuel E. Driver, and Craig C. Mello. Potent and specific genetic interference by double-stranded RNA in *Caenorhabditis elegans*. *Nature*, 391(6669):806–811, February 1998.
- [4] David P Bartel. MicroRNAs: Genomics, Biogenesis, Mechanism, and Function. *Cell*, 116(2):281–297, January 2004. Publisher: Elsevier.
- [5] Heidi Schwarzenbach, Naohiro Nishida, George A. Calin, and Klaus Pantel. Clinical relevance of circulating cell-free microRNAs in cancer. *Nature Reviews. Clinical Oncology*, 11(3):145–156, March 2014.
- [6] Minju Ha and V. Narry Kim. Regulation of microRNA biogenesis. *Nature Reviews Molecular Cell Biology*, 15(8):509–524, August 2014.
- [7] Julia Höck and Gunter Meister. The Argonaute protein family. *Genome Biology*, 9(2):210, 2008.
- [8] Jacob O’Brien, Heyam Hayder, Yara Zayed, and Chun Peng. Overview of MicroRNA Biogenesis, Mechanisms of Actions, and Circulation. *Frontiers in Endocrinology*, 9:402, August 2018.
- [9] Kioomars Saliminejad, Hamid Reza Khorram Khorshid, Shahrzad Soleymani Fard, and Seyed Hamidollah Ghaffari. An overview of microRNAs: Biology, functions,

- therapeutics, and analysis methods: SALIMINEJAD et al.. *Journal of Cellular Physiology*, 234(5):5451–5465, May 2019.
- [10] George Adrian Calin, Calin Dan Dumitru, Masayoshi Shimizu, Roberta Bichi, Simona Zupo, Evan Noch, Hansjuerg Aldler, Sashi Rattan, Michael Keating, Kanti Rai, Laura Rassenti, Thomas Kipps, Massimo Negrini, Florencia Bullrich, and Carlo M. Croce. Frequent deletions and down-regulation of micro- RNA genes miR15 and miR16 at 13q14 in chronic lymphocytic leukemia. *Proceedings of the National Academy of Sciences of the United States of America*, 99(24):15524–15529, November 2002.
- [11] Yong Peng and Carlo M. Croce. The role of MicroRNAs in human cancer. *Signal Transduction and Targeted Therapy*, 1:15004, 2016.
- [12] Anna Elisa Roser, Lucas Caldi Gomes, Jonas Schünemann, Fabian Maass, and Paul Lingor. Circulating miRNAs as Diagnostic Biomarkers for Parkinson’s Disease. *Frontiers in Neuroscience*, 12:625, September 2018.
- [13] Eiichiro Satake, Marcus G. Pezzolesi, Zaipul I. Md Dom, Adam M. Smiles, Monika A. Niewczasz, and Andrzej S. Krolewski. Circulating miRNA Profiles Associated With Hyperglycemia in Patients With Type 1 Diabetes. *Diabetes*, 67(5):1013–1023, 2018.
- [14] Simona Ultimo, Giorgio Zauli, Alberto M. Martelli, Marco Vitale, James A. McCubrey, Silvano Capitani, and Luca M. Neri. Cardiovascular disease-related miRNAs expression: potential role as biomarkers and effects of training exercise. *Oncotarget*, 9(24):17238–17254, March 2018.
- [15] G. A. Calin and C. M. Croce. MicroRNAs and chromosomal abnormalities in cancer cells. *Oncogene*, 25(46):6202–6210, October 2006.
- [16] H. Tagawa and M. Seto. A microRNA cluster as a target of genomic amplification in malignant lymphoma. *Leukemia*, 19(11):2013–2016, November 2005.
- [17] Yoji Hayashita, Hirotaka Osada, Yoshio Tatematsu, Hideki Yamada, Kiyoshi Yanagisawa, Shuta Tomida, Yasushi Yatabe, Katsunobu Kawahara, Yoshitaka Sekido, and Takashi Takahashi. A polycistronic microRNA cluster, miR-17-92, is overexpressed in human lung cancers and enhances cell proliferation. *Cancer Research*, 65(21):9628–9632, November 2005.
- [18] Kathryn A. O’Donnell, Erik A. Wentzel, Karen I. Zeller, Chi V. Dang, and Joshua T. Mendell. c-Myc-regulated microRNAs modulate E2F1 expression. *Nature*, 435(7043):839–843, June 2005.

- [19] Tsung-Cheng Chang, Duonan Yu, Yun-Sil Lee, Erik A. Wentzel, Dan E. Arking, Kristin M. West, Chi V. Dang, Andrei Thomas-Tikhonenko, and Joshua T. Mendell. Widespread microRNA repression by Myc contributes to tumorigenesis. *Nature Genetics*, 40(1):43–50, January 2008.
- [20] Lin He, Xingyue He, Lee P. Lim, Elisa de Stanchina, Zhenyu Xuan, Yu Liang, Wen Xue, Lars Zender, Jill Magnus, Dana Ridzon, Aimee L. Jackson, Peter S. Linsley, Caifu Chen, Scott W. Lowe, Michele A. Cleary, and Gregory J. Hannon. A microRNA component of the p53 tumour suppressor network. *Nature*, 447(7148):1130–1134, June 2007.
- [21] Yoko Karube, Hisaaki Tanaka, Hirotaka Osada, Shuta Tomida, Yoshio Tatematsu, Kiyoshi Yanagisawa, Yasushi Yatabe, Junichi Takamizawa, Shinichiro Miyoshi, Tetsuya Mitsudomi, and Takashi Takahashi. Reduced expression of Dicer associated with poor prognosis in lung cancer patients. *Cancer Science*, 96(2):111–115, February 2005.
- [22] M. S. Iliou, V. da Silva-Diz, F. J. Carmona, J. Ramalho-Carvalho, H. Heyn, A. Villanueva, P. Muñoz, and M. Esteller. Impaired DICER1 function promotes stemness and metastasis in colon cancer. *Oncogene*, 33(30):4003–4015, July 2014.
- [23] Lin He, J. Michael Thomson, Michael T. Hemann, Eva Hernando-Monge, David Mu, Summer Goodson, Scott Powers, Carlos Cordon-Cardo, Scott W. Lowe, Gregory J. Hannon, and Scott M. Hammond. A microRNA polycistron as a potential human oncogene. *Nature*, 435(7043):828–833, June 2005.
- [24] Mark E. Hatley, David M. Patrick, Matthew R. Garcia, James A. Richardson, Rhonda Bassel-Duby, Eva van Rooij, and Eric N. Olson. Modulation of K-Ras-dependent lung tumorigenesis by MicroRNA-21. *Cancer Cell*, 18(3):282–293, September 2010.
- [25] Jessica A. Weber, David H. Baxter, Shile Zhang, David Y. Huang, Kuo How Huang, Ming Jen Lee, David J. Galas, and Kai Wang. The microRNA spectrum in 12 body fluids. *Clinical Chemistry*, 56(11):1733–1741, November 2010.
- [26] Xi Chen, Hongwei Liang, Junfeng Zhang, Ke Zen, and Chen-Yu Zhang. Secreted microRNAs: a new form of intercellular communication. *Trends in Cell Biology*, 22(3):125–132, March 2012.
- [27] Patrick S. Mitchell, Rachael K. Parkin, Evan M. Kroh, Brian R. Fritz, Stacia K. Wyman, Era L. Pogosova-Agadjanyan, Amelia Peterson, Jennifer Noteboom, Kathy C. O’Briant, April Allen, Daniel W. Lin, Nicole Urban, Charles W. Drescher, Beatrice S.

- Knudsen, Derek L. Stirewalt, Robert Gentleman, Robert L. Vessella, Peter S. Nelson, Daniel B. Martin, and Muneesh Tewari. Circulating microRNAs as stable blood-based markers for cancer detection. *Proceedings of the National Academy of Sciences of the United States of America*, 105(30):10513–10518, July 2008.
- [28] Sarah Roush and Frank J. Slack. The let-7 family of microRNAs. *Trends in Cell Biology*, 18(10):505–516, October 2008.
- [29] Haifeng Dong, Jianping Lei, Lin Ding, Yongqiang Wen, Huangxian Ju, and Xueji Zhang. MicroRNA: Function, Detection, and Bioanalysis. *Chemical Reviews*, 113(8):6207–6233, August 2013.
- [30] Zev Williams, Iddo Z. Ben-Dov, Rony Elias, Aleksandra Mihailovic, Miguel Brown, Zev Rosenwaks, and Thomas Tuschl. Comprehensive profiling of circulating microRNA via small RNA sequencing of cDNA libraries reveals biomarker potential and limitations. *Proceedings of the National Academy of Sciences*, 110(11):4255–4260, March 2013.
- [31] Aurora Esquela-Kerscher and Frank J. Slack. Oncomirs - microRNAs with a role in cancer. *Nature Reviews. Cancer*, 6(4):259–269, April 2006.
- [32] Susan R. Pfeffer, Chuan He Yang, and Lawrence M. Pfeffer. The Role of miR-21 in Cancer: The Role of miR-21 In Cancer. *Drug Development Research*, 76(6):270–277, September 2015.
- [33] Jun Lu, Gad Getz, Eric A. Miska, Ezequiel Alvarez-Saavedra, Justin Lamb, David Peck, Alejandro Sweet-Cordero, Benjamin L. Ebert, Raymond H. Mak, Adolfo A. Ferrando, James R. Downing, Tyler Jacks, H. Robert Horvitz, and Todd R. Golub. MicroRNA expression profiles classify human cancers. *Nature*, 435(7043):834–838, June 2005.
- [34] Nozomu Yanaihara, Natasha Caplen, Elise Bowman, Masahiro Seike, Kensuke Kumamoto, Ming Yi, Robert M. Stephens, Aikou Okamoto, Jun Yokota, Tadao Tanaka, George Adrian Calin, Chang-Gong Liu, Carlo M. Croce, and Curtis C. Harris. Unique microRNA molecular profiles in lung cancer diagnosis and prognosis. *Cancer Cell*, 9(3):189–198, March 2006.
- [35] Mustafa Kahraman, Anne Röske, Thomas Laufer, Tobias Fehlmann, Christina Backes, Fabian Kern, Jochen Kohlhaas, Hannah Schrörs, Anna Saiz, Cassandra Zabler, Nicole Ludwig, Peter A. Fasching, Reiner Strick, Matthias Rübner, Matthias W. Beckmann, Eckart Meese, Andreas Keller, and Michael G. Schrauder. MicroRNA in diagnosis

- and therapy monitoring of early-stage triple-negative breast cancer. *Scientific Reports*, 8(1):11584, December 2018.
- [36] Huo Zhang, Mingxia Zhu, Xia Shan, Xin Zhou, Tongshan Wang, Jinying Zhang, Jinsong Tao, Wenfang Cheng, Gang Chen, Jian Li, Ping Liu, Qiang Wang, and Wei Zhu. A panel of seven-miRNA signature in plasma as potential biomarker for colorectal cancer diagnosis. *Gene*, 687:246–254, March 2019.
- [37] Tetsuya Ueda, Stefano Volinia, Hiroshi Okumura, Masayoshi Shimizu, Cristian Tac-cioli, Simona Rossi, Hansjuerg Alder, Chang-gong Liu, Naohide Oue, Wataru Yasui, Kazuhiro Yoshida, Hiroki Sasaki, Sachiyo Nomura, Yasuyuki Seto, Michio Kaminishi, George A. Calin, and Carlo M. Croce. Relation between microRNA expression and progression and prognosis of gastric cancer: a microRNA expression analysis. *The Lancet. Oncology*, 11(2):136–146, February 2010.
- [38] Srinivasulu Yerukala Sathipati and Shinn-Ying Ho. Identifying a miRNA signature for predicting the stage of breast cancer. *Scientific Reports*, 8(1):16138, December 2018.
- [39] Xiu-Hui Shi, Xu Li, Hang Zhang, Rui-Zhi He, Yan Zhao, Min Zhou, Shu-Tao Pan, Chun-Le Zhao, Ye-Chen Feng, Min Wang, Xing-Jun Guo, and Ren-Yi Qin. A Five-microRNA Signature for Survival Prognosis in Pancreatic Adenocarcinoma based on TCGA Data. *Scientific Reports*, 8(1):7638, December 2018.
- [40] Guillaume Gines, Roberta Menezes, Wenjin Xiao, Yannick Rondelez, and Valerie Taly. Emerging isothermal amplification technologies for microRNA biosensing: Applications to liquid biopsies. *Molecular Aspects of Medicine*, 72:100832, April 2020.
- [41] Caifu Chen, Dana A. Ridzon, Adam J. Broomer, Zhaohui Zhou, Danny H. Lee, Julie T. Nguyen, Maura Barbisin, Nan Lan Xu, Vikram R. Mahuvakar, Mark R. Andersen, Kai Qin Lao, Kenneth J. Livak, and Karl J. Guegler. Real-time quantification of microRNAs by stem-loop RT-PCR. *Nucleic Acids Research*, 33(20):e179, November 2005.
- [42] Rui Shi and Vincent L. Chiang. Facile means for quantifying microRNA expression by real-time PCR. *BioTechniques*, 39(4):519–525, October 2005.
- [43] Paola Tiberio, Maurizio Callari, Valentina Angeloni, Maria Grazia Daidone, and Valentina Appierto. Challenges in using circulating miRNAs as cancer biomarkers. *BioMed Research International*, 2015:731479, 2015.

- [44] Christopher K. Raymond, Brian S. Roberts, Phillip Garrett-Engele, Lee P. Lim, and Jason M. Johnson. Simple, quantitative primer-extension PCR assay for direct monitoring of microRNAs and short-interfering RNAs. *RNA (New York, N. Y.)*, 11(11):1737–1744, November 2005.
- [45] Pieter Mestdagh, Nicole Hartmann, Lukas Baeriswyl, Ditte Andreasen, Nathalie Bernard, Caifu Chen, David Cheo, Petula D’Andrade, Mike DeMayo, Lucas Dennis, Stefaan Derveaux, Yun Feng, Stephanie Fulmer-Smentek, Bernhard Gerstmayer, Julia Gouffon, Chris Grimley, Eric Lader, Kathy Y Lee, Shujun Luo, Peter Mouritzen, Aishwarya Narayanan, Sunali Patel, Sabine Peiffer, Silvia Rüberg, Gary Schroth, Dave Schuster, Jonathan M Shaffer, Elliot J Shelton, Scott Silveria, Umberto Ulmanella, Vamsi Veeramachaneni, Frank Staedtler, Thomas Peters, Toumy Guettouche, Linda Wong, and Jo Vandesompele. Evaluation of quantitative miRNA expression platforms in the microRNA quality control (miRQC) study. *Nature Methods*, 11(8):809–815, August 2014.
- [46] Vladimir Benes and Mirco Castoldi. Expression profiling of microRNA using real-time quantitative PCR, how to use it and what is available. *Methods*, 50(4):244–249, April 2010.
- [47] Carsten A. Raabe, Thean-Hock Tang, Juergen Brosius, and Timofey S. Rozhdestvensky. Biases in small RNA deep sequencing data. *Nucleic Acids Research*, 42(3):1414–1426, February 2014.
- [48] Stephen A. Bustin, Vladimir Benes, Jeremy A. Garson, Jan Hellemans, Jim Huggett, Mikael Kubista, Reinhold Mueller, Tania Nolan, Michael W. Pfaffl, Gregory L. Shipley, Jo Vandesompele, and Carl T. Wittwer. The MIQE guidelines: minimum information for publication of quantitative real-time PCR experiments. *Clinical Chemistry*, 55(4):611–622, April 2009.
- [49] Peter Androvic, Lukas Valihrach, Julie Elling, Robert Sjoback, and Mikael Kubista. Two-tailed RT-qPCR: a novel method for highly accurate miRNA quantification. *Nucleic Acids Research*, 45(15):e144–e144, September 2017.
- [50] Jiangyan Zhang, Zhengping Li, Hui Wang, Yucong Wang, Hongxia Jia, and Jingli Yan. Ultrasensitive quantification of mature microRNAs by real-time PCR based on ligation of a ribonucleotide-modified DNA probe. *Chemical Communications (Cambridge, England)*, 47(33):9465–9467, September 2011.

- [51] P. Kumar, B. H. Johnston, and S. A. Kazakov. miR-ID: A novel, circularization-based platform for detection of microRNAs. *RNA*, 17(2):365–380, February 2011.
- [52] Ryan T. Fuchs, Zhiyi Sun, Fanglei Zhuang, and G. Brett Robb. Bias in Ligation-Based Small RNA Sequencing Library Construction Is Determined by Adaptor and RNA Structure. *PLOS ONE*, 10(5):e0126049, May 2015.
- [53] Jingmin Jin, Sophie Vaud, Alexander M. Zhelkovsky, Janos Posfai, and Larry A. McReynolds. Sensitive and specific miRNA detection method using SplintR Ligase. *Nucleic Acids Research*, 44(13):e116–e116, July 2016.
- [54] Eugene J. H. Wee and Matt Trau. Simple Isothermal Strategy for Multiplexed, Rapid, Sensitive, and Accurate miRNA Detection. *ACS Sensors*, 1(6):670–675, June 2016.
- [55] Sarah L. Daubendiek, Kevin Ryan, and Eric T. Kool. Rolling-Circle RNA Synthesis: Circular Oligonucleotides as Efficient Substrates for T7 RNA Polymerase. *Journal of the American Chemical Society*, 117(29):7818–7819, July 1995.
- [56] Dongyu Liu, Sarah L. Daubendiek, Martin A. Zillman, Kevin Ryan, and Eric T. Kool. Rolling Circle DNA Synthesis: Small Circular Oligonucleotides as Efficient Templates for DNA Polymerases. *Journal of the American Chemical Society*, 118(7):1587–1594, February 1996.
- [57] Søren Peter Jonstrup, Jørn Koch, and Jørgen Kjems. A microRNA detection system based on padlock probes and rolling circle amplification. *RNA (New York, N.Y.)*, 12(9):1747–1752, September 2006.
- [58] Hirokazu Takahashi, Masahiko Ohkawachi, Kyohei Horio, Toshiro Kobori, Tsunehiro Aki, Yukihiko Matsumura, Yutaka Nakashimada, and Yoshiko Okamura. RNase H-assisted RNA-primed rolling circle amplification for targeted RNA sequence detection. *Scientific Reports*, 8(1):7770, December 2018.
- [59] Tomasz Krzywkowski and Mats Nilsson. Fidelity of RNA templated end-joining by chlorella virus DNA ligase and a novel iLock assay with improved direct RNA detection accuracy. *Nucleic Acids Research*, 45(18):e161–e161, October 2017.
- [60] Ruijie Deng, Longhua Tang, Qianqian Tian, Ying Wang, Lei Lin, and Jinghong Li. Toehold-initiated Rolling Circle Amplification for Visualizing Individual MicroRNAs In Situ in Single Cells. *Angewandte Chemie International Edition*, 53(9):2389–2393, February 2014.

- [61] Xiaoli Zhu, Yalan Shen, Jiepei Cao, Li Yin, Fangfang Ban, Yongqian Shu, and Genxi Li. Detection of microRNA SNPs with ultrahigh specificity by using reduced graphene oxide-assisted rolling circle amplification. *Chemical Communications*, 51(49):10002–10005, 2015.
- [62] Tingting Fan, Yu Mao, Qinsheng Sun, Feng Liu, Jin-Shun Lin, Yajie Liu, Junwei Cui, and Yuyang Jiang. Branched rolling circle amplification method for measuring serum circulating microRNA levels for early breast cancer detection. *Cancer Science*, 109(9):2897–2906, September 2018.
- [63] Haiyun Liu, Lu Li, Lili Duan, Xu Wang, Yanxia Xie, Lili Tong, Qian Wang, and Bo Tang. High Specific and Ultrasensitive Isothermal Detection of MicroRNA by Padlock Probe-Based Exponential Rolling Circle Amplification. *Analytical Chemistry*, 85(16):7941–7947, August 2013.
- [64] Jeffrey Van Ness, Lori K. Van Ness, and David J. Galas. Isothermal reactions for the amplification of oligonucleotides. *Proceedings of the National Academy of Sciences of the United States of America*, 100(8):4504–4509, April 2003.
- [65] Eric Tan, Jennifer Wong, Doris Nguyen, Yolanda Zhang, Barbara Erwin, Lori K. Van Ness, Shenda M. Baker, David J. Galas, and Angelika Niemz. Isothermal DNA Amplification Coupled with DNA Nanosphere-Based Colorimetric Detection. *Analytical Chemistry*, 77(24):7984–7992, December 2005.
- [66] Hongxia Jia, Zhengping Li, Chenghui Liu, and Yongqiang Cheng. Ultrasensitive detection of microRNAs by exponential isothermal amplification. *Angewandte Chemie (International Ed. in English)*, 49(32):5498–5501, July 2010.
- [67] Yongqiang Cheng, Lijuan Dong, Jiangyan Zhang, Yaqing Zhao, and Zhengping Li. Recent advances in microRNA detection. *The Analyst*, 143(8):1758–1774, 2018.
- [68] Eric Tan, Barbara Erwin, Shale Dames, Tanya Ferguson, Megan Buechel, Bruce Irvine, Karl Voelkerding, and Angelika Niemz. Specific versus Nonspecific Isothermal DNA Amplification through Thermophilic Polymerase and Nicking Enzyme Activities[†]. *Biochemistry*, 47(38):9987–9999, September 2008.
- [69] Jifeng Qian, Tanya M. Ferguson, Deepali N. Shinde, Alissa J. Ramírez-Borrero, Arend Hintze, Christoph Adami, and Angelika Niemz. Sequence dependence of isothermal DNA amplification via EXPAR. *Nucleic Acids Research*, 40(11):e87–e87, June 2012.

- [70] Kevin Montagne, Guillaume Gines, Teruo Fujii, and Yannick Rondelez. Boosting functionality of synthetic DNA circuits with tailored deactivation. *Nature Communications*, 7(1):13474, December 2016.
- [71] Guillaume Gines, Roberta Menezes, Kaori Nara, Anne-Sophie Kirstetter, Valerie Taly, and Yannick Rondelez. Isothermal digital detection of microRNAs using background-free molecular circuit. *Science Advances*, 6(4):eaay5952, January 2020.
- [72] Jun Chen, Xueqing Zhou, Yingjun Ma, Xiulian Lin, Zong Dai, and Xiaoyong Zou. Asymmetric exponential amplification reaction on a toehold/biotin featured template: an ultrasensitive and specific strategy for isothermal microRNAs analysis. *Nucleic Acids Research*, page gkw504, June 2016.
- [73] Jun Chen, Taixue An, Yingjun Ma, Bo Situ, Danping Chen, Yuzhi Xu, Li Zhang, Zong Dai, and Xiaoyong Zou. Isothermal Amplification on a Structure-Switchable Symmetric Toehold Dumbbell-Template: A Strategy Enabling MicroRNA Analysis at the Single-Cell Level with Ultrahigh Specificity and Accuracy. *Analytical Chemistry*, 90(1):859–865, January 2018.
- [74] Dmitry A. Shagin, Denis V. Rebrikov, Valery B. Kozhemyako, Ilia M. Altshuler, Alex S. Shcheglov, Pavel A. Zhulidov, Ekaterina A. Bogdanova, Dmitry B. Staroverov, Valery A. Rasskazov, and Sergey Lukyanov. A novel method for SNP detection using a new duplex-specific nuclease from crab hepatopancreas. *Genome Research*, 12(12):1935–1942, December 2002.
- [75] Veronika E. Anisimova, Denis V. Rebrikov, Dmitry A. Shagin, Valery B. Kozhemyako, Natalia I. Menzorova, Dmitry B. Staroverov, Rustam Ziganshin, Laura L. Vagner, Valery A. Rasskazov, Sergey A. Lukyanov, and Alex S. Shcheglov. Isolation, characterization and molecular cloning of Duplex-Specific Nuclease from the hepatopancreas of the Kamchatka crab. *BMC Biochemistry*, 9(1):14, 2008.
- [76] Bin-Cheng Yin, Yu-Qiang Liu, and Bang-Ce Ye. One-Step, Multiplexed Fluorescence Detection of microRNAs Based on Duplex-Specific Nuclease Signal Amplification. *Journal of the American Chemical Society*, 134(11):5064–5067, March 2012.
- [77] Yingcun Li, Jiangyan Zhang, Jingjing Zhao, Likun Zhao, Yongqiang Cheng, and Zhengping Li. A simple molecular beacon with duplex-specific nuclease amplification for detection of microRNA. *The Analyst*, 141(3):1071–1076, 2016.

- [78] Hui Zhou, Chao Yang, Huifang Chen, Xun Li, Yongdong Li, and Xiaolin Fan. A simple G-quadruplex molecular beacon-based biosensor for highly selective detection of microRNA. *Biosensors and Bioelectronics*, 87:552–557, January 2017.
- [79] Junjie Li, Shuangshuang Yang, Chen Zuo, Ling Dai, Yongcan Guo, and Guoming Xie. Applying CRISPR-Cas12a as a Signal Amplifier to Construct Biosensors for Non-DNA Targets in Ultralow Concentrations. *ACS Sensors*, page accsensors.9b02305, March 2020.
- [80] Yacui Liu, Jiangyan Zhang, Jingxiao Tian, Xiaofei Fan, Hao Geng, and Yongqiang Cheng. Multiplex detection of microRNAs by combining molecular beacon probes with T7 exonuclease-assisted cyclic amplification reaction. *Analytical and Bioanalytical Chemistry*, 409(1):107–114, January 2017.
- [81] Robert M. Dirks and Niles A. Pierce. Triggered amplification by hybridization chain reaction. *Proceedings of the National Academy of Sciences of the United States of America*, 101(43):15275–15278, October 2004.
- [82] Suvir Venkataraman, Robert M. Dirks, Paul W. K. Rothemund, Erik Winfree, and Niles A. Pierce. An autonomous polymerization motor powered by DNA hybridization. *Nature Nanotechnology*, 2(8):490–494, August 2007.
- [83] Harry M T Choi, Joann Y Chang, Le A Trinh, Jennifer E Padilla, Scott E Fraser, and Niles A Pierce. Programmable in situ amplification for multiplexed imaging of mRNA expression. *Nature Biotechnology*, 28(11):1208–1212, November 2010.
- [84] Qingsheng Guo, Feika Bian, Yuqian Liu, Xiaojun Qu, Xianyun Hu, and Qingjiang Sun. Hybridization chain reactions on silica coated Qbeads for the colorimetric detection of multiplex microRNAs. *Chemical Communications (Cambridge, England)*, 53(36):4954–4957, May 2017.
- [85] Harry M. T. Choi, Victor A. Beck, and Niles A. Pierce. Next-generation in situ hybridization chain reaction: higher gain, lower cost, greater durability. *ACS nano*, 8(5):4284–4294, May 2014.
- [86] Maayan Schwarzkopf and Niles A. Pierce. Multiplexed miRNA northern blots via hybridization chain reaction. *Nucleic Acids Research*, page gkw503, June 2016.
- [87] David Yu Zhang and Erik Winfree. Control of DNA Strand Displacement Kinetics Using Toehold Exchange. *Journal of the American Chemical Society*, 131(47):17303–17314, December 2009.

- [88] Cuiping Ma, Wenshuo Wang, Zhaoxin Li, Lijie Cao, and Qingyin Wang. Simple colorimetric DNA detection based on hairpin assembly reaction and target-catalytic circuits for signal amplification. *Analytical Biochemistry*, 429(2):99–102, October 2012.
- [89] Jinfeng Chen, Bo Liu, Xiaorong Song, Ping Tong, Huanghao Yang, and Lan Zhang. Enzyme-free amplified detection of microRNA using target-catalyzed hairpin assembly and magnesium ion-dependent deoxyribozyme. *Science China Chemistry*, 58(12):1906–1911, December 2015.
- [90] Yi Liu, Tian Shen, Jing Li, Hang Gong, Chunyan Chen, Xiaoming Chen, and Changqun Cai. Ratiometric Fluorescence Sensor for the MicroRNA Determination by Catalyzed Hairpin Assembly. *ACS Sensors*, 2(10):1430–1434, October 2017.
- [91] Anna Valoczi, Csaba Hornyik, Nora Varga, Jozsef Burgyan, Sakari Kauppinen, and Zoltan Havelda. Sensitive and specific detection of microRNAs by northern blot analysis using LNA-modified oligonucleotide probes. *Nucleic Acids Research*, 32(22):e175, December 2004.
- [92] Tinglan Ouyang, Zhiyu Liu, Zhiyi Han, and Qinyu Ge. MicroRNA Detection Specificity: Recent Advances and Future Perspective. *Analytical Chemistry*, 91(5):3179–3186, March 2019. Publisher: American Chemical Society.
- [93] Ehsan Arefian, Jafar Kiani, Masoud Soleimani, S. Ali M. Shariati, Seyed Hamid Aghaee-Bakhtiari, Amir Atashi, Yousof Gheisari, Naser Ahmadbeigi, Ali M. Banaei-Moghaddam, Mahmood Naderi, Nabiolah Namvarasl, Liam Good, and Omid R. Faridani. Analysis of microRNA signatures using size-coded ligation-mediated PCR. *Nucleic Acids Research*, 39(12):e80–e80, July 2011.
- [94] Arun Richard Chandrasekaran, Molly MacIsaac, Paromita Dey, Oksana Levchenko, Lifeng Zhou, Madeline Andres, Bijan K. Dey, and Ken Halvorsen. Cellular microRNA detection with miRacles: microRNA- activated conditional looping of engineered switches. *Science Advances*, 5(3):eaau9443, March 2019.
- [95] Ruei-Min Jiang, Yu-Sun Chang, Shu-Jen Chen, Jian-Hung Chen, Hua-Chien Chen, and Po-Ling Chang. Multiplexed microRNA detection by capillary electrophoresis with laser-induced fluorescence. *Journal of Chromatography A*, 1218(18):2604–2610, May 2011.
- [96] Pengbo Zhang, Ye Liu, Yajing Zhang, Chenghui Liu, Zhibin Wang, and Zhengping Li. Multiplex ligation-dependent probe amplification (MLPA) for ultrasensitive mul-

- tiplexed microRNA detection using ribonucleotide-modified DNA probes. *Chemical Communications*, 49(85):10013, 2013.
- [97] Kaiji Wei, Jingjin Zhao, Yingfeng Qin, Shuting Li, Yong Huang, and Shulin Zhao. A novel multiplex signal amplification strategy based on microchip electrophoresis platform for the improved separation and detection of microRNAs. *Talanta*, 189:437–441, November 2018.
- [98] Jeongkyeong Na, Gi Won Shin, Heehwa G. Son, Seung-Jae V. Lee, and Gyoo Yeol Jung. Multiplex quantitative analysis of microRNA expression via exponential isothermal amplification and conformation-sensitive DNA separation. *Scientific Reports*, 7(1):11396, December 2017.
- [99] Tong Qi, Chang Song, Jing He, Wei Shen, Dezhao Kong, Haiwei Shi, Li Tan, Ruirong Pan, Sheng Tang, and Hian Kee Lee. Highly Sensitive Detection of Multiple MicroRNAs by High-Performance Liquid Chromatography Coupled with Long and Short Probe-Based Recycling Amplification. *Analytical Chemistry*, 92(7):5033–5040, April 2020.
- [100] Salvatore A. E. Marras, Sanjay Tyagi, Dan-Oscar Antson, and Fred Russell Kramer. Color-coded molecular beacons for multiplex PCR screening assays. *PloS One*, 14(3):e0213906, 2019.
- [101] Aditya Rajagopal, Axel Scherer, Andrew Homyk, and Emil Kartalov. Supercolor Coding Methods for Large-Scale Multiplexing of Biochemical Assays. *Analytical Chemistry*, 85(16):7629–7636, August 2013.
- [102] Felix Moltzahn, Adam B. Olshen, Lauren Baehner, Andrew Peek, Lawrence Fong, Hubert Stöppler, Jeffrey Simko, Joan F. Hilton, Peter Carroll, and Robert Blemloch. Microfluidic-based multiplex qRT-PCR identifies diagnostic and prognostic microRNA signatures in the sera of prostate cancer patients. *Cancer Research*, 71(2):550–560, January 2011.
- [103] Zongwen Jin, Daniel Geißler, Xue Qiu, K. David Wegner, and Niko Hildebrandt. A Rapid, Amplification-Free, and Sensitive Diagnostic Assay for Single-Step Multiplexed Fluorescence Detection of MicroRNA. *Angewandte Chemie International Edition*, 54(34):10024–10029, August 2015.
- [104] Xue Qiu and Niko Hildebrandt. Rapid and Multiplexed MicroRNA Diagnostic Assay Using Quantum Dot-Based Förster Resonance Energy Transfer. *ACS Nano*, 9(8):8449–8457, August 2015.

- [105] Xue Qiu, Jiajia Guo, Zongwen Jin, Alexandra Petreto, Igor L. Medintz, and Niko Hildebrandt. Multiplexed Nucleic Acid Hybridization Assays Using Single-FRET-Pair Distance-Tuning. *Small*, 13(25):1700332, July 2017.
- [106] Jiajia Guo, Carlos Mingoos, Xue Qiu, and Niko Hildebrandt. Simple, Amplified, and Multiplexed Detection of MicroRNAs Using Time-Gated FRET and Hybridization Chain Reaction. *Analytical Chemistry*, 91(4):3101–3109, February 2019.
- [107] Jingyue Xu, Jiajia Guo, Nicole Golob-Schwarzl, Johannes Haybaeck, Xue Qiu, and Niko Hildebrandt. Single-Measurement Multiplexed Quantification of MicroRNAs from Human Tissue Using Catalytic Hairpin Assembly and Förster Resonance Energy Transfer. *ACS Sensors*, 5(6):1768–1776, June 2020.
- [108] Xue Qiu, Jiajia Guo, Jingyue Xu, and Niko Hildebrandt. Three-Dimensional FRET Multiplexing for DNA Quantification with Attomolar Detection Limits. *The Journal of Physical Chemistry Letters*, 9(15):4379–4384, August 2018.
- [109] Wen-Qi Ye, Yi-Xuan Wei, Ying-Zhi Zhang, Chun-Guang Yang, and Zhang-Run Xu. Multiplexed detection of micro-RNAs based on microfluidic multi-color fluorescence droplets. *Analytical and Bioanalytical Chemistry*, 412(3):647–655, January 2020.
- [110] Ruixuan Wang, Xianxian Zhao, Xiaohui Chen, Xiaopei Qiu, Guangchao Qing, Hong Zhang, Liangliang Zhang, Xiaolin Hu, Zhuoqi He, Daidi Zhong, Ying Wang, and Yang Luo. Rolling Circular Amplification (RCA)-Assisted CRISPR/Cas9 Cleavage (RACE) for Highly Specific Detection of Multiple Extracellular Vesicle MicroRNAs. *Analytical Chemistry*, 92(2):2176–2185, January 2020.
- [111] Yaqin Tang, Xiao He, Rui Yuan, Xingming Liu, Yi Zhao, Tingting Wang, Hui Chen, and Xuli Feng. Logic-signal-based multiplex detection of MiRNAs with high tension hybridization and multiple signal amplification. *The Analyst*, 145(12):4314–4320, 2020.
- [112] Liang Cui, Xiaoyan Lin, Ninghang Lin, Yanling Song, Zhi Zhu, Xi Chen, and Chaoyong James Yang. Graphene oxide-protected DNA probes for multiplex microRNA analysis in complex biological samples based on a cyclic enzymatic amplification method. *Chem. Commun.*, 48(2):194–196, 2012.
- [113] Mingshu Xiao, Tiantian Man, Changfeng Zhu, Hao Pei, Jiye Shi, Li Li, Xiangmeng Qu, Xizhong Shen, and Jiang Li. MoS₂ Nanoprobe for MicroRNA Quantification Based on Duplex-Specific Nuclease Signal Amplification. *ACS Applied Materials & Interfaces*, 10(9):7852–7858, March 2018.

- [114] Samuel Robinson, Marie Follo, David Haenel, Maximilian Mauler, Daniela Stallmann, Lukas Andreas Heger, Thomas Helbing, Daniel Duerschmied, Karlheinz Peter, Christoph Bode, Ingo Ahrens, and Marcus Hortmann. Chip-based digital PCR as a novel detection method for quantifying microRNAs in acute myocardial infarction patients. *Acta Pharmacologica Sinica*, 39(7):1217–1227, July 2018.
- [115] S. Robinson, M. Follo, D. Haenel, M. Mauler, D. Stallmann, M. Tewari, D. Duerschmied, K. Peter, C. Bode, I. Ahrens, and M. Hortmann. Droplet digital PCR as a novel detection method for quantifying microRNAs in acute myocardial infarction. *International Journal of Cardiology*, 257:247–254, April 2018.
- [116] Qun Zhong, Smiti Bhattacharya, Steven Kotsopoulos, Jeff Olson, Valérie Taly, Andrew D. Griffiths, Darren R. Link, and Jonathan W. Larson. Multiplex digital PCR: breaking the one target per color barrier of quantitative PCR. *Lab on a Chip*, 11(13):2167, 2011.
- [117] Yannick Rondelez and Guillaume Gines. Multiplex Digital MicroRNA Detection Using Cross-Inhibitory DNA Circuits. *ACS Sensors*, page acssensors.0c00593, July 2020.
- [118] Lucas D. Smith, Yang Liu, Mohammad U. Zahid, Taylor D. Canady, Liang Wang, Manish Kohli, Brian T. Cunningham, and Andrew M. Smith. High-Fidelity Single Molecule Quantification in a Flow Cytometer Using Multiparametric Optical Analysis. *ACS Nano*, 14(2):2324–2335, February 2020.
- [119] M. Monsur Ali, Feng Li, Zhiqing Zhang, Kaixiang Zhang, Dong-Ku Kang, James A. Ankrum, X. Chris Le, and Weian Zhao. Rolling circle amplification: a versatile tool for chemical biology, materials science and medicine. *Chemical Society Reviews*, 43(10):3324–3341, May 2014.
- [120] Zhian Hu, Fujian Xu, Gongwei Sun, Sichun Zhang, and Xinrong Zhang. Homogeneous multiplexed digital detection of microRNA with ligation-rolling circle amplification. *Chemical Communications*, 56(40):5409–5412, 2020.
- [121] Malte Kühnemund, Iván Hernández-Neuta, Mohd Istiaq Sharif, Matteo Cornaglia, Martin A.M. Gijs, and Mats Nilsson. Sensitive and inexpensive digital DNA analysis by microfluidic enrichment of rolling circle amplified single-molecules. *Nucleic Acids Research*, page gkw1324, January 2017.
- [122] Sergio Barberán-Soler, Jenny M. Vo, Ryan E. Hogans, Anne Dallas, Brian H. Johnston, and Sergei A. Kazakov. Decreasing miRNA sequencing bias using a single adapter and circularization approach. *Genome Biology*, 19(1):105, December 2018.

- [123] Marc R. Friedländer, Wei Chen, Catherine Adamidi, Jonas Maaskola, Ralf Einspanier, Signe Knespel, and Nikolaus Rajewsky. Discovering microRNAs from deep sequencing data using miRDeep. *Nature Biotechnology*, 26(4):407–415, April 2008.
- [124] Vivek Priy Dave, Tien Anh Ngo, Anna-Karin Pernestig, Diana Tilevik, Krishna Kant, Trieu Nguyen, Anders Wolff, and Dang Duong Bang. MicroRNA amplification and detection technologies: opportunities and challenges for point of care diagnostics. *Laboratory Investigation*, 99(4):452–469, April 2019.
- [125] Travis C. Glenn. Field guide to next-generation DNA sequencers. *Molecular Ecology Resources*, 11(5):759–769, September 2011.
- [126] Shahar Alon, Francois Vigneault, Seda Eminaga, Danos C. Christodoulou, Jonathan G. Seidman, George M. Church, and Eli Eisenberg. Barcoding bias in high-throughput multiplex sequencing of miRNA. *Genome Research*, 21(9):1506–1511, September 2011.
- [127] Yuan-Jyue Chen, Christopher N. Takahashi, Lee Organick, Callista Bee, Siena Dumas Ang, Patrick Weiss, Bill Peck, Georg Seelig, Luis Ceze, and Karin Strauss. Quantifying molecular bias in DNA data storage. *Nature Communications*, 11(1):3264, December 2020.
- [128] Shirley Tam, Richard de Borja, Ming-Sound Tsao, and John D McPherson. Robust global microRNA expression profiling using next-generation sequencing technologies. *Laboratory Investigation*, 94(3):350–358, March 2014.
- [129] Qiyuan Yang, Jimin Lin, Miao Liu, Ronghong Li, Bin Tian, Xue Zhang, Beiyong Xu, Mofang Liu, Xuan Zhang, Yiping Li, Huijuan Shi, and Ligang Wu. Highly sensitive sequencing reveals dynamic modifications and activities of small RNAs in mouse oocytes and early embryos. *Science Advances*, 2(6):e1501482, 2016.
- [130] Anna M. L. Coenen-Stass, Helena Sork, Sole Gatto, Caroline Godfrey, Amarjit Bhomra, Kaarel Krjutškov, Jonathan R. Hart, Jakub O. Westholm, Liz O’Donovan, Andreas Roos, Hanns Lochmüller, Pier Lorenzo Puri, Samir El Andaloussi, Matthew J. A. Wood, and Thomas C. Roberts. Comprehensive RNA-Sequencing Analysis in Serum and Muscle Reveals Novel Small RNA Signatures with Biomarker Potential for DMD. *Molecular Therapy. Nucleic Acids*, 13:1–15, December 2018.
- [131] Cuiyun Yang, Baoting Dou, Kai Shi, Yaqin Chai, Yun Xiang, and Ruo Yuan. Multiplexed and amplified electronic sensor for the detection of microRNAs from cancer cells. *Analytical Chemistry*, 86(23):11913–11918, December 2014.

- [132] Yuanyuan Chang, Zhongyu Wu, Qianxin Sun, Ying Zhuo, Yaqin Chai, and Ruo Yuan. Simply Constructed and Highly Efficient Classified Cargo-Discharge DNA Robot: A DNA Walking Nanomachine Platform for Ultrasensitive Multiplexed Sensing. *Analytical Chemistry*, 91(13):8123–8128, July 2019.
- [133] Sai Xu, Yuanyuan Chang, Zhongyu Wu, Yunrui Li, Ruo Yuan, and Yaqin Chai. One DNA circle capture probe with multiple target recognition domains for simultaneous electrochemical detection of miRNA-21 and miRNA-155. *Biosensors and Bioelectronics*, 149:111848, February 2020.
- [134] Wenyuan Zhu, Xingpeng Su, Xiaoyu Gao, Zong Dai, and Xiaoyong Zou. A label-free and PCR-free electrochemical assay for multiplexed microRNA profiles by ligase chain reaction coupling with quantum dots barcodes. *Biosensors and Bioelectronics*, 53:414–419, March 2014.
- [135] Jingrui Wang, Zhixuan Lu, Hailin Tang, Ling Wu, Zixiao Wang, Minghua Wu, Xinyao Yi, and Jianxiu Wang. Multiplexed Electrochemical Detection of MiRNAs from Sera of Glioma Patients at Different Stages via the Novel Conjugates of Conducting Magnetic Microbeads and Diblock Oligonucleotide-Modified Gold Nanoparticles. *Analytical Chemistry*, 89(20):10834–10840, October 2017.
- [136] Sawsen Azzouzi, Zina Fredj, Anthony P. F. Turner, Mounir Ben Ali, and Wing Cheung Mak. Generic Neutravidin Biosensor for Simultaneous Multiplex Detection of MicroRNAs via Electrochemically Encoded Responsive Nanolabels. *ACS Sensors*, 4(2):326–334, February 2019.
- [137] Rui Liu, Shixi Zhang, Chao Wei, Zhi Xing, Sichun Zhang, and Xinrong Zhang. Metal Stable Isotope Tagging: Renaissance of Radioimmunoassay for Multiplex and Absolute Quantification of Biomolecules. *Accounts of Chemical Research*, 49(5):775–783, May 2016.
- [138] Shixi Zhang, Rui Liu, Zhi Xing, Sichun Zhang, and Xinrong Zhang. Multiplex miRNA assay using lanthanide-tagged probes and the duplex-specific nuclease amplification strategy. *Chemical Communications*, 52(99):14310–14313, 2016.
- [139] E. C. Le Ru, E. Blackie, M. Meyer, and P. G. Etchegoin. Surface Enhanced Raman Scattering Enhancement Factors: A Comprehensive Study. *The Journal of Physical Chemistry C*, 111(37):13794–13803, September 2007.

- [140] Jing Su, Dongfang Wang, Lena Nörbel, Jianlei Shen, Zhihan Zhao, Yanzhi Dou, Tianhuan Peng, Jiye Shi, Sanjay Mathur, Chunhai Fan, and Shiping Song. Multicolor Gold–Silver Nano-Mushrooms as Ready-to-Use SERS Probes for Ultrasensitive and Multiplex DNA/miRNA Detection. *Analytical Chemistry*, 89(4):2531–2538, February 2017.
- [141] Wen Zhou, Ya-Fei Tian, Bin-Cheng Yin, and Bang-Ce Ye. Simultaneous Surface-Enhanced Raman Spectroscopy Detection of Multiplexed MicroRNA Biomarkers. *Analytical Chemistry*, 89(11):6120–6128, 2017.
- [142] Hsin-Neng Wang, Bridget M. Crawford, Andrew M. Fales, Michelle L. Bowie, Victoria L. Seewaldt, and Tuan Vo-Dinh. Multiplexed Detection of MicroRNA Biomarkers Using SERS-Based Inverse Molecular Sentinel (iMS) Nanoprobes. *The Journal of Physical Chemistry C*, 120(37):21047–21055, September 2016.
- [143] Woo Hyun Kim, Jong Uk Lee, Sojin Song, Soohyun Kim, Young Jae Choi, and Sang Jun Sim. A label-free, ultra-highly sensitive and multiplexed SERS nanoplasmonic biosensor for miRNA detection using a head-flocked gold nanopillar. *The Analyst*, 144(5):1768–1776, 2019.
- [144] Gary K. Geiss, Roger E. Bumgarner, Brian Birditt, Timothy Dahl, Naeem Dowidar, Dwayne L. Dunaway, H. Perry Fell, Sean Ferree, Renee D. George, Tammy Grogan, Jeffrey J. James, Malini Maysuria, Jeffrey D. Mitton, Paola Oliveri, Jennifer L. Osborn, Tao Peng, Amber L. Ratcliffe, Philippa J. Webster, Eric H. Davidson, Leroy Hood, and Krassen Dimitrov. Direct multiplexed measurement of gene expression with color-coded probe pairs. *Nature Biotechnology*, 26(3):317–325, March 2008.
- [145] Ido Amit, Manuel Garber, Nicolas Chevrier, Ana Paula Leite, Yoni Donner, Thomas Eisenhaure, Mitchell Guttman, Jennifer K. Grenier, Weibo Li, Or Zuk, Lisa A. Schubert, Brian Birditt, Tal Shay, Alon Goren, Xiaolan Zhang, Zachary Smith, Raquel Deering, Rebecca C. McDonald, Moran Cabili, Bradley E. Bernstein, John L. Rinn, Alex Meissner, David E. Root, Nir Hacohen, and Aviv Regev. Unbiased reconstruction of a mammalian transcriptional network mediating pathogen responses. *Science (New York, N. Y.)*, 326(5950):257–263, October 2009.
- [146] Yi-Hsien Su, Enhu Li, Gary K. Geiss, William J. R. Longabaugh, Alexander Krämer, and Eric H. Davidson. A perturbation model of the gene regulatory network for oral and aboral ectoderm specification in the sea urchin embryo. *Developmental Biology*, 329(2):410–421, May 2009.

- [147] Weixin Wang, Meghan Corrigan-Cummins, Justin Hudson, Irina Maric, Olga Simakova, Sattva S. Neelapu, Larry W. Kwak, John E. Janik, Barry Gause, Elaine S. Jaffe, and Katherine R. Calvo. MicroRNA profiling of follicular lymphoma identifies microRNAs related to cell proliferation and tumor response. *Haematologica*, 97(4):586–594, April 2012.
- [148] Catherine Foye, Irene K. Yan, Waseem David, Neha Shukla, Yacob Habboush, Lori Chase, Kristen Ryland, Vivek Kesari, and Tushar Patel. Comparison of miRNA quantitation by Nanostring in serum and plasma samples. *PloS One*, 12(12):e0189165, 2017.
- [149] Ana Kozomara, Maria Birgaoanu, and Sam Griffiths-Jones. miRBase: from microRNA sequences to function. *Nucleic Acids Research*, 47(D1):D155–D162, January 2019.
- [150] Athina Giannoudis, Kim Clarke, Rasheed Zakaria, Damir Varešlija, Mosavar Farahani, Lucille Rainbow, Angela Platt-Higgins, Stuart Ruthven, Katherine A. Brougham, Philip S. Rudland, Michael D. Jenkinson, Leonie S. Young, Francesco Falciani, and Carlo Palmieri. A novel panel of differentially-expressed microRNAs in breast cancer brain metastasis may predict patient survival. *Scientific Reports*, 9(1):18518, December 2019.
- [151] Selam B. Dejene, Anders W. Ohman, Wei Du, Deepinder Randhawa, Anand Bradley, Niraj Yadav, Kevin M. Elias, Daniela M. Dinulescu, and Sunita R. Setlur. Defining fallopian tube-derived miRNA cancer signatures. *Cancer Medicine*, 8(15):6709–6716, November 2019.
- [152] Eric A. Hunt, David Broyles, Trajen Head, and Sapna K. Deo. MicroRNA Detection: Current Technology and Research Strategies. *Annual Review of Analytical Chemistry*, 8(1):217–237, July 2015.
- [153] Mohamed Guled, Leo Lahti, Pamela M. Lindholm, Kaisa Salmenkivi, Izhar Bagwan, Andrew G. Nicholson, and Sakari Knuutila. *CDKN2A*, *NF2*, and *JUN* are dysregulated among other genes by miRNAs in malignant mesothelioma-A miRNA microarray analysis. *Genes, Chromosomes and Cancer*, 48(7):615–623, July 2009.
- [154] Jian-Jun Zhao, Juhua Yang, Jianhong Lin, Nan Yao, Yihua Zhu, Jianlong Zheng, Jianhua Xu, Jin Q. Cheng, Jian-Yin Lin, and Xu Ma. Identification of miRNAs associated with tumorigenesis of retinoblastoma by miRNA microarray analysis. *Child's Nervous System*, 25(1):13–20, January 2009.

- [155] E. M. Southern. DNA microarrays. History and overview. *Methods in Molecular Biology (Clifton, N.J.)*, 170:1–15, 2001.
- [156] T. Babak. Probing microRNAs with microarrays: Tissue specificity and functional inference. *RNA*, 10(11):1813–1819, November 2004.
- [157] J Michael Thomson, Joel Parker, Charles M Perou, and Scott M Hammond. A custom microarray platform for analysis of microRNA gene expression. *Nature Methods*, 1(1):47–53, October 2004.
- [158] R.-Q. Liang. An oligonucleotide microarray for microRNA expression analysis based on labeling RNA with quantum dot and nanogold probe. *Nucleic Acids Research*, 33(2):e17–e17, January 2005.
- [159] C.-G. Liu, G. A. Calin, B. Meloon, N. Gamliel, C. Sevignani, M. Ferracin, C. D. Dumitru, M. Shimizu, S. Zupo, M. Dono, H. Alder, F. Bullrich, M. Negrini, and C. M. Croce. An oligonucleotide microchip for genome-wide microRNA profiling in human and mouse tissues. *Proceedings of the National Academy of Sciences*, 101(26):9740–9744, June 2004.
- [160] Scott Baskerville and David P. Bartel. Microarray profiling of microRNAs reveals frequent coexpression with neighboring miRNAs and host genes. *RNA (New York, N.Y.)*, 11(3):241–247, March 2005.
- [161] Eric A. Miska, Ezequiel Alvarez-Saavedra, Matthew Townsend, Akira Yoshii, Nenad Sestan, Pasko Rakic, Martha Constantine-Paton, and H. Robert Horvitz. Microarray analysis of microRNA expression in the developing mammalian brain. *Genome Biology*, 5(9):R68, 2004.
- [162] James Q. Yin, Robert C. Zhao, and Kevin V. Morris. Profiling microRNA expression with microarrays. *Trends in Biotechnology*, 26(2):70–76, February 2008.
- [163] M. Castoldi. A sensitive array for microRNA expression profiling (miChip) based on locked nucleic acids (LNA). *RNA*, 12(5):913–920, March 2006.
- [164] Somenath Roy, Jun Hui Soh, and Jackie Y. Ying. A microarray platform for detecting disease-specific circulating miRNA in human serum. *Biosensors and Bioelectronics*, 75:238–246, January 2016.
- [165] Jong Uk Lee, Woo Hyun Kim, Hye Sun Lee, Kyong Hwa Park, and Sang Jun Sim. Quantitative and Specific Detection of Exosomal miRNAs for Accurate Diagnosis of

- Breast Cancer Using a Surface-Enhanced Raman Scattering Sensor Based on Plasmonic Head-Flocked Gold Nanopillars. *Small*, 15(17):1804968, April 2019.
- [166] Xia Liu, Rongrong Tian, Jiaxue Gao, Dianjun Liu, and Zhenxin Wang. Multiplexed detection of microRNAs by a competitive DNA microarray-based resonance light scattering assay. *The Analyst*, 142(23):4529–4535, 2017.
- [167] Andrea Sguassero, Alvaro Artiga, Carlo Morasso, Rafael Ramirez Jimenez, Rafael Martín Rapún, Roberta Mancuso, Simone Agostini, Ambra Hernis, Arturs Abols, Aija Linē, Alice Gualerzi, Silvia Picciolini, Marzia Bedoni, Marco Rovaris, Furio Gramatica, Jesus M. de la Fuente, and Renzo Vanna. A simple and universal enzyme-free approach for the detection of multiple microRNAs using a single nanostructured enhancer of surface plasmon resonance imaging. *Analytical and Bioanalytical Chemistry*, 411(9):1873–1885, March 2019.
- [168] Wing Kiu Yeung, Huai-Yi Chen, Juan-Jie Sun, Tung-Han Hsieh, Mansoureh Z. Mousavi, Hsi-Hsien Chen, Kuang-Li Lee, Heng Lin, Pei-Kuen Wei, and Ji-Yen Cheng. Multiplex detection of urinary miRNA biomarkers by transmission surface plasmon resonance. *The Analyst*, 143(19):4715–4722, 2018.
- [169] Abraham J. Qavi, Jared T. Kindt, Martin A. Gleeson, and Ryan C. Bailey. Anti-DNA:RNA Antibodies and Silicon Photonic Microring Resonators: Increased Sensitivity for Multiplexed microRNA Detection. *Analytical Chemistry*, 83(15):5949–5956, August 2011.
- [170] Stefan Hofmann, Yiwei Huang, Peter Paulicka, Andreas Kappel, Hugo A. Katus, Andreas Keller, Benjamin Meder, Cord Friedrich Stähler, and Walter Gumbrecht. Double-Stranded Ligation Assay for the Rapid Multiplex Quantification of MicroRNAs. *Analytical Chemistry*, 87(24):12104–12111, December 2015.
- [171] Yanli Wen, Lanying Li, Jiang Li, Meihua Lin, Gang Liu, Wen Liang, Li Xu, Yan Li, Xiaolei Zuo, Suzhen Ren, and Ying Zhu. DNA Framework-Mediated Electrochemical Biosensing Platform for Amplification-Free MicroRNA Analysis. *Analytical Chemistry*, 92(6):4498–4503, March 2020.
- [172] Hyewon Lee, Jiseok Lee, Seung-Goo Lee, and Patrick S. Doyle. Hydrogel-Based Colorimetric Assay for Multiplexed MicroRNA Detection in a Microfluidic Device. *Analytical Chemistry*, page acs.analchem.9b05043, April 2020.

- [173] Woongsun Choi, Sang Yun Yeom, Junsun Kim, Seungwon Jung, Seungho Jung, Tae Soup Shim, Sang Kyung Kim, Ji Yoon Kang, Soo Hyun Lee, Il-Joo Cho, Jungkyu Choi, and Nakwon Choi. Hydrogel micropost-based qPCR for multiplex detection of miRNAs associated with Alzheimer's disease. *Biosensors & Bioelectronics*, 101:235–244, March 2018.
- [174] Seungwon Jung, Won Jin Kim, Bong Kyun Kim, Junsun Kim, Mi Jung Kim, Kwang Pyo Kim, and Sang Kyung Kim. In-particle stem-loop RT-qPCR for specific and multiplex microRNA profiling. *Biosensors and Bioelectronics*, 163:112301, September 2020.
- [175] Koji Hashimoto, Mika Inada, and Keiko Ito. Multiplex Real-Time Loop-Mediated Isothermal Amplification Using an Electrochemical DNA Chip Consisting of a Single Liquid-Flow Channel. *Analytical Chemistry*, 91(5):3227–3232, 2019.
- [176] Kazuo Hosokawa, Takahiro Sato, Yasunobu Sato, and Mizuo Maeda. DNA detection on a power-free microchip with laminar flow-assisted dendritic amplification. *Analytical Sciences: The International Journal of the Japan Society for Analytical Chemistry*, 26(10):1053–1057, 2010.
- [177] Andreas Mader, Ulrike Riehle, Thomas Brandstetter, Elmar Stickeler, and Juergen Ruehe. Universal nucleic acid sequence-based amplification for simultaneous amplification of messengerRNAs and microRNAs. *Analytica Chimica Acta*, 754:1–7, November 2012.
- [178] John P. Nolan and Larry A. Sklar. Suspension array technology: evolution of the flat-array paradigm. *Trends in Biotechnology*, 20(1):9–12, January 2002.
- [179] Limor Cohen, Mark R. Hartman, Aaron Amardey-Wellington, and David R. Walt. Digital direct detection of microRNAs using single molecule arrays. *Nucleic Acids Research*, 45(14):e137–e137, August 2017.
- [180] Filippo Causa, Anna Aliberti, Angela M. Cusano, Edmondo Battista, and Paolo A. Netti. Supramolecular Spectrally Encoded Microgels with Double Strand Probes for Absolute and Direct miRNA Fluorescence Detection at High Sensitivity. *Journal of the American Chemical Society*, 137(5):1758–1761, February 2015.
- [181] Xiaojun Qu, Haojun Jin, Yuqian Liu, and Qingjiang Sun. Strand Displacement Amplification Reaction on Quantum Dot-Encoded Silica Bead for Visual Detection of Multiplex MicroRNAs. *Analytical Chemistry*, 90(5):3482–3489, March 2018.

- [182] Jia-Jia Wang, Caishang Zheng, Yong-Zhong Jiang, Zhenhua Zheng, Miao Lin, Yi Lin, Zhi-Ling Zhang, Hanzhong Wang, and Dai-Wen Pang. One-Step Monitoring of Multiple Enterovirus 71 Infection-Related MicroRNAs Using Core–Satellite Structure of Magnetic Nanobeads and Multicolor Quantum Dots. *Analytical Chemistry*, 92(1):830–837, January 2020.
- [183] Dongbei Li, Yinan Wang, Chaiwan Lau, and Jianzhong Lu. xMAP Array Microspheres Based Stem–Loop Structured Probes as Conformational Switches for Multiplexing Detection of miRNAs. *Analytical Chemistry*, 86(20):10148–10156, October 2014.
- [184] Guangyu Tao, Tiancheng Lai, Xiao Xu, Yurou Ma, Xi Wu, Xiaojing Pei, Feng Liu, and Na Li. Colocalized Particle Counting Platform for Zeptomole Level Multiplexed Quantification. *Analytical Chemistry*, 92(5):3697–3706, March 2020.
- [185] David M. Rissin, Cheuk W. Kan, Todd G. Campbell, Stuart C. Howes, David R. Fournier, Linan Song, Tomasz Piech, Purvish P. Patel, Lei Chang, Andrew J. Rivnak, Evan P. Ferrell, Jeffrey D. Randall, Gail K. Provuncher, David R. Walt, and David C. Duffy. Single-molecule enzyme-linked immunosorbent assay detects serum proteins at subfemtomolar concentrations. *Nature Biotechnology*, 28(6):595–599, June 2010.
- [186] David M. Rissin, David R. Fournier, Tomasz Piech, Cheuk W. Kan, Todd G. Campbell, Linan Song, Lei Chang, Andrew J. Rivnak, Purvish P. Patel, Gail K. Provuncher, Evan P. Ferrell, Stuart C. Howes, Brian A. Pink, Kaitlin A. Minnehan, David H. Wilson, and David C. Duffy. Simultaneous detection of single molecules and singulated ensembles of molecules enables immunoassays with broad dynamic range. *Analytical Chemistry*, 83(6):2279–2285, March 2011.
- [187] Linan Song, David W. Hanlon, Lei Chang, Gail K. Provuncher, Cheuk W. Kan, Todd G. Campbell, David R. Fournier, Evan P. Ferrell, Andrew J. Rivnak, Brian A. Pink, Kaitlin A. Minnehan, Purvish P. Patel, David H. Wilson, Mary A. Till, William A. Faubion, and David C. Duffy. Single molecule measurements of tumor necrosis factor alpha and interleukin-6 in the plasma of patients with Crohn’s disease. *Journal of Immunological Methods*, 372(1-2):177–186, September 2011.
- [188] Danlu Wu, Milena Dumont Milutinovic, and David R. Walt. Single molecule array (Simoa) assay with optimal antibody pairs for cytokine detection in human serum samples. *The Analyst*, 140(18):6277–6282, 2015.
- [189] Linan Song, Dandan Shan, Mingwei Zhao, Brian A. Pink, Kaitlin A. Minnehan, Lyndsey York, Melissa Gardel, Sean Sullivan, Aaron F. Phillips, Ryan B. Hayman,

- David R. Walt, and David C. Duffy. Direct Detection of Bacterial Genomic DNA at Sub-Femtomolar Concentrations Using Single Molecule Arrays. *Analytical Chemistry*, 85(3):1932–1939, February 2013.
- [190] Seungwon Jung, Junsun Kim, Dong Jin Lee, Eun Hae Oh, Hwasup Lim, Kwang Pyo Kim, Nakwon Choi, Tae Song Kim, and Sang Kyung Kim. Extensible Multiplex Real-time PCR of MicroRNA Using Microparticles. *Scientific Reports*, 6(1):22975, March 2016.
- [191] Stephen C. Chapin and Patrick S. Doyle. Ultrasensitive Multiplexed MicroRNA Quantification on Encoded Gel Microparticles Using Rolling Circle Amplification. *Analytical Chemistry*, 83(18):7179–7185, September 2011.
- [192] Hyewon Lee, Sarah J. Shapiro, Stephen C. Chapin, and Patrick S. Doyle. Encoded Hydrogel Microparticles for Sensitive and Multiplex microRNA Detection Directly from Raw Cell Lysates. *Analytical Chemistry*, 88(6):3075–3081, March 2016.
- [193] Maxwell B. Nagarajan, Augusto M. Tentori, Wen Cai Zhang, Frank J. Slack, and Patrick S. Doyle. Nonfouling, Encoded Hydrogel Microparticles for Multiplex MicroRNA Profiling Directly from Formalin-Fixed, Paraffin-Embedded Tissue. *Analytical Chemistry*, 90(17):10279–10285, September 2018.
- [194] Nidhi Juthani and Patrick S. Doyle. A platform for multiplexed colorimetric microRNA detection using shape-encoded hydrogel particles. *The Analyst*, 145(15):5134–5140, 2020.
- [195] Jae Jung Kim, Lynna Chen, and Patrick S. Doyle. Microparticle parking and isolation for highly sensitive microRNA detection. *Lab on a Chip*, 17(18):3120–3128, 2017.
- [196] Shengquan Liu, Han Fang, Chengjiao Sun, Nana Wang, and Jiong Li. Highly sensitive and multiplexed miRNA analysis based on digitally encoded silica microparticles coupled with RCA-based cascade amplification. *The Analyst*, 143(21):5137–5144, 2018.
- [197] Y. Xia, B. Gates, Y. Yin, and Y. Lu. Monodispersed Colloidal Spheres: Old Materials with New Applications. *Advanced Materials*, 12(10):693–713, May 2000. Publisher: John Wiley & Sons, Ltd.
- [198] Feika Bian, Jindao Wu, Huan Wang, Lingyu Sun, Changmin Shao, Yu Wang, Zhiyang Li, Xuehao Wang, and Yuanjin Zhao. Bioinspired Photonic Barcodes with Graphene Oxide Encapsulation for Multiplexed MicroRNA Quantification. *Small*, 14(52):1803551, December 2018.

- [199] Yueshuang Xu, Huan Wang, Chengxin Luan, Fanfan Fu, Baoan Chen, Hong Liu, and Yuanjin Zhao. Porous Hydrogel Encapsulated Photonic Barcodes for Multiplex MicroRNA Quantification. *Advanced Functional Materials*, 28(1):1704458, January 2018.
- [200] Xiaowei Wei, Feika Bian, Xiaoxiao Cai, Yu Wang, Lijun Cai, Jian Yang, Yefei Zhu, and Yuanjin Zhao. Multiplexed Detection Strategy for Bladder Cancer MicroRNAs Based on Photonic Crystal Barcodes. *Analytical Chemistry*, 92(8):6121–6127, April 2020.
- [201] Regina Bilan, Amagoia Ametzazurra, Kristina Brazhnik, Sergio Escorza, David Fernández, María Uríbarri, Igor Nabiev, and Alyona Sukhanova. Quantum-dot-based suspension microarray for multiplex detection of lung cancer markers: preclinical validation and comparison with the Luminex xMAP® system. *Scientific Reports*, 7(1):44668, April 2017.
- [202] Ningning Wang, Liran Song, Ting Deng, and Jishan Li. Microsphere-based suspension array for simultaneous recognition and quantification of multiple cancer-associated miRNA via DNAzyme-Mediated signal amplification. *Analytica Chimica Acta*, 1140:69–77, December 2020.
- [203] Kayeong Shin, Jaeyeong Choi, Yeojun Kim, Yoonjeong Lee, Jooheon Kim, Seungho Lee, and Hoeil Chung. Feasibility study for combination of field-flow fractionation (FFF)-based separation of size-coded particle probes with amplified surface enhanced Raman scattering (SERS) tagging for simultaneous detection of multiple miRNAs. *Journal of Chromatography A*, 1556:97–102, June 2018.
- [204] Akihisa Miyagawa, Makoto Harada, and Tetsuo Okada. Multiple MicroRNA Quantification Based on Acoustic Levitation of Single Microspheres after One-Pot Sandwich Interparticle Hybridizations. *Analytical Chemistry*, 90(22):13729–13735, November 2018.
- [205] Sungi Kim, Jeong-Eun Park, Woosung Hwang, Jinyoung Seo, Young-Kwang Lee, Jae-Ho Hwang, and Jwa-Min Nam. Optokinetically Encoded Nanoprobe-Based Multiplexing Strategy for MicroRNA Profiling. *Journal of the American Chemical Society*, 139(9):3558–3566, March 2017.
- [206] Huiting Lu, Keke Guo, Yu Cao, Fan Yang, Dongdong Wang, Lei Dou, Yayun Liu, and Haifeng Dong. Cancer Cell Membrane Vesicle for Multiplex MicroRNA Imaging in Living Cells. *Analytical Chemistry*, 92(2):1850–1855, January 2020.
- [207] Jing Li, Jin Huang, Xiaohai Yang, Yanjing Yang, Ke Quan, Nuli Xie, Yanan Wu, Changbei Ma, and Kemin Wang. Two-Color-Based Nanoflares for Multiplexed MicroRNAs Imaging in Live Cells. *Nanotheranostics*, 2(1):96–105, 2018.

- [208] Qian Lu, Daniel Ericson, Yang Song, Chengzhou Zhu, Ranfeng Ye, Songqin Liu, Joseph A. Spornyak, Dan Du, He Li, Yun Wu, and Yuehe Lin. MnO₂ Nanotube-Based NanoSearchlight for Imaging of Multiple MicroRNAs in Live Cells. *ACS Applied Materials & Interfaces*, 9(28):23325–23332, July 2017.
- [209] Yafeng Wu, Jianyu Han, Peng Xue, Rong Xu, and Yuejun Kang. Nano metal–organic framework (NMOF)-based strategies for multiplexed microRNA detection in solution and living cancer cells. *Nanoscale*, 7(5):1753–1759, 2015.
- [210] Jiantao Yu, Sihui He, Chen Shao, Haoran Zhao, Jing Li, and Leilei Tian. A common anchor facilitated GO-DNA nano-system for multiplex microRNA analysis in live cells. *Nanoscale*, 10(15):7067–7076, 2018.
- [211] Xianjiu Liao, Quanbo Wang, and Huangxian Ju. Simultaneous sensing of intracellular microRNAs with a multi-functionalized carbon nitride nanosheet probe. *Chem. Commun.*, 50(88):13604–13607, September 2014.
- [212] Wenjiao Zhou, Daxiu Li, Chengyi Xiong, Ruo Yuan, and Yun Xiang. Multicolor-Encoded Reconfigurable DNA Nanostructures Enable Multiplexed Sensing of Intracellular MicroRNAs in Living Cells. *ACS Applied Materials & Interfaces*, 8(21):13303–13308, June 2016.
- [213] Zhixin Zhou, Yang Sung Sohn, Rachel Nechushtai, and Itamar Willner. DNA Tetrahedra Modules as Versatile Optical Sensing Platforms for Multiplexed Analysis of miRNAs, Endonucleases, and Aptamer–Ligand Complexes. *ACS Nano*, 14(7):9021–9031, July 2020.
- [214] Fan Yang, Yaru Cheng, Yiyi Zhang, Wei Wei, Haifeng Dong, Huiting Lu, and Xueji Zhang. Bioinspired Framework Nucleic Acid Capture Sensitively and Rapidly Resolving MicroRNAs Biomarkers in Living Cells. *Analytical Chemistry*, 92(6):4411–4418, March 2020.
- [215] Huiting Lu, Keke Guo, Yu Cao, Fan Yang, Dongdong Wang, Lei Dou, Yayun Liu, and Haifeng Dong. Cancer Cell Membrane Vesicle for Multiplex MicroRNA Imaging in Living Cells. *Analytical Chemistry*, 92(2):1850–1855, January 2020.
- [216] Xiangdan Meng, Kai Zhang, Wenhao Dai, Yu Cao, Fan Yang, Haifeng Dong, and Xueji Zhang. Multiplex microRNA imaging in living cells using DNA-capped-Au assembled hydrogels. *Chemical Science*, 9(37):7419–7425, 2018.

- [217] Shue Wang, Nicholas J. Emery, and Allen P. Liu. A Novel Synthetic Toehold Switch for MicroRNA Detection in Mammalian Cells. *ACS Synthetic Biology*, 8(5):1079–1088, May 2019.
- [218] Zixun Wang, Lin Qi, Yang Yang, Mingxing Lu, Kai Xie, Xi Zhao, Elvis Hung Chi Cheung, Yuan Wang, Xuezheng Jiang, Wenjun Zhang, Linfeng Huang, Xin Wang, and Peng Shi. High-throughput intracellular biopsy of microRNAs for dissecting the temporal dynamics of cellular heterogeneity. *Science Advances*, 6(24):eaba4971, June 2020.
- [219] Wen Zhou, Qiang Li, Huiqiao Liu, Jie Yang, and Dingbin Liu. Building Electromagnetic Hot Spots in Living Cells *via* Target-Triggered Nanoparticle Dimerization. *ACS Nano*, 11(4):3532–3541, April 2017.
- [220] Seungwon Jung, Bong Kyun Kim, Sangjoon Lee, Seungmin Yoon, Heh-In Im, and Sang Kyung Kim. Multiplexed on-chip real-time PCR using hydrogel spot array for microRNA profiling of minimal tissue samples. *Sensors and Actuators B: Chemical*, 262:118–124, June 2018.
- [221] G. Seelig, D. Soloveichik, D. Y. Zhang, and E. Winfree. Enzyme-Free Nucleic Acid Logic Circuits. *Science*, 314(5805):1585–1588, December 2006.
- [222] Ke Quan, Jing Li, Jiaoli Wang, Nuli Xie, Qiaomei Wei, Jinlu Tang, Xiaohai Yang, Kemin Wang, and Jin Huang. Dual-microRNA-controlled double-amplified cascaded logic DNA circuits for accurate discrimination of cell subtypes. *Chemical Science*, 10(5):1442–1449, 2019.
- [223] Xiaoyi Ma, Xifeng Chen, Yuguo Tang, Ruhong Yan, and Peng Miao. Triple-Input Molecular AND Logic Gates for Sensitive Detection of Multiple miRNAs. *ACS Applied Materials & Interfaces*, 11(44):41157–41164, November 2019.
- [224] Siqi Zhang, Jiayi Cheng, Wei Shi, Kai-Bin Li, De-Man Han, and Jing-Juan Xu. Fabrication of a Biomimetic Nanochannel Logic Platform and Its Applications in the Intelligent Detection of miRNA Related to Liver Cancer. *Analytical Chemistry*, 92(8):5952–5959, April 2020.
- [225] Chao Zhang, Yumeng Zhao, Xuemei Xu, Rui Xu, Haowen Li, Xiaoyan Teng, Yuzhen Du, Yanyan Miao, Hsiao Chu Lin, and Da Han. Cancer diagnosis with DNA molecular computation. *Nature Nanotechnology*, 15:709–715, May 2020.
- [226] Kazuo Hosokawa, Takahiro Sato, Yasunobu Sato, and Mizuo Maeda. DNA detection on a power-free microchip with laminar flow-assisted dendritic amplification. *Analytical*

Sciences: The International Journal of the Japan Society for Analytical Chemistry, 26(10):1053–1057, 2010.

- [227] Cong Wang, Qiang Ding, Pamela Plant, Mayada Basheer, Chuance Yang, Eriny Tawadrous, Adriana Krizova, Carl Boulos, Mina Farag, Yufeng Cheng, and George M. Yousef. Droplet digital PCR improves urinary exosomal miRNA detection compared to real-time PCR. *Clinical Biochemistry*, 67:54–59, May 2019.
- [228] Teruo Fujii and Yannick Rondelez. Predator–Prey Molecular Ecosystems. *ACS Nano*, 7(1):27–34, January 2013.
- [229] Kevin Montagne, Raphael Plasson, Yasuyuki Sakai, Teruo Fujii, and Yannick Rondelez. Programming an *in vitro* DNA oscillator using a molecular networking strategy. *Molecular Systems Biology*, 7(1):466, January 2011.
- [230] Alexandre Baccouche, Kevin Montagne, Adrien Padirac, Teruo Fujii, and Yannick Rondelez. Dynamic DNA-toolbox reaction circuits: A walkthrough. *Methods*, 67(2):234–249, May 2014.

List of publications

European patent 19305670.2: *Method of digital multiplex detection and/or quantification of biomolecules*

Inventors: GINES, Guillaume; RONDELEZ, Yannick; TALY, Valérie; JET, Thomas.

Filed 2019.05.27

Advances in multiplexed techniques for the detection and quantification of microRNAs

Authors: JET, Thomas; GINES, Guillaume; RONDELEZ, Yannick; TALY, Valérie.

Accepted at Chemical Society Reviews.

Digital and multiplex microRNA detection with microcompartmentalized bead assay

Authors: JET, Thomas; GINES, Guillaume; RONDELEZ, Yannick; TALY, Valérie.

Under preparation.

Communications

Poster presentation: MicroTAS 2020 conference (October 2020)

Digital and multiplex microRNA detection with microcompartmentalized bead assay

Résumé :

Les microARN sont de courts ARN simple brins, non codants, impliqués dans la régulation post transcriptionnelle de l'expression génétique. De nombreuses études ont montré que les concentrations de miARN dans les fluides corporels sont dérégulées dans de nombreuses conditions pathologiques, comme les cancers, les maladies cardiovasculaires ou bien encore la maladie d'Alzheimer, en faisant de potentiels indicateurs de ces maladies. De plus, les miARN sont libérés dans les fluides corporels, notamment le sang, sous la forme de complexes protéiques, ce qui leur confère une meilleure stabilité, en comparaison d'autres marqueurs circulants, dans ces fluides. Pour ces raisons, les miARN apparaissent comme des cibles de choix pour le développement de nouvelles méthodes de diagnostic. Ces méthodes requièrent cependant de hauts niveaux de sensibilité, de spécificité et de quantitativité, qui sont autant de défis technologiques. De plus, le potentiel diagnostique des miARN se situe probablement dans l'analyse chez le patient de différents miARN, formant un profil pouvant être comparé avec les signatures miARN typiques des conditions pathologiques ou non-pathologiques. Ainsi, la capacité de quantifier différents miARN en parallèle est également cruciale. Dans cette thèse, nous présentons les différentes étapes du développement d'une méthode permettant la quantification absolue et multiplexe de miARN. Cette méthode combine l'utilisation d'un réseau de réactions chimiques permettant l'amplification exponentielle d'un signal moléculaire avec la production de microémulsions par microfluidique. La technique développée permet la quantification de 20 miARNs simultanément, une capacité bien supérieure à celle de la RT-qPCR, méthode standard pour la détection de miARN. La sensibilité de notre méthode est adaptée pour l'analyse de miARN dans les fluides corporels humains, avec une limite de détection de l'ordre du femtomolaire.

Mots-clés : microRNA; diagnostic; multiplex; digital; biologie synthétique; microfluidique; cytométrie en flux.

Summary:

MicroRNAs are short, non-coding, single-stranded RNA molecules involved in post-transcriptional regulation of protein expression. A plethora of studies reported that the concentrations of some miRNAs are dysregulated in numerous pathological conditions, such as cancers, cardiovascular or Alzheimer's diseases, making them potential markers of these diseases. Additionally, the miRNAs released in bodily fluids are protected by protein complexes, which improves their stability in these fluids. For those reasons, miRNAs appear as promising targets for the development of new diagnostic methods. MiRNA-based diagnostics however require high levels of sensitivity, specificity and quantitativity. Additionally, the potential of miRNAs as biomarkers most likely lies in the parallelized analysis of several miRNAs, forming a profile of the patient, which is then compared to pathological and non-pathological miRNA signatures. The ability to detect several miRNAs simultaneously is therefore of prime importance. In this PhD thesis, we report on the development of a high-multiplex and digital miRNA detection method. The technique combines a chemical network allowing exponential amplification of a molecular signal and droplet microfluidics. The developed method allows the absolute quantification of up to 20 miRNAs, outperforming the gold-standard method for miRNA detection, RT-qPCR. The sensitivity of the method is suited for miRNA detection from bodily fluids, with a limit of detection in the femtomolar range.

Keywords: microRNA; diagnostics; multiplex; digital; synthetic biology; microfluidics; flow cytometry.

Résumé :

Les microARN sont de courts ARN simple brins, non codants, impliqués dans la régulation post transcriptionnelle de l'expression génétique. De nombreuses études ont montré que les concentrations de miARN dans les fluides corporels sont dérégulées dans de nombreuses conditions pathologiques, comme les cancers, les maladies cardiovasculaires ou bien encore la maladie d'Alzheimer, en faisant de potentiels indicateurs de ces maladies. De plus, les miARN sont libérés dans les fluides corporels, notamment le sang, sous la forme de complexes protéiques, ce qui leur confère une meilleure stabilité, en comparaison d'autres marqueurs circulants, dans ces fluides. Pour ces raisons, les miARN apparaissent comme des cibles de choix pour le développement de nouvelles méthodes de diagnostic. Ces méthodes requièrent cependant de hauts niveaux de sensibilité, de spécificité et de quantitativité, qui sont autant de défis technologiques. De plus, le potentiel diagnostique des miARN se situe probablement dans l'analyse chez le patient de différents miARN, formant un profil pouvant être comparé avec les signatures miARN typiques des conditions pathologiques ou non-pathologiques. Ainsi, la capacité de quantifier différents miARN en parallèle est également cruciale. Dans cette thèse, nous présentons les différentes étapes du développement d'une méthode permettant la quantification absolue et multiplexe de miARN. Cette méthode combine l'utilisation d'un réseau de réactions chimiques permettant l'amplification exponentielle d'un signal moléculaire avec la production de microémulsions par microfluidique. La technique développée permet la quantification de 20 miARNs simultanément, une capacité bien supérieure à celle de la RT-qPCR, méthode standard pour la détection de miARN. La sensibilité de notre méthode est adaptée pour l'analyse de miARN dans les fluides corporels humains, avec une limite de détection de l'ordre du femtomolaire.

Mots-clés : microRNA; diagnostic; multiplex; digital; biologie synthétique; microfluidique; cytométrie en flux.

Summary:

MicroRNAs are short, non-coding, single-stranded RNA molecules involved in post-transcriptional regulation of protein expression. A plethora of studies reported that the concentrations of some miRNAs are dysregulated in numerous pathological conditions, such as cancers, cardiovascular or Alzheimer's diseases, making them potential markers of these diseases. Additionally, the miRNAs released in bodily fluids are protected by protein complexes, which improves their stability in these fluids. For those reasons, miRNAs appear as promising targets for the development of new diagnostic methods. MiRNA-based diagnostics however require high levels of sensitivity, specificity and quantitativity. Additionally, the potential of miRNAs as biomarkers most likely lies in the parallelized analysis of several miRNAs, forming a profile of the patient, which is then compared to pathological and non-pathological miRNA signatures. The ability to detect several miRNAs simultaneously is therefore of prime importance. In this PhD thesis, we report on the development of a high-multiplex and digital miRNA detection method. The technique combines a chemical network allowing exponential amplification of a molecular signal and droplet microfluidics. The developed method allows the absolute quantification of up to 20 miRNAs, outperforming the gold-standard method for miRNA detection, RT-qPCR. The sensitivity of the method is suited for miRNA detection from bodily fluids, with a limit of detection in the femtomolar range.

Keywords: microRNA; diagnostics; multiplex; digital; synthetic biology; microfluidics; flow cytometry.